Structure and Thermal Stability of Selected Organic Inclusion Compounds

NOTHEMBA SILWANA

Cape Peninsula
University of Technology

Structure and Thermal Stability of Selected Organic Inclusion Compounds

Composed by: NOTHEMBA SILWANA

A thesis submitted to: Cape Peninsula University of Technology

In fulfillment of: Masters Degree in Technology (Chemistry)

Department of Chemistry

April 2012

DECLARATION

I, _____ declare that the contents of this dissertation/thesis represent my own work, and that the dissertation/thesis has not previously been submitted for academic examination towards any qualification. Furthermore, it represents my own opinions and not necessarily those of the Cape Peninsula University of Technology.

Signed **Date**

_____ _____

Acknowledgements

I Thank the LORD Almighty for the enabling strength throughout this journey. His guidance in leading me to be custodian of the invaluable knowledge, technical expertise and love, offered to me by the following individuals and organisations to whom I feel wholly indebted.

My supervisor "Prof J" Prof. Ayesha Jacobs your dedication to this field is inspiring you are an epitome of diligence. I am grateful for your patience, constant guidance, support, encouragement and all the energy that you've poured in to making sure that I pull through.

Prof. L. R. Nassimbeni our oracle. Your presence brought about enlightenment, discomfort and a lot of entertainment. Thank you for your support, and words of encouragement. Your scientific and worldly knowledge is unmatched in my view.

Dr. Nikoletta B. Báthori thank you for your open door policy, your support and motivation. You've been wonderful.

Mrs Merrill Wicht I am grateful for the Mandela Rhodes scholarship nomination a life changing experience was afforded to me because of that. Thank you for the support.

Mrs Lorna Marshall thank you for your encouragement and willingness to help however you could.

Mr Cornelius Botha, I appreciate your willing assistance.

Group members Karabo Sebogisi, Yav Rodriquez Kabwit, Amina Sayed, Mr Mawonga Mei an incredible team. I couldn't have done it without your assistance, support and encouragement.

My mother thank you for all the love, patience, and support Ndiyabulela Mamyirha. My father your presence makes that much of a difference. Thank you for your guidance and support.

Christel Kimene-Kaya, thank you for believing in me. Thank you for your assistance. Your worth in my life is immeasurable.

I would like to thank my family oSilwana, Dibakoane, Mditshwa, Mzamo, Jacobs, Thene nabakwa Mbali your love and support kept me going.

Friends Bulelwa Fongoma, Nwabisa Majola, Tsidi Malapane and Mbuyiselo Gunguluza thank you for the encouragement love and support.

I would also like to extend a big thank you to The Mandela Rhodes foundation for the financial support and for tuning my mind to issues concerning leadership, reconciliation, entrepreneurship and education.

I acknowledge the Cape Peninsula University of Technology for financial support, and for facilities and learning resources afforded to postgraduates. It made a difference.

ABSTRACT

Title: Structure and Thermal Stability of Selected Organic Inclusion Compounds

Author: Nothemba Silwana

Date: April 2012

Crystal engineering is the synthesis of new crystalline materials with specific chemical and physical properties which allows the comprehensive understanding of the non covalent interactions that occur between molecules in the crystalline state. This has lead to extensive work being done in terms of host design. The study of non-covalent interactions formed by these materials is crucial to understanding many biological processes.

This study focuses on the inclusion compounds of 1, 4-bis (diphenylhydroxymethyl) benzene **H**, a host compound engineered by E Weber, that conforms to Weber's rules for host design as it is bulky, rigid, and has hydroxyl moieties that act as hydrogen-bonding donors. A Cambridge Structural Database (CSD version 5.33) search has revealed that no research has been conducted on this host compound. Characterization of the compounds were conducted using thermogravimetric analysis (TGA), differential scanning calorimetry (DSC), hot stage microscopy (HS), gas chromatography (GC), powder X-ray diffraction(PXRD) and single X -ray diffraction. Host: guest ratios determined from TG analysis were correlated with structural analysis results.

We have successfully prepared inclusion compounds with *N, N*- dimethylformamide(DMF) *N, N*- dimethylacetamide (DMA), *N*-methylformamide (NMF) and *N*-methylacetamide (NMA), 2-picoline, 3-picoline, 4-picoline, pyridine and morpholine. Following which a series of competition experiments were conducted to establish the selectivity profile of the host by dissolving the host in an excess of two guests pairs, between DMF: DMA, DMF: NMF, DMF: NMA, DMA: NMF, DMA: NMA and NMF: NMA. The results of the competition experiment showed that the host had high selectivity for DMF and the selectivity profile follows a trend as follows DMF>NMA>NMF>DMA. The results for the competition experiments between the picolines, pyridine and morpholine were inconclusive.

PUBLICATIONS AND CONFERENCES

Parts of this thesis were published in :

Inclusion of 1,4-bis(diphenylhydroxymethyl)benzene with amides: Structure and selectivity, Ayesha Jacobs, Luigi R. Nassimbeni, Nothemba Silwana, Nikoletta B. Báthori and Edwin Weber, *CrystEngComm*, 13,2011,7014-7018

Parts of this thesis were presented in :

Poster entitled: Selectivity of Amides by host-guest inclusion, at Cape Peninsula University of Technology Research day, 3 December,2011

TABLE OF CONTENTS

1. CHAPTER 1- Introduction

1.1 Supramolecular Chemistry

Supramolecular chemistry refers to multidisciplinary research encompassing chemical, physical, biological and technological aspects. It is the study of complex chemical systems, based on multi-component molecular assemblies, where the component structures are bridged by a variety of weaker (non-covalent) interactions.[1] These intermolecular interactions define the molecular crystal. Supramolecular principles make it possible to combine molecules into new chemical species bearing an individual set of physical and chemical properties.

It can be depicted by the relationship between a host and guest molecule:

$$Host_{(s)} + Guest_{(s,\ g\ or\ l)} \rightarrow Host{\cdot}Guest_{(s)}$$

Depending on the compatibility of the guest to the host, the guest interacts with the host. Their association by means of intermolecular bonds describes their relationship in terms of their function, size, shape and geometric complementarities.

In its broadest sense supramolecules are aggregates whereby molecular components form bonds either spontaneously or by design to form a larger entity with properties derived from its components. Inclusion chemistry is one aspect of supramolecular chemistry. These are supramolecular systems formed as a result of inclusion of guest molecules into cavities formed by host molecules.[2]

Supramolecular chemistry is resonant within living species. It has proven to be at the core of human existence from a biological perspective, considering the hydrogen bonds that hold the DNA helical structure together.[3] There have been numerous applications of supramolecular studies as discussed by H.Dodzuik.

"The study of supramolecular chemistry is not only focused on the understanding of the nature of the supramolecular aggregates but also on the formation of devices of industrial importance.....numerous exciting ventures in electronics e.g. the miniaturization of computers and the development of nano sized tools capable of manipulating them, supramolecular sensors for environmental protection, photochemical processes leading to more effective and environmentally friendly energy use and generation. Drug design and

administration has been explored and liquid crystalline displays and cylodextrin complexes in the pharmaceutical and food industry, in cleaning and cosmetics are those few bringing profits today."[4]

Literature Review of Supramolecular chemistry

Supramolecular chemistry dates back to 1810 when Sir Humphrey Davy first prepared a chlorine hydrate ($Cl_2.6H_2O$).[5] Further advances were made in 1893 when Alfred Werner discovered coordination theory. This concept was further studied by Emil Fisher who in 1894 introduced the lock and key concept, the main topic associated with molecular recognition.[6] *(Molecular recognition investigates how host molecules recognize guests and how they associate.)*

In 1948 H. M. Powell proposed a structure for β-quinol inclusion compounds and introduced the term clathrate to describe the total encapsulation of a guest within a host framework cavity.[7] In 1967 Pederson observed that crown ethers showed molecular recognition, making them the first artificial molecule found to do so.[8] D. J Cram and J. M Cram introduced the term host–guest where the host compound accommodates the guest.[9] In 1978 J. M Lehn defined supramolecular chemistry as "the chemistry of the non-covalent bond."[10]

The field has made great leaps since, it has become one of the fastest growing fields of the chemical landscape with numerous journals, Comprehensive supramolecular publications, Encyclopedia of supramolecular chemistry and the Cambridge structural data base growing rapidly annually.

1.2 The Interactions

Molecular complexes are composed of two or more molecules or ions held together by weak non-covalent electrostatic forces. These complexes are usually held together by hydrogen bonding, ion pairing π-acid and π-base interactions, metal to ligand binding and/or van der Waals attractive forces.[11]

The hydrogen bond is one of the most important non-covalent interactions in the design of supramolecular structures because of its strength and high degree of directionality.[12,13] These bonds have been extensively investigated using spectroscopic tools such as infra red (IR) and nuclear magnetic resonance (NMR) spectroscopy and neutron/X-ray diffraction.[1] Figure. 1.1 illustrates the main types of hydrogen bonds which have been characterized. The hydrogen bond is an interaction between a hydrogen bond donor, D and an acceptor, A in the same (intramolecular) or in different (intermolecular) molecules usually represented as D–H···A. D is an electronegative atom such as O, N, F, P, S, Cl, Br, or I. A can be any electron rich atom such as N, O, P, S, Cl, Br, alkenes, alkynes, aromatic π systems or transition metals. If the acceptor and donor groups have low electronegativity the hydrogen bond is said to be weak. Another important type of intermolecular interaction is π-π interactions which can be divided into two types: face-to-face and edge-to-face as indicated in Figure. 1.2.

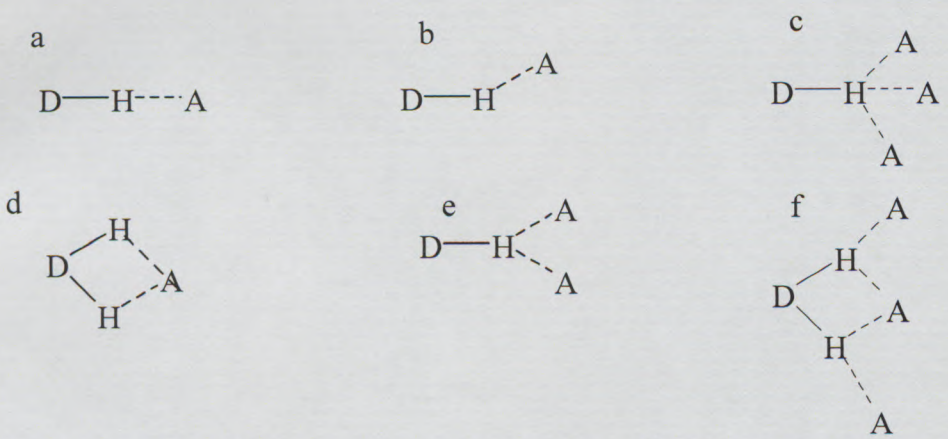

Figure 1.1 Different types of hydrogen bonding geometries: a-linear, b-bent, c-trifurcated, d-accepting bifurcated, e-donating bifurcated and f-three centre bifurcated.

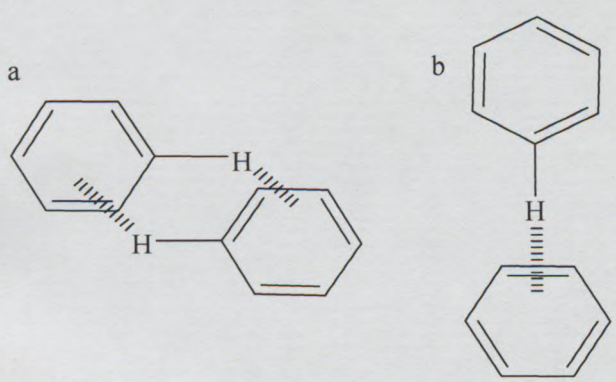

Figure 1.2 Illustration of two types of π- π interactions a-face to face and b –edge-to-face

Hydrogen bonds are considered to be strong or weak based on their ability to hold or control the supramolecular structure. The strength of a hydrogen bond can vary from the weakest (~4kJ/mol) to the strongest (~120kJ/mol) depending on the interaction direction. Table 1.1 shows the strength of the hydrogen bond according to distance and bond angle. It is usually bent rather than linear.[14,15] Linear hydrogen bonds are understood to be the strongest and the strength can be related to the length of the bond. The weak hydrogen bonds are even less linear and in some cases can form perpendicular interactions as in the case of C–H··· π, where the C–H bonds point directly towards the conjugated system.

Table 1.1 Parameter of Hydrogen bonds[15, 16]

Hydrogen bond type	Strong	Moderate	Weak
Length D···A (Å)	1.2-1.5	1.5-2.2	2.2-3.2
Angle (°)	175-180	130-180	90-150

The hydrogen bond is an important consideration for the molecular assembly, molecular recognition and crystal engineering. The relationships explored in this study are aimed at investigating host-guest systems in order to build an in depth understanding of the intermolecular interactions occurring in these compounds, which is an essential step towards gaining control over the assembly of such compounds.

1.3 Crystal Engineering

Crystal engineering has been able to advance rapidly in recent years. Today the subject covers a community of at least 150 independent research groups, with many specialist journals including Crystal Growth and Design and CrystEngComm—and even a dedicated webpage and a Wikipedia site maintained by the latter society.[2,17,18] The term crystal engineering was first used in 1971 by Schmidt.[19] Desiraju describes it as "the understanding of intermolecular interactions in the context of crystal packing and utilization of such understanding in the design of new solids with desired physical and chemical properties."[18] It can then be understood as the application of the concepts of supramolecular chemistry to the solid state in the formation of new crystalline solids as a result of weak but directional

intermolecular forces and reproducible recognition events of supramolecular synthons. Scientists have long been working on a supramolecular blueprint which is prone to produce successful outcomes, allowing the synthesis of new solid phases with predictable stoichiometry and architecture.

It was Dunitz who first expressed this notion of a crystal being an example of a "supramolecule par excellence" in that the crystal is *: a lump of matter, of macroscopic dimensions, millions of molecules long, held together in a periodic arrangement by just the same kind of interactions as are responsible for molecular recognition and complexation at all levels - ion-ion, ion-dipole, dipole-dipole interactions, hydrogen bonding, London forces, and so on.*[20] Knowledge and control of intermolecular interactions is as vital to crystal synthesis as is control of the covalent bond to molecular synthesis. After metal-coordination bonds and ionic interactions the strongest interactions in crystal engineering are hydrogen bonds which is focal to this study.[22,23,24]

Molecular recognition plays a major role in crystal engineering. It typically involves an interaction between complementary hydrogen-bonding faces or a metal and a ligand. The term supramolecular synthon (a reproducible, frequently occurring kind of non-covalent interaction found in molecular crystal structures which can be used in crystal designs) was coined by Desiraju to describe building blocks that are common to many structures and can be used to order specific groups in the solid state. The most common type of intermolecular bonding that sustains supramolecular synthons is the hydrogen bond.[22,24,25] Typical supramolecular synthons based on hydrogen bonding that have been used in crystal engineering studies are shown in Figure. 1.3.

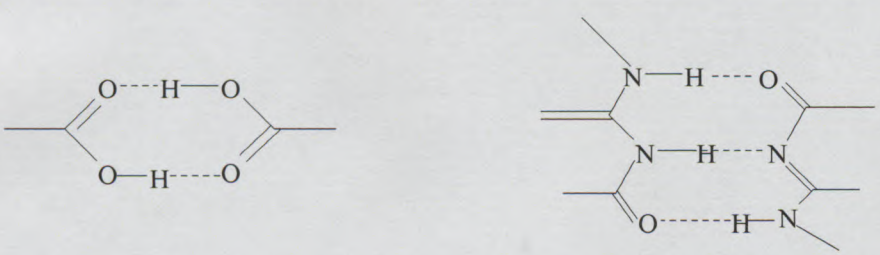

Figure 1.3 Supramolecular synthons based on hydrogen bonds.

1.4 Polymorphism

The term polymorphism has been used since the early 1820's when Mitsherlich reported the existence of several distinct structures for arsenate/phosphate salts.[26] Though there seems to be a lot of debate about the ambiguity of the term with regard to dynamic isomers, tautomers and solvates,[27,28,29,30,31] Desiraju believes that the term polymorph should be restricted to single component crystals.[29]

Despite the continual debates about the subject McCrones's definition has been the most commonly accepted, that a polymorph is a solid crystalline phase of a given compound resulting from the possibility of at least two different arrangements of the molecules of that compound.[32] Thus a simple explanation that will suffice is that polymorphs are different crystal forms of the same chemical compound or substance. Buerger further defined polymorphs as crystal forms with different properties.[33]

Polymorphism has an impact in many spheres ranging from processing (drug compounding and stability) to biomedical (establishment of therapeutic dosage) to legal (potential loss of patent protection).

1.5 Host-guest complexes

Clathrates or inclusion compounds are a typical representative of a supermolecular species. They may be defined as compounds formed by inclusion of one kind of molecule, called guest molecules, into the cavities of the crystalline framework composed of molecules of another kind called host molecules (or into a cavity of one large host molecule). It is different to traditional chemical synthesis in that it is not chemical reactivity but favourable spatial complementarity of the guest and the host subsystems that plays an important role in formation of these compounds from components.[34]

The term clathrate was introduced by Powell in 1948,[7] for inclusion compound of β-quinone that possessed a crystalline framework with cavities shaped as isometric cages in which the guest molecules were located. There are two distinct topologies in which host-guest complexes have been found to occur. The first being molecular complexes where the host is a single molecule and is able to encapsulate the guest molecule or molecules as seen in Figure 1.4. The second is termed lattice inclusion where a number of host molecules

assemble into a framework which in turn is able to encapsulate the guest molecule or molecules.[35] (Figure 1.5)

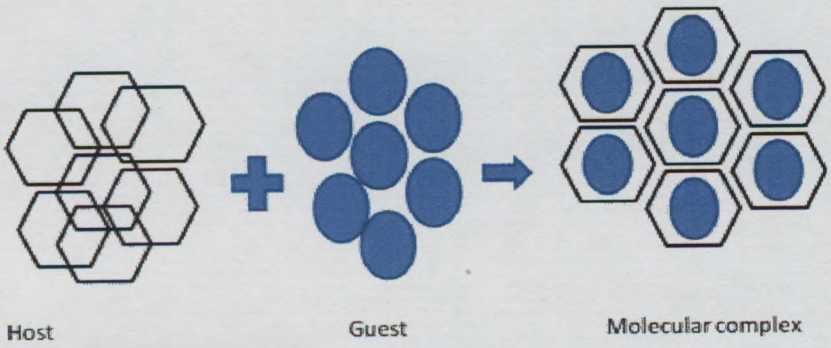

Figure 1.4 Formation of a molecular complex.

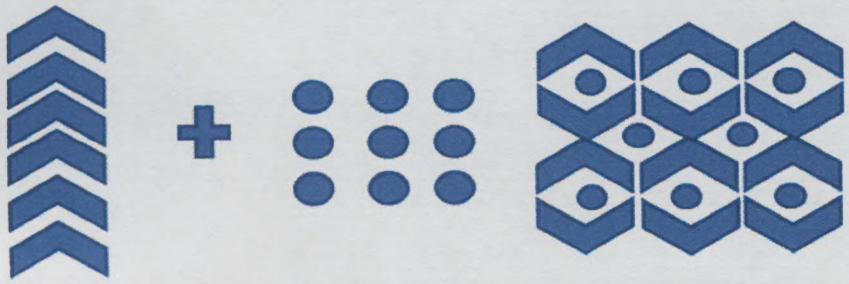

Figure 1.5 Formation of lattice inclusion

Host molecules belonging to the first topology are crown ethers, cyclodextrins, corands, cavitands and cryptands, all of which have a central cavity into which the guest is able to associate. Dianin's compound, urea and tri-o-thymotide are examples of hosts which partake in lattice inclusion, the host and guest molecules form aggregates, known as clathrates.

The compounds can be further subdivided into supramolecular host-guest compounds based on the forces between the host and guest. If the host-guest aggregate is held together by electrostatic forces including ion-dipole, dipole–dipole, hydrogen bonding, etc., the term "complex" is used. Species held together by less specific and often weaker non-directional interactions such as hydrophobic, van der Waals, or crystal close-packing effects, then the terms "cavitate" and "clathrate" are more appropriate. These interactions are described in detail in Table.1.2.

Table 1.2 Table listing the strength of the various intermolecular interactions

Interaction	Strength (kJ mol^{-1})
Ion-ion	200-300
Ion-dipole	50-200
Dipole- dipole	5-50
Hydrogen bonding	4-120
Cation- π	5-80
π-π	0-50
Van der Waals	< 5 but variable depending on surface area
Hydrophobic	Related to solvent-solvent interaction energy

1.6 Competition Experiments

Selectivity in supramolecular complexation is an important property in determining the molecular recognition ability of the host molecule that discriminates among different guest species. The ratio of the binding constant (the equilibrium constant for the binding process), K for the corresponding complexation is usually treated as a measure of selectivity. In some supramolecular systems the temperature plays a huge role in the selectivity. Therefore thermodynamic parameters: enthalpy (ΔH), entropy (ΔS) and Gibbs free energy (ΔG) are more suitable criteria for expressing molecular recognition abilities.[36,37,38]

The ratio of binding constants (K) as shown in Eq 1.1 of the corresponding complexation is usually treated as a measure of selectivity. The binding constant has been the basic evaluation criterion of the host-guest complexation process.

$$H + G \leftrightarrow H{\cdot}G$$

$$K = [H{\cdot}G]/[H][G] \qquad \text{Eq 1.1}$$

This gives a quantitative measure of the molecular recognition occurring between host and guest provided one defines the standard state as 1 mol dm^{-3}. Incidentally supramolecular selection between two species is the ratio of the binding constants for two different guests (Eq 1.2). The relationship between the binding constant of any given supramolecular complex is directly related to the change in free energy during the association process (Eq 1.3).

$$K = K_{GUEST1}/K_{GUEST2} \qquad \text{Eq 1.2}$$

$$\Delta G = -R\,T\,\ln K \qquad \text{Eq 1.3}$$

where R = gas constant and T = temperature in Kelvin.

The selectivity of a host compound for a guest molecule can be determined using a suitable analytical technique, such as gas chromatography (GC), nuclear magnetic resonance (NMR), thermogravimetry (TG) or differential scanning calorimetry (DSC). Powder X-ray diffraction (PXRD) and single crystal X-ray diffraction are used to analyze crystals obtained from competition experiments. The preferred method will then be to measure the selectivity constant of a given guest G_A versus a comparative guest G_B for a particular host. The method requires one to perform a series of competition experiments in which a given host is exposed to a number of guest mixtures of varying, but known mole fraction:

X_A	0	0.2	0.4	0.6	0.8	1.0
X_B	1.0	0.8	0.6	0.4	0.2	0

A fixed quantity of host is placed in each vial, allowed to dissolve in the guest mixture, and the host guest complex allowed to crystallize. The mole fraction of the guest Z_A is established and the selectivity coefficient of the host is then given as:

$$K_{G_A:G_B} = \frac{Z_A}{Z_B} \times \frac{X_B}{X_A}$$

Z_A, Z_B are the mole fractions of the guest in the crystal

X_A, X_B are the mole fractions of the guest in the mother liquor.

In addition to the binding constant the temperature dependence of selectivity is also important to gain insight into the origin of supramolecular functions.[38] Different kinds of selectivity profiles may arise between the guests G_A and G_B as shown in the Figure 1.6.

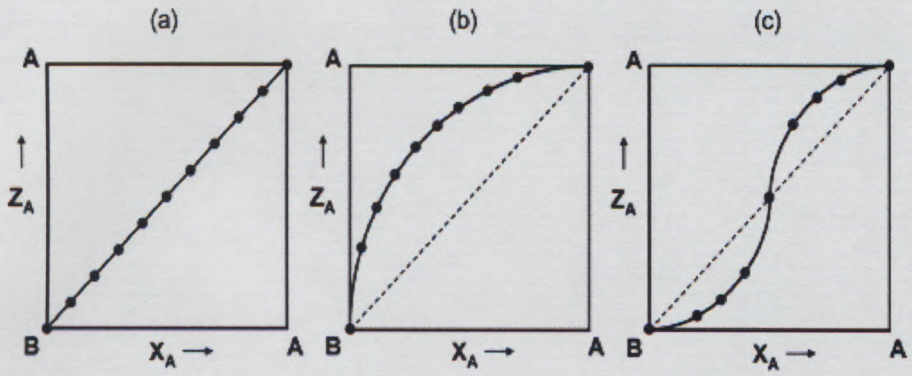

Figure 1.6 An illustration of selectivity profiles for competition experiments[39]

In graph a, the selectivity is zero or close to zero, $K_{G_A:G_B} \approx 1$

In graph b, G_A is preferred over G_B over the whole range.

In graph c, the selectivity is concentration dependent.

The method of analysis used for the competition experiment depends on the molecular properties of the two guests G_A and G_B. NMR methods may be employed if the host-guest system is suitable, soluble in deuterated solvents such as $CDCl_3$, and there are no overlaps between the signals of the host, and guests.

The competition experiments may also be carried out using mixtures of more than two guests. This is conducted by altering the mole fraction for each guest. For example a mole fraction could be considered as $(X_A + X_B + X_C) = 1$ maintained throughout all three experiments and where $(X_A + X_B + X_C + X_D) = 1$ throughout all four experiments. The results for a three-component competition experiment are plotted on a triangular graph where each apex represents one of the pure guests and a four point experiment is illustrated using a tetrahedral plot.

1.7 Thermal Stability of Inclusion compounds

The formation of an inclusion compound follows a general format:

$$H_{(s,\alpha)} + nG_{(s,l,g)} \leftrightarrow H{\cdot}nG_{(s,\beta)}$$

where H represents the host molecule in its nonporous α-phase (the apohost), G is the guest solvent which can be liquid or vapour and H·nG is the β-phase held together by non-covalent interactions.[39]

Thermal analysis is one of the most important techniques in the analysis of inclusion compounds. There are usually two types of thermal analysis techniques used in conjunction with each other. Thermogravimetry (TG) which measures the loss of guest from a crystal upon heating translates as a loss in the total mass of the crystal, thus giving accurate measurements of host:guest ratios. The other technique is differential scanning calorimetry (DSC), which measures enthalpy, melting and other changes as the guest is released. The onset temperature, T_{onset}, of the guest released gives an indication of the stability of a compound. An inclusion compound can decompose in various ways. Each of these decomposition methods will show a mass loss in the TG as well as an accompanying endotherm in the DSC (Figure 1.9).

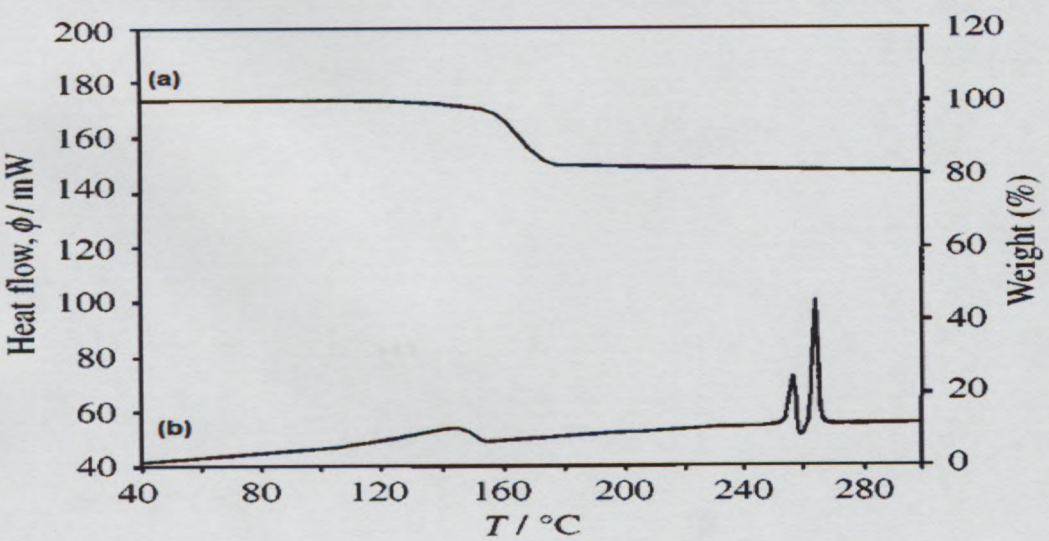

Figure 1.7 An example of thermal analysis curves a) TG single step mass loss b) corresponding DSC scan for the decomposition.[40]

The technique of thermal analysis has been extensively documented.[41,42,43,44] In addition other techniques, such as hotstage analysis, X-ray diffraction or IR spectroscopy, can be used to yield thermo-analytical information.

1.8 Kinetics

There are many types of solid-state reactions but our focus will be on reactions that involve a single solid reactant. A simple reaction is one which follows the reaction scheme below:

$$A\,(s) \rightarrow B\,(s) + C\,(g)$$

A being the clathrate, B is the host and C the released guest.

Solid-state desolvation is a reaction that obeys the above scheme because it involves the removal of solvent as vapour from a crystalline solvate below its melting point.[45] The rate of the reaction is dependent on the amount or fraction of the reactant raised at an integer power[46] according to

$$Rate \propto [A]^n$$

In solids, reactions often occur or are initiated at defects in the crystal lattice or at crystal surfaces, edges or corners. [47]

Experimentally solid state kinetics are measured isothermally or non-isothermally and can be evaluated by many mathematical methods. These generally fall into two categories: model fitting which determine the kinetic triplet (model, frequency factor and activation energy) and the model free (isoconversional) methods which generate the activation energy as a function of reaction progress. [48]

In our study kinetics of desolvation were measured using non-isothermal TG methods. The sample was collected from its mother liquor and crushed using filter paper to form a powder.

The weight loss was measured as a function of temperature change at different heating rates. The weight loss curves are then converted to a normalized form: the conversion fraction (α) vs temperature. The conversion fraction ranges from 0 to 1. Nonisothermally the conversion fraction (α) at any time is:

$$\alpha = \frac{m_0 - m_T}{m_0 - m_\infty} \qquad \text{Eq 1.4}$$

Where, m_0 is the initial sample weight, where, m_T is the sample weight at temperature, T, and m_∞ is the final sample weight.

The equation $\frac{dC}{dT} = \left(\frac{A}{\beta}\right) f(C) e^{-Ea/RT}$ Eq 1.5

Gives the rate of the reaction, C= degree of mass loss β= heating rate.

The equation can be re-written as:

$$\frac{d\log\beta}{d\frac{1}{T}} \cong \left(\frac{0.457}{R}\right) Ea \qquad \text{Eq 1. 6}$$

The resultant curves were analysed by plotting –log β vs 1/T where T = absolute temperature (K). The activation energy range can then be calculated.[49, 50]

1.9 Host Design

The aim of crystal engineering is to gain topological control over crystalline form and hence control over crucial physical phenomena such as melting point, optical properties, thermal stability, solubility, colour, porosity, conductivity, crystal habit and mechanical strength. Topological analyses simplifies complicated frameworks and provides a better understanding for targeting particular packing arrangements and their associated

properties.[51] When the molecules bond together into a crystal it is generally expected that they will pack as a regular component array as close to each other as possible in order to reach the lowest state of potential energy. This close packing is not always the case, it is dependent on the attractive forces that have strong directional requirements.[52] In general a detailed understanding of supramolecular chemistry of functional groups is a prerequisite for the design of novel compounds.[53] The development of a host compound is therefore of prime importance.

There are general requirements and guidelines for the design of host molecules. These include:[54]

Rigid basic frameworks - to maintain cavities

Bulky substituents - for low density packing

Strategically positioned functional groups - to provide suitable host-guest interactions

Degree of symmetry

The characteristic examples are scissor – type,[55] roof-shaped,[56] or small ring,[57] dicarboxylic host molecules, dog–bone or wheel-and-axle type, which are typical diol- host molecules. [58]

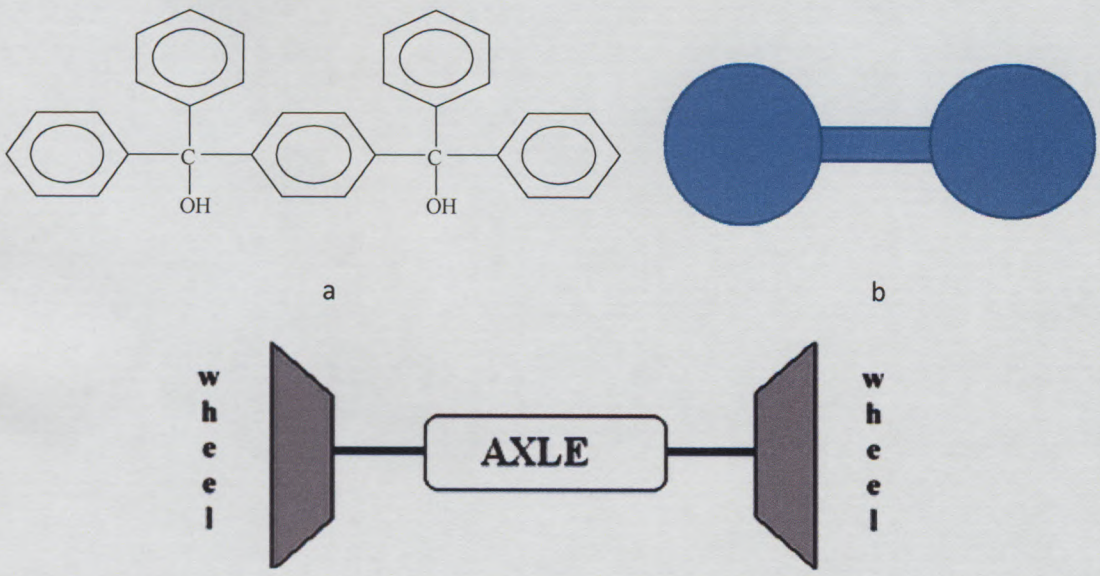

Figure 1.8 Diagram of : a host molecule b illustration of a dog-bone c wheel-and-axle[59] designed host molecule.

Molecules comprising two diphenylhydroxymethyl moieties attached to a rigid central unit are commonly known as "diol hosts".[60] The host compound used in this study can be classified as the dog-bone type, which can also be referred to as wheel-and-axle type. This host compound conforms to the requirements stated above. The host possesses hydroxyl functional groups which act as H- bond sites for the guest as well as encouraging host-host interactions thus achieving high selectivity.

1.10 Aims and Objectives of the Study

There has been a lot of focus on the design of suitable host compounds following Weber's specified guidelines. The dog-bone has been one of the most successful host designs which was derived from its precursor 1,1,6,6-tetraphenylhexa-2,4-diyne-1-6-diol. This host was first reported by Toda and Akagi.[61] Weber et al. have further explored these design concepts which has lead to the synthesis of host compounds possessing 9- hydroxyl-9-fluorenyl or analogous groups separated by linear spacers.[62]

The main aim of this study was to investigate the inclusion ability of a particular diol host compound. The selectivity of the host compound for a series of guests was also determined. An important facet of inclusion chemistry is that the interaction between the host and guest components should be selective. This concept dates back to 1894 as the lock-and-key method proposed by Emil Fischer.[6,63] The question then focuses on the choice of suitable host and guest compounds. We have chosen a host compound which is rigid, bulky and possesses hydroxyl moieties which can act as hydrogen bond donors. The guests selected contain hydrogen acceptor groups such as amine and amide moieties. These were liquid at room temperature with the exception of *N*-methylacetamide. The compound under investigation is 1,4-bis (diphenylhydroxymethyl)benzene **(H)**. The following guests were used; *N,N*-dimethylacetamide (DMA), *N,N*–dimethylformamide (DMF), *N*-methylacetamide (NMA), *N*-methylformamide (NMF), morpholine, 2-picoline, 3-picoline, 4-picoline and pyridine.

The structures of these inclusion compounds were elucidated using single crystal X-ray diffraction. Thermal analysis was completed to characterize the resultant compounds. Hotstage microscopy analyses were conducted in correlation with DSC and TG analysis. Selectivity experiments were conducted between the host and selected guests. The resultant material was analysed using single crystal X-ray diffraction, powder X-ray diffraction and GC. The PXRD was used to confirm that a bulk powdered sample matched that of the corresponding crystal. This study is therefore geared towards the ultimate aim of supramolcular chemistry becoming the "science of informed matter"[64].

1.11 References

1. J. L. Atwood, J. E. D. Davies, D. D. MacNicol and F. Vögtle *Comprehensive Supramolecular Chemistry*, 1996, **Vol. 1-10** eds., Pergamon, Oxford
2. D. V. Soldatov I. S. Terekhova, *J of Struc.l Chem.*, 2005, **46,** S1-S8
3. R. H. Petrucci, General Chemistry: Principles and Modern Applications; **5**th Edition.; Macmillan Publishing Company: New York, 1989
4. H. Dodzuik, Introduction to Supramolecular Chemistry, Kluwer Academic, 2002
5. H. Davy, *Philos. Trans. R. Soc.* London, 1811, **101**, 1
6. E. Fisher, *Ber. Deutsch. Chem. Ges.*, 1894, **27**, 2985
7. H. J. Powell, *J. Chem. Soc.*, 1961, **73**, 5691
8. K. A. Toyoki Kunitake, Supramolecular Chemistry Fundamentals and Applications, Springer-Verlag, 2006
9. D. J. Cram and J. M. Cram, *Science*, 1974, **183**, 803
10. M. Lehn, *Pure Appl. Chem.*, 1978, **50**, 85
11. F. Vögtle, Supramolecular Chemistry, John Wiley & Sons, Chichester, 1991, Chapter 5
12. J. L. Prins, D. N Reinhoudt, P. Timmerman, *Angew Chem,* 2001, **40,** 2382
13. D. Braga, F. Grepioni, *Acc. Chem.* 2000, **33**, 601
14. D. B. Smithrud, E. M. Sanford, I. Chao, S. B. Ferguson, D. R. Carcanague, J. D, Evanseck, K.N Houk, and F. Diederich, *Pure Appl Chem.*, 1990, **62**, 2227
15. J. W. Steed, J. L. Atwood, Supramolecular Chemistry, John Wiley & Sons, Chichester, 2000
16. G. A. Jeffery , *Oxford University Press*, Oxford, UK, 1997
17. A. D. Burrows, Concepts in Crystal Engineering: J. W. Steed in Encyclopedia of Sup. Chem. **Vol 1**, eds. J. L. Atwood and J. W. Steed, Marcel Dekker, Inc., New York, 2004, 319
18. G. R. Desiraju, *Angew. Chem., Int. Ed. Engl.*,2007, Vol **46** Issue 44, 8342
19. G. M. J Schmidt, *Pure App. Chem.*, 1971, **27**, 64
20. G. R. Desiraju, *Elsevier,* 1989, Ch **5**
21. J. D. Dunitz, *Pure Appl. Chem.*, 1991, **63**, 177
22. C. B. Aakeröy and K. R Seddon, *Chem. Soc. Rev.*, 1993, **22**, 397

23. R. E. Meléndez, A. D. *Hamilton* Topics. in Current Chemistry. Chem., 1998, **198**, 97

24. M. J. Zaworotko, *Chem. Comm.*, 2001, **1**, 1

25. G. R. Desiraju, *Angew. Chem., Int. Ed. Engl.*, 1995, **34 (21),** 2311

26. E. Mitscherlich. *Abhl Akad,* Berlin, 1822, **23**, 43

27. M. R. Huaser, L Zhakarov, K. M. Doxsee T. Li *Cryst. Growth Des.,* 2008, **8,** 4428

28. G. R. Desiraju, *Cryst. Growth Des.* , 2008, **8(1)**, 3

29. G. R. Desiraju, *Cryst. Growth Des.*, 2004, **4(6)**, 1089

30. J. Bernstein, *Cryst Growth Des.*, 2005, ***5*** **(5),** 1661

31. K. R. Seddon, *Cryst. Growth Des.*, 2004, ***4*** **(6),** 1087

32. W. C. McCrone. In Physics and Chemistry of the Organic Solid State; D. Fox; Labes, M. M., Weissberger, Eds, Wiley Interscience; New York, 1965, **Vol 2**, pp 725

33. M. J. Buerger, M. C. Bloom, *Kristallogr*, 1937, **A96,** 182

34. Y. A. Dyadin, I. S Terekhova; J. W. Steed in Encyclopedia of Sup. Chem. **Vol 1**, eds. J. L. Atwood and J. W. Steed, Marcel Dekker, Inc., New York, 2004, 319

35. E. Weber, *J. Incl Phenom*, 1983, **1,** 79

36. C. A. Shalley, Analytical methods in supramolecular chemistry , Wiley-VCH verlag GmBH & Co, 2007

37. P. Franz Shmidtchen; Selectivity: Thermodynamic and Kinetic, J. W. Steed in Encyclopedia of Sup. Chem. **Vol 1**, eds. J. L. Atwood and J. W. Steed, M. Dekker, Inc., New York, 2004, 319-325 K. A Connors, *John Wiley & Sons*, Ltd Chichester, UK, 1987

38. K. A. Connors, John Wiley & Sons, Ltd Chichester, UK, 1987

39. L. R. Nassimbeni, *Acc. Chem. Res* 2003, **36**, 631-

40. S. Apel, M. Czugler, V. J. Griffith, L. R. Nassimbeni and E. Weber *J. Chem. Soc., Perkin Trans.* ***2****, 1997*

41. P. J. Haines, Thermal methods of analysis-technique application, Chapman and Hall, London, 1995

42. M. E. Brown, Introduction to Thermal analysis- Techniques and Applications, Chapman and Hall, London,1998

43. K. J. Laidler, Chemical Kinetics, McGraw-Hill, New York, 1965

44. M. R. Caira and L.R Nassimbeni, Comprehensive Supramolecular Chemistry, **Vol 6**, eds. D. D MacNicol, F. Toda and R. Bishop, Pergamon, Oxford, 1996, Chapter **2**

45. A. K. Galwey, *Thermochim. Acta* 2000, **355,**181

46. J. I. Steinfeld; J. S. Francisco and W. L. Hase. *Chemical Kinetics and Dynamics*, second ed., Prentice Hall, Upper Saddle River, N.J., 1999

47. I. C. Paul and D. Y. Curtin, *Acc. Chem. Res.* 1973, **6:** 217

48. K. J. Laidler, *J. Chem. Educ.* 1984, **61:** 494

49. J. H. Flynn, L. A. Wall, *J. Polym Sci, Part B: Poly. Lett.*, 1996, **4**, 323

50. T. Ozawa, *Bull. Chem. Soc.*, 1965, **38,** 1881

51. K. Biradha, C. Y. Su, and J. J. Vittal, *Cryst. Growth Des.*,2011, **11**, 875

52. I. Y. H. Chan, V. T. Nguyen, R. Bishop, D. C. Craig, and Marcia L. Scudder, *Cryst. Growth Des.,2010,* **10,** 4582

53. T. R. Shattock, K. K. Arora, P. Vishweshwar, and M. J. Zaworotko, *Cryst. Growth Des.,* 2008, **8,** No 12, 4533

54. E. Weber, Inclusion compounds, Vol.4 eds. J. L. Atwood, J. E. D. Davies and D. D. MacNicol, Oxford University Press, 1991,188

55. E. Weber, I. Csöregh, B. Stenslan and M. Czulger, *Org chem. Soc,* 1984, **106**, 3297

56. E. Weber, J. *Mol. Graphics*, 1989, **7**, 12

57. E. Weber, M. Hecker, I. Csöregh, and M. Czugler, *J. Am Chem. Soc.*, 1989, **111**,7866

58. E. Weber, K. Skobridis, A. Wierig, L. R. Nassimbeni and L. Johnson, *J. Chem. Soc Perkin Trans.* 2 , 1992, 2123

59. F. Toda and K. Akagi, *Tetrahedron Lett.*, 1968, **9**, 3695.

60. C. B. Aakeröy, N. R. Champness and C. Janiak, *CrystEngComm*, 2010, **12**, 22

61. G. Paraskevopoulos, V. Theodorou, W. Seichter, E. Weber, *Cryst. Growth Des.,* 2011, **11**, 5275

62. E. Weber, S. Nitche, A. Wierig and I. Csöregh, *Eur. J. Org. Chem.,* 2002, 856

63. J.-P. Behr, The Lock and Key Principle, Perspectives in Supramolecular Chemistry, Wiley, Chichester, 1994, **vol. 1**.

64. M. C. T. Fyfe and J. F. Stoddart, *J. Am Chem. Soc 1997*, **30(10)**

2. CHAPTER 2 - Experimental

2.1 Host Compounds

The compound 1,4-bis(diphenylhydroxymethyl)benzene (Figure 2.1) employed in this study was synthesised by E Weber (Technische Universitat Bergakademie in Freiberg, Germany).[1] A Cambridge Structural Database (CSD version 5.30)[2] search has revealed that no research has been conducted on this host compound.

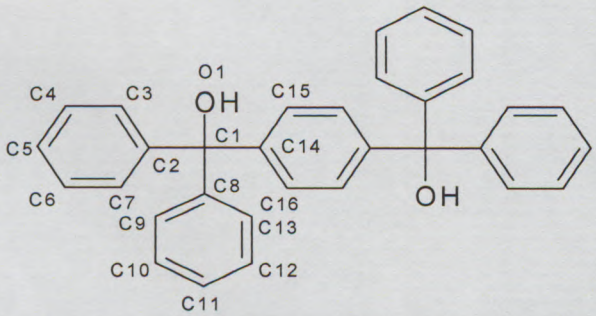

1,4-bis(diphenylhydroxymethyl)benzene (H)

Figure 2.1 Schematic representation of 1, 4-bis (diphenylhydroxymethyl) benzene

2.2 Guests

The guest compounds were purchased from Sigma Aldrich, Merck, Uni-lab and BDH Chemicals. The guests are of more than 99% chemical purity. The amide guests used have similar molecular and structural arrangements. The picoline isomers differ by the position of the methyl group and were studied comparatively with pyridine and morpholine. The physical properties of the guests are listed in Table 2. 1 below.

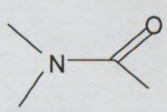

N,N-dimethylacetamide
DMA

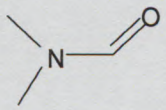

N,N-dimethylformamide
DMF

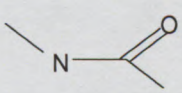

N-methylacetamide
NMA

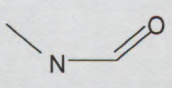

N-methylformamide
NMF

Figure 2.2 Diagrammatic representations of amide guests.

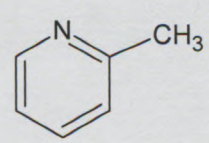

2-Picoline

2PIC

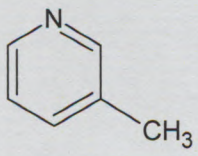

3-Picoline

3PIC

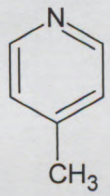

4-Picoline

4PIC

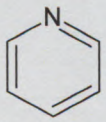

Pyridine

PYR

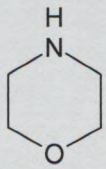

Morpholine

MORPH

Figure 2.3 Diagrammatic representations of picolines, pyridine and morpholine guests.

Table 2.1 Physical properties of guest compunds[3]

Guest compounds	Abbreviation	Molecular formula	Molar mass ($gmol^{-1}$)	Boiling point (K)	Melting point (K)
N,N-Dimethylacetamide	DMA	C_4H_9NO	87.12	437.7-439	253
N, N -Dimethylformamide	DMF	C_3H_7NO	73.09	426	212
N-Methylacetamide	NMA	C_3H_7NO	73.00	477-479	299-301
N-Methylformamide	NMF	C_2H_5NO	59.07	198-199	269
Morpholine	MORPH	C_4H_9NO	87.12	401	268.1
2-Picoline	2PIC	C_6H_7N	93.12	401-402	203
3-Picoline	3PIC	C_6H_7N	93.12	416-417	291
4-Picoline	4PIC	C_6H_7N	93.12	418	276.6
Pyridine	PYR	C_5H_5N	79.10	388	231

2.3 Crystal Growth

Inclusion compounds were prepared by dissolving the host in an excess of the liquid guest by gentle stirring on a hot plate. The solutions were covered with pierced parafilm and left to crystallise by slow evaporation at room temperature (caution should be taken for solution to remain at the bottom of the vial to avoid crystals forming at the side of the vials).

2.4 Thermal Analysis

Thermal analysis is a group of methods used to measure a characteristic of a sample while it is subjected to a controlled temperature programme in a specified atmosphere. Such a programme can compose both heating and cooling at certain rates of temperature change.[4]

The designs of all thermal analysis techniques are very similar. The sample of interest is placed in a furnace controlled by a computer (system) in order to perform the desired temperature programme. The atmosphere in the furnace is controlled by means of a suitable device. A simple set up has a constant flow of inert purge gas. A sensor detects the changes in a property that is to be recorded. The signal is then amplified, processed and finally fed into a data collection and processing computer.

The techniques used in this study are thermogravimetry analysis (TGA) and differential scanning calorimetry (DSC). These differ particularly in sensory mechanisms, corresponding sample size and heating systems.

TGA measures changes in sample mass with high accuracy, as a function of either temperature or time. It is used for the measurement of stoichiometry of inclusion compounds. The mass loss is a result of guest molecules being released during the volatilisation process. The theoretical stoichiometry of the inclusion compounds are calculated and used to establish confidence limits of measured results. The results are

measured as percentage weight loss. The host:guest ratio is then calculated. TGA is also used for measuring chemical dynamics such as kinetics.

In TGA the sample is removed from the mother liquor, crushed and dried using filter paper. It is then placed in a ceramic sample holder, which is held in a thermobalance. Sample masses of about 1 - 5mg were used.

DSC measures the difference in heat flow between the sample and reference in a controlled atmosphere as a function of temperature while the sample and reference are subjected to the same temperature programme. The difference in enthalpy is associated with different thermal events, guest release, phase transformations and melting points. DSC experiments are used to measure the onset temperatures and enthalpy changes associated with thermal events. The DSC and TGA results are interpreted and then correlated accordingly.

In DSC experiments the sample is taken out of the mother liquor, crushed and dried using filter paper. Sample masses in the ranges of 2 - 5mg were placed in aluminium pans, crimped and placed in the furnace. Calibrations were carried out using indium with known onset temperatures of 429.6 K.

Both TGA and DSC were conducted on a Perkin Elmer PC6 Series system using Pyris software. Temperature programmes from 303 K to 573 K at 10 K /min were used. Samples were purged with dry nitrogen gas flowing 20cm^3/min.

In addition hotstage microscopy analysis was performed. The hotstage is used for the visual characterization of all kinds of thermal transitions e.g. loss of guest, changes in shape and colour of crystal. The technique also allows phase transitions to be characterised and provides information on expansion and shrinkage behaviour. The information obtained from

hotstage microscopy is complimentary to data obtained from the DSC and TG. This assists with the interpretation of results.

The crystals were dried on filter paper, sample placed on sample holder and immersed in silicone oil. The hotstage model used is a Linkam T95-PE and samples were viewed using Meijie EMZ-8TR Microscope fitted with a Canon EOS kiss F camera.

2.5 Competition Experiments

Competition experiments were used to determine selectivity of a host compound for a series of guests in a given mixture of such guests. Crystals obtained were analysed using PXRD or GC. Two component competition experiments were prepared initially using guest mole fraction ratios of 1:1. If both guests were included further experiments were performed where the mole ratio of the guest components vary from 0 to 1. The solutions were left to crystallize by slow evaporation at room temperature. The crystals were filtered, dried and analysed by PXRD.

2.6 X-ray Powder Diffraction (PXRD)

This technique is used as a fingerprint to identify and compare compounds. This is done by careful comparison of the experimental PXRD patterns with the PXRD traces calculated from refined crystallographic data. The ideal pattern is generated using cell parameters, space group symmetry, atomic coordinates and thermal parameters from refined coordinates derived from single structure analysis as input. The three dimensional reciprocal spaces studied in single X-ray diffraction can be equally projected into a single dimensional X-ray powdered diffraction (PXRD). In PXRD the angle between the beam angle and the ring is called the scattering angle and in crystallography is denoted as 2θ. Results are depicted in a diffractogram in which the diffracted intensity I is shown as a function of the scattering angle 2θ.

Crystals were crushed and placed on Mylar film. The intensities were measured using a Huber imaging plate D83253, a Guiner camera 670, a Huber MC 9300 power supply unit and a Philips PW11200/00 X-ray generator and high temperature controller HTC 9634 unit was

used with capillary rotation device 670.2. The generator was kept constant at 20 mA and 40 kV while the sample is bombarded with CuK_α radiation (λ=1.5418Å). A 2θ range of 4 to 100 with a step size of 0.005 was used.

Lazy Pulverix [5] was used to generate idealised X-ray powder traces from single crystal data.

2.7 Gas Chromatography

Evaluations for isomer composition were analyzed by gas chromatography (GC). The samples were prepared by growing crystals from host dissolved in 1:1 guest mixtures. These crystals were then dissolved in chloroform, and the solution was filtered using microfilters. The pure 1:1 guest solvent mixtures were extracted in chloroform, calibrated and compared against data obtained from the samples analyzed.

Analyses were performed using an Agilent 7890 GC equipped with a flame ionization detector. The isomers were well separated using a Varian CP wax capillary column, 25 m x 320 μm x 0 μm ID, Detector gas flow rates were Hydrogen, 32 ml/min, Air 380 ml/min, Nitrogen 28 ml/min (Make up). Nitrogen 1.092 ml/min (Carrier), Temperature programming was linear at 10 ^{0}C/min, initial temperature 40 ^{0}C (3 min), final temperature 180 ^{0}C held for 11 min, the total run time was approximately 28min.The injector and detector temperatures were set at 220 ^{0}C and 250 ^{0}C respectively. The split ratio was set at 100:1. A sample volume of 1 μl was injected. The components were identified by their elution times

2.8 Crystal Structure Analysis

For the elucidation of crystal structures, suitable quality single crystals of sufficient stability based on their ability to extinguish plane polarised light uniformly were analysed and subjected to single crystal X-ray diffraction. Data collection is carried out mostly at low temperatures.

Crystals were mounted onto the top of glass fibres with paratone N oil. The glass resided on a goniometer head. For low temperature data collections, crystals were cooled and maintained at 173 K by a Cryostream cooler with a constant stream of nitrogen gas flowing at 20 cm^3/min.

Crystal intensity data were collected on a Nonius Kappa CCD (charge coupled device) single crystal X-ray diffractometer, using graphite monochromated MoKα radiation (t = 0.7107 Å) generated by a Nonius FR590 generator at 50 kV and 30 mA.

Data collection was evaluated using COLLECT[6] software. Accurate unit cell parameters were refined on all data.

SHELXS[7] was used to solve the structures by direct methods. Refinements were completed with SHELXL [7] by employing full matrix least squares. X-Seed[8] was employed as a graphical interface to SHELX for the solution and refinement of the structures.

SHELX-97 uses full matrix least squares refinement against F^2 for unique reflections. The residual index, R, shows the agreement between the observed structure factors (F_o) and the calculated structure factors (F_c) The residual index R, is the agreement between the observed and calculated structure factors based on F, while the residual index, R_2 is the agreement based on F^2. Both are quoted for comparison.

$$R_1 = \frac{\sum \left| |F_0| - |F_c| \right|}{\sum |F_0|}$$

$$wR_2 = \sqrt{\frac{\sum w\left(F_0^2 - F_c^2\right)^2}{\sum w\left(F_o^2\right)}}$$

where w is the weighing scheme and was refined for each structure.

$$w = \frac{1}{\sigma^2 F_0^2 + (aP)^2 + bP}$$

where $P = \frac{\max(0, F_0^2) + 2F_c^2}{3}$ and a, and b were refined for each structure.

The Goodness of Fit is based on F^2

$$S = \left(\frac{\sum w\left(F_0^2 - F_c^2\right)^2}{n - p} \right)^{\frac{1}{2}}$$

where n is the number of reflections and p is the total number of parameters refined.

The program examines the analysis of variance and prints a warning that an extinction coefficient, x, should be refined if S is significantly higher than unity. When necessary an extinction parameter x was refined by least-squares, where F_c is multiplied by:

$$\left[\frac{\left(1+0.001*x*F_c^2*3x\right)}{\sin(2\theta)}\right]^{-1/4}$$

The expression is empirical and covering both primary and secondary extinction.

2.9 Computing Packages

Layer [9] - Intensity data is displayed as simulated precession photographs of the reciprocal lattice levels and allows for the investigation of the systematic absences which occur.

Lazy Pulverix [5]- was used to generate idealised X-ray powder traces from single crystal data.

Section [10] - Gives a graphical interpretation of the packing in the structure, by effectively cutting slices through the unit cell. The guest molecules can be removed and the host shown with its van der Waals radii so that channels or cavities can be investigated

PovRay [11]- Renders graphics for structures.

ConQuest[2]- Cambridge Structural Database (CSD) provides informative and comparative structure details.

WingGX[12]- WinGX is a MS-Windows system of programs for solving, refining and analyzing single crystal X-ray or neutron diffraction data.

Platon[12]- Programme used in conjunction to WingX as an interface for the bond length analysis.

2.10 References

1. E. Weber, K. Skobridis, A Wierig, L. R. Nassembeni, L. Johnson, J. *Chem.*

Soc, Perkin Trans, 1999, **2**, 2123

2. ConQuest, a program for the search of CSD structural details, version **5.3**

3. The Merck Index, Encyclopedia of Chemical and Drugs, 1976, **9**th edition

4. M. E. Brown. 'Introduction to thermal analysis' Chapman and Hall, London 1988

5. K. Yvon, W. Jeistchko and E. Parthé, *J. Appl. Cryst.*, 1977, **10**, 73

6. COLLECT, Data collection software, Nonius, Delft, The Netherlands, 1999

7. G. M. Sheldrick, SHELX-97, Program for crystal structure determination, University of Göttingen, Germany, 1997

8. L. J. Barbour, *J. Supramol. Chem.*, 2001, **1**, 189; J. L. Atwood, L. J. Barbour, *Cryst. Growth. Des.*, 2003, **3**, 3

9. L. J. Barbour, LAYER, A computer program for graphic display of intensity data as simulated precession photographs, *J. Appl. Cryst.*, 1999, **32**, 351

10. L. J. Barbour, SECTION, A computer programme for graphic display of cross sections through a unit cell, *J. Appl. Cryst.*, 1999, **32**,353

12. Pov-Ray for Windows, Version **3.61**, watcomwin32, The persistence of Vision Development Team, 1999-2003

13. L. J. Farrugia. *J. Appl. Cryst.*, 1999, **32**, 837

3. CHAPTER 3- Results and discussions

We have successfully prepared inclusion compounds with *N, N*- dimethylformamide (DMF) *N, N*-dimethylacetamide (DMA), *N*-methylformamide (NMF) and *N*-methylacetamide (NMA), water 2-picoline, 3-picoline, 4-picoline, pyridine and morpholine. The abbreviations used in this text for the inclusion compounds obtained are:

H·2DMF	1, 4-bis (diphenylhydroxymethyl) benzene dimethylformamide clathrate
H·2DMA(a)	1, 4-bis (diphenylhydroxymethyl) benzene dimethylacetamide clathrate
H·2DMA(b)	1, 4-bis (diphenylhydroxymethyl) benzene dimethylacetamide clathrate polymorph
H·NMF	1, 4-bis (diphenylhydroxymethyl) benzene N-methylformamide clathrate
H·2NMA	1, 4-bis (diphenylhydroxymethyl) benzene N-methylacetamide clathrate
$H{\cdot}2H_2O$	1, 4-bis (diphenylhydroxymethyl) benzene dihydrate
H·2PIC	1,4 bis (diphenylhydroxymethyl)benzene-2-methlylpyridine
H·2(3PIC)	1, 4-bis (diphenylhydroxymethyl) benzene-3-methylpyridine clathrate
H·2(4PIC)	1, 4-bis (diphenylhydroxymethyl) benzene-4-methylpyridine clathrate
H·2PYR	1,4 bis (diphenylhydroxymethyl) benzene pyridine
H·2MORPH	1,4 bis (diphenylhydroxymethyl) benzne morpholine

3.1 Thermal Analysis

3.1.1 Thermal analysis of host

A DSC (Figure 3.1) analysis of the host compound was performed to establish its decomposition profile. The DSC shows three sharp peaks, A, B and C which indicate a progressive phase change at A and B and the complete host melts at C. The T_{onset} values for each of the endotherms are shown in Table 3.1.

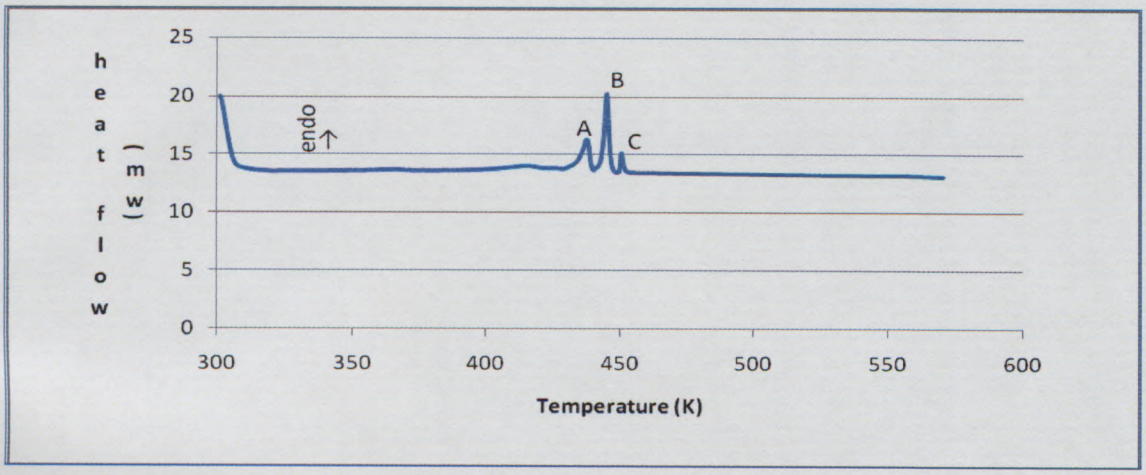

Figure 3.1 DSC curve for host compound **H**.

Table 3.1 Thermal analysis results of the host

DSC	
Endotherm	T_{onset} (K)
A	433.2
B	443.2
C	450.6

3.1.2 Thermal analysis of H·2DMA

The DSC and TG traces of **H·2DMA** are shown in Figure 3.2. The TG shows two distinct mass losses in the temperature range of approximately 270 - 500 K. The individual mass loss percentages were found to be 9.0 and 19.1% respectively. The total mass loss of 28.1 % represents the release of the two guest molecules. The DSC shows a single sharp endotherm (A) at 371 K which can be attributed to the loss of guest and concomitant dissolution of the host (B). Table 3.2 show results obtained from DSC and TG analysis.

Table 3.2 Thermal analysis results of **H·2DMA**

	Endotherm	T_{onset} (K)	Normal bp of DMA(K)
DSC	A	371.3	438-439
	B	422.2	
	Exp. % weight loss	Calc. % weight loss	H:G ratio
TG	28.1	28.3	1:2

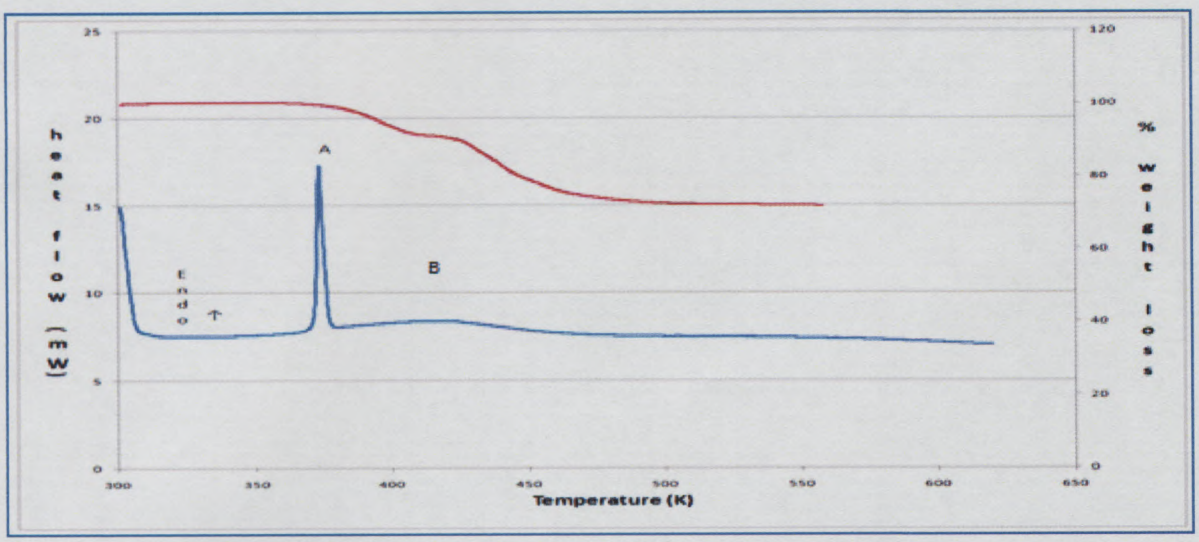

Figure 3.2 DSC and TG traces of **H·2DMA**.

3.1.3 Thermal analysis of H·2DMF

DSC and TG curves of **H·2DMF** are shown in Figure 3.3. The TG gives a single mass loss step which represents the loss of two guest molecules. The DSC shows three endotherms. The two endotherms A and B correspond to the loss of the two guest molecules at temperatures of 401.1 and 426 K respectively, and C can be attributed to the melt of the host at 449.7 K. The DSC and TG results are listed in Table 3.3.

Table 3.3 Thermal analysis results of **H·2DMF**

	Endotherm	T_{onset} (°C)	Normal bp of DMF (K)
DSC	A	401.1	
	B	426.0	426
	C	449.7	
	Exp. % weight loss	Calc.% weight loss	H:G ratio
TG	24.7	24.8	1:2

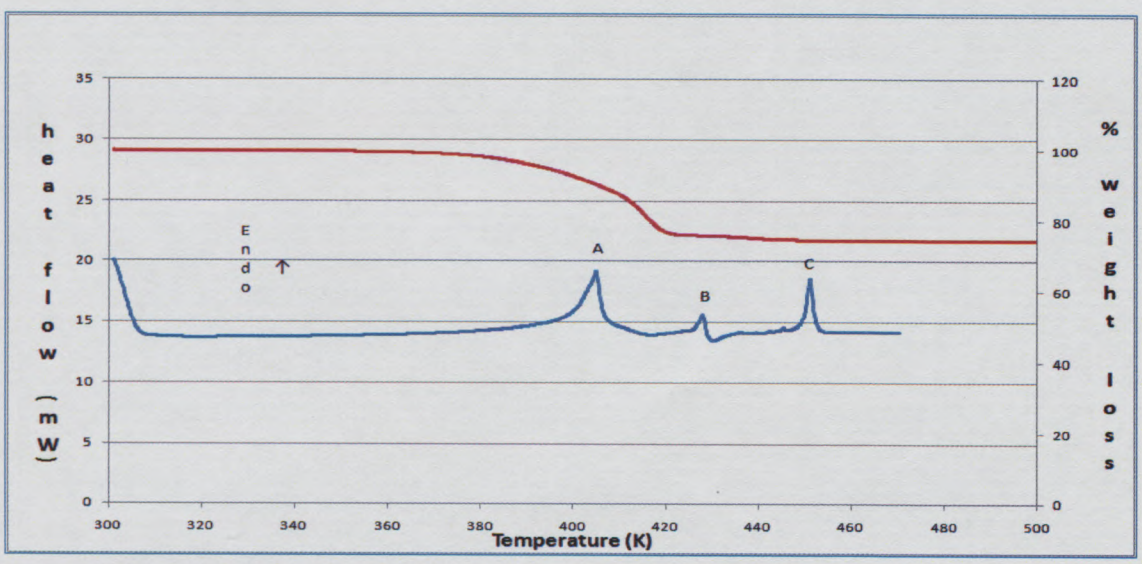

Figure 3.3 DSC and TG traces of **H·2DMF**.

3.1.4 Thermal analysis of H·2NMA

TG and DSC traces for **H·2NMA** are illustrated in Figure 3.4. The TG trace shows a two-step mass loss. The decomposition is non-stoichiometric with the first mass loss of 19.7 % followed by a 5 % loss. Overall, the percentage mass loss (24.7 %) corresponds to the loss of two guest molecules. The DSC curve shows one endotherm, A, due to the loss of the guest and B dissolution of the host. The onset temperatures and total percentage mass losses are listed in Table 3.4.

Table 3.4 Thermal analysis results of **H·2NMA**

	Endotherm	T_{onset}(K)	Normal bp of NMA (K)
DSC	A	401.6	
	B	420.0	479-481
	Exp. % weight loss	Calc. %weight loss	H:G ratio
TG	24.7	24.7	1:2

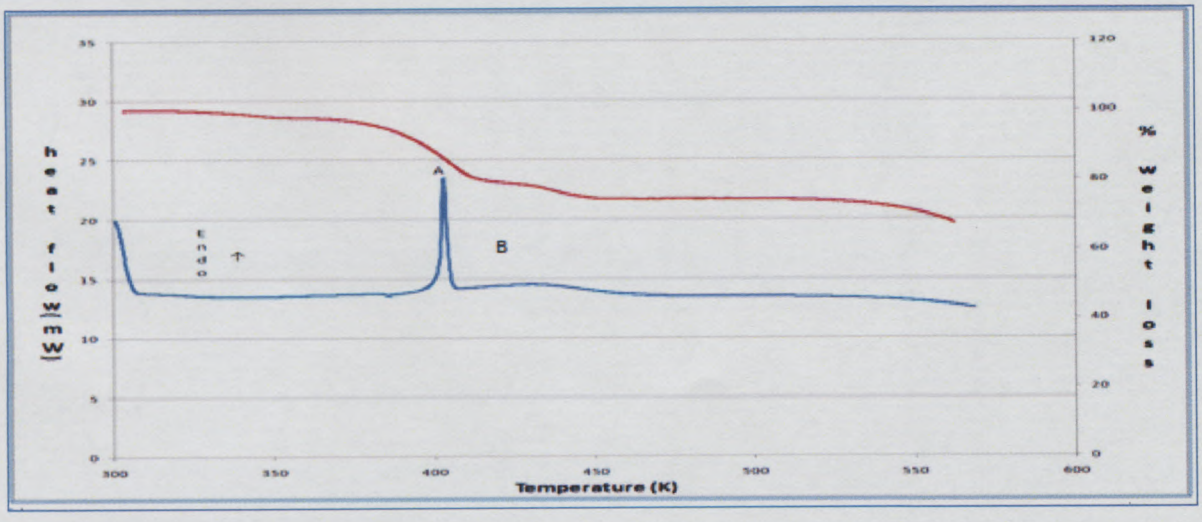

Figure 3.4 DSC and TG traces of **H·2NMA**.

3.1.5 Thermal analysis of H·NMF

The DSC and TG curves of **H·NMF** are shown in Figure 3.5. The TG trace appears as a diffuse two-step process. The curve is non-stoichiometric with the individual mass losses at 10.5 and 1.4 % respectively. The total mass loss of 11.9 % can be attributed to the release of one guest molecule. The DSC shows two peaks. A sharp endothermic peak, A, and a broad peak B, which can be attributed to the loss of guest and dissolution of the host. The results are shown in Table 3.5.

Table 3.5 Thermal analysis results of **H·NMF**

	Endothem	T_{onset} (K)	Normal bp of NMF (K)
	A	397.8	
DSC	B	411	471-472
	Exp. % weight loss	Calc. % weight loss	H:G ratio
TG	11.9	11.8	1:1

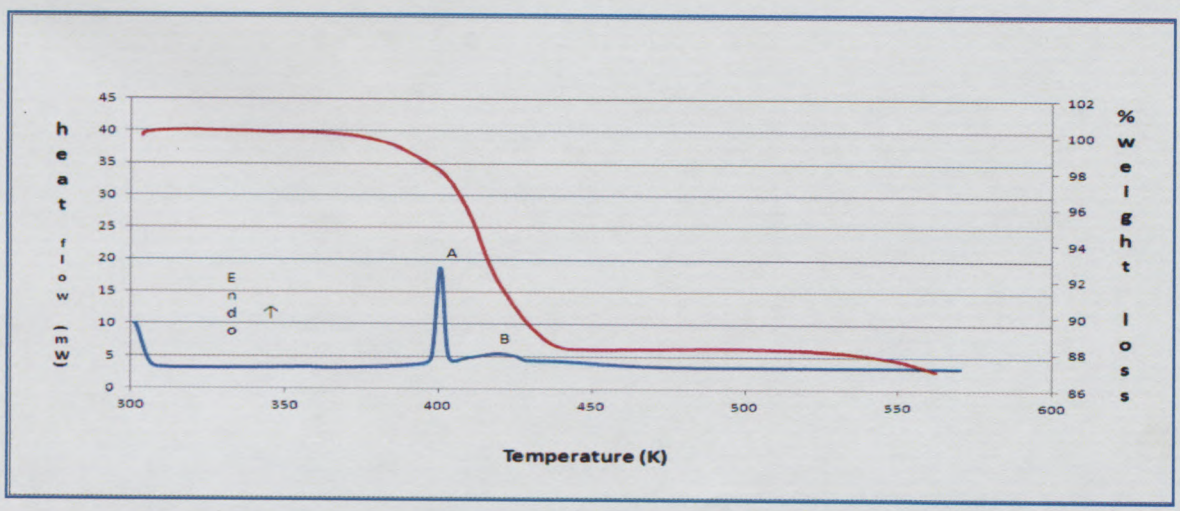

Figure 3.5 TG and DSC traces of **H·NMF**

3.1.6 Thermal analysis of H·2PIC

The DSC and TG of **H·2PIC** are shown in Figure 3.6. The TG curve indicates a non-stoichiometric two step process. The individual mass losses are 15.0 % and 2.9 % respectively. The total mass loss of 17.9 % represents the complete loss of one guest molecule. The DSC shows two endotherms. Endotherm A can be attributed to the loss of guest at 364K and endotherm B corresponds to the loss of the remaining guest and the host melts. The onset temperatures and % mass losses are given in Table 3.6.

Table 3.6 Thermal analysis results of **H·2PIC**

	Endotherm	T_{onset} (K)	Normal bp of 2PIC (K)
DSC	A	364.0	
	B	442.5	388
	Exp. % weight loss	Calc.% weight loss	H:G ratio
TG	17.9	17.4	1:1

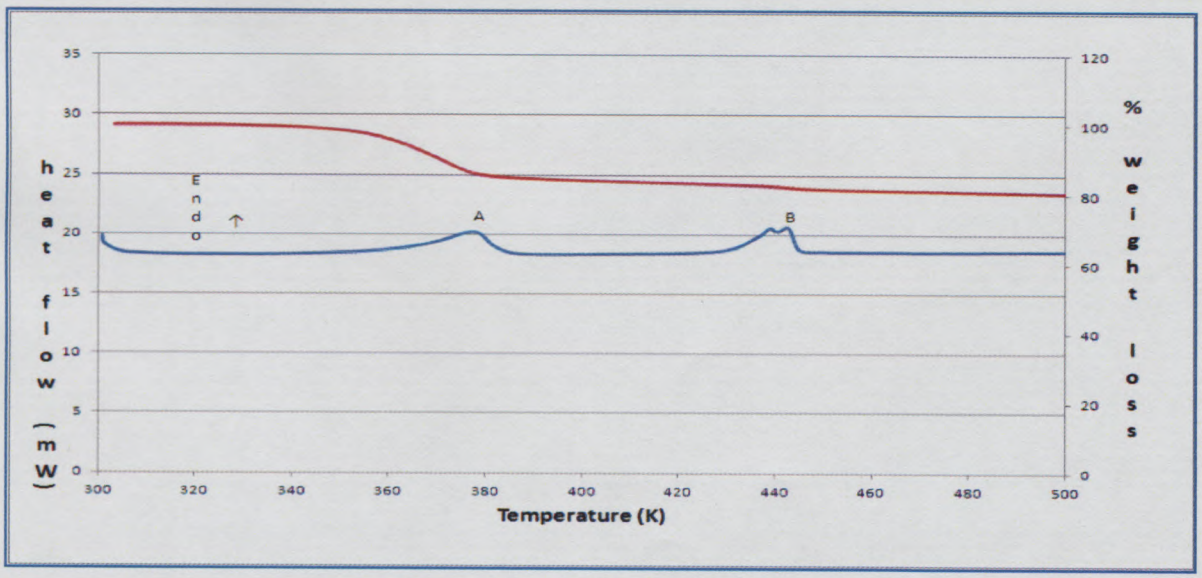

Figure 3.6 DSC and TG traces of **H·2PIC.**

3.1.7 Thermal analysis of H·2(3PIC)

DSC and TG curves of **H·2(3PIC)** are shown in Figure 3.7. The TG gives a two step mass loss curve. The individual percentage mass losses are 25.5 and 3.7% respectively. The total mass loss of 29.2 % corresponds to a H:G ratio of 1:2. The DSC shows three endotherms labeled A, B and C. The loss of guest occurs at 363.6 K and at 433K followed by the host melt at 449 K. The % mass loss results are listed in Table 3.7.

Table 3.7 Thermal analysis results of **H·2(3PIC)**

	Endotherm	T_{onset} (K)	Normal bp of 3PIC (K)
DSC	A	363.6	
	B	433.0	417
	C	449.0	
	Exp. % weight loss	Calc. % weight loss	H:G ratio
TG	29.2	29.6	1:2

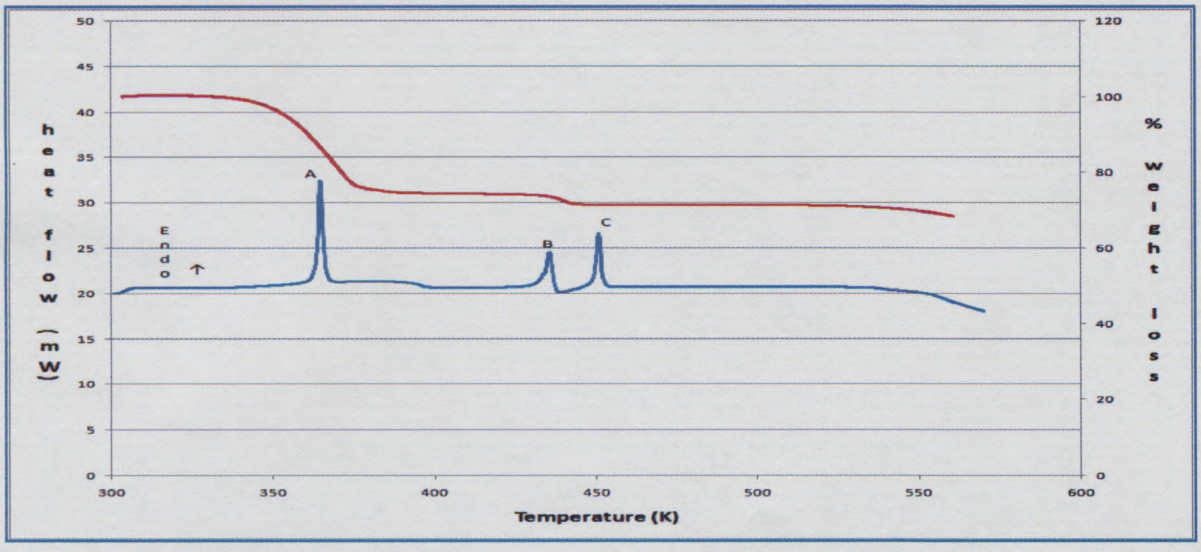

Figure 3.7 DSC and TG traces of **H·2(3PIC).**

3.1.8 Thermal analysis of H·2(4PIC)

The DSC and TG traces of **H·2(4PIC)** are shown in Figure 3.8. The TG curve shows a two step mass loss which is non-stoichiometric. The individual mass losses are 28.6 and 1.0 % with the total mass loss of 29.6 % representing a loss of two guest molecules. The DSC shows three peaks A, B and C. Endotherm A can be attributed to the loss of guest, B and C correspond to the host phase change at 430.4K and the host melt at 450.2K. The T_{onset} and % mass losses are given in Table 3.8.

Table 3.8 Thermal analysis results of **H·2(4PIC)**

	Endotherm	T_{onset} (K)	Normal bp of 4PIC (K)
DSC	A	387.4	
	B	430.4	418
	C	450.2	
	Exp. % weight loss	Calc.% weight loss	H:G ratio
TG	29.6	29.6	1:2

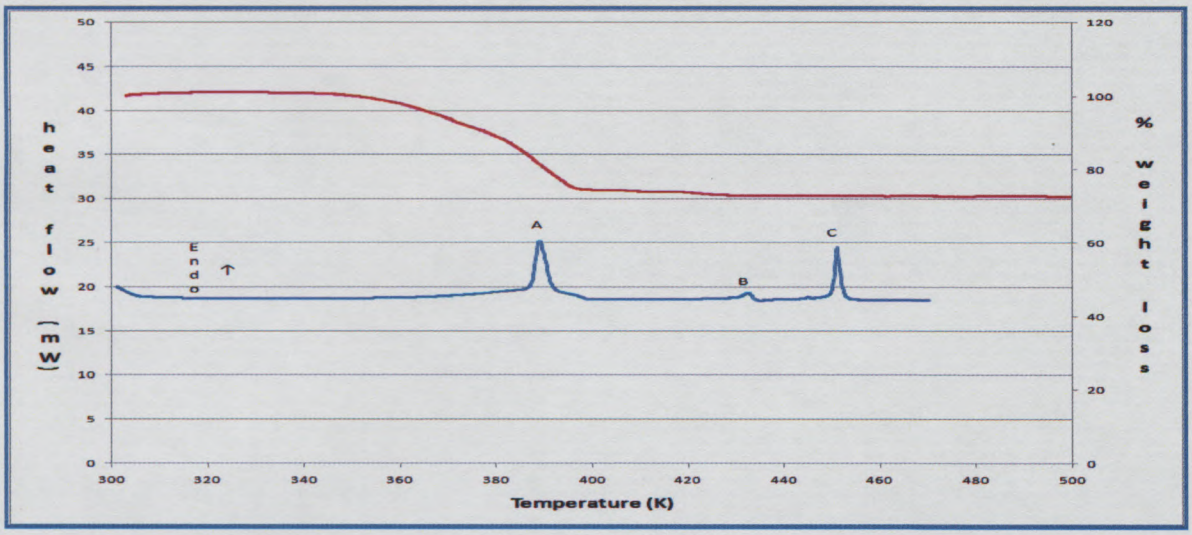

Figure 3.8 DSC and TG traces of **H·2(4PIC).**

3.1.9 Thermal analysis of H·2PYR

The DSC and TG traces of **H·2PYR** are shown in Figure 3.9. The TG trace shows a three step mass loss with individual mass losses of 14.9, 7.3 and 4.0 % respectively. The total mass loss of 26.2 % can be attributed to the loss of two guest molecules. The resultant H:G ratio is 1:2. The DSC shows three endotherms. The endotherm A is due to the loss of guest, endotherms B host phase change and C can be ascribed to the host melt. The onset temperatures and % mass losses are given in Table 3.9.

Table 3.9 Thermal analysis results of **H·2PYR**

	Endotherm	T_{onset} (K)	Normal bp of PYR (K)
DSC	A	392.2	
	B	431.8	388
	C	450.6	
	Exp. % weight loss	Calc. % weight loss	Ratio
TG	26.1	26.3	1:2

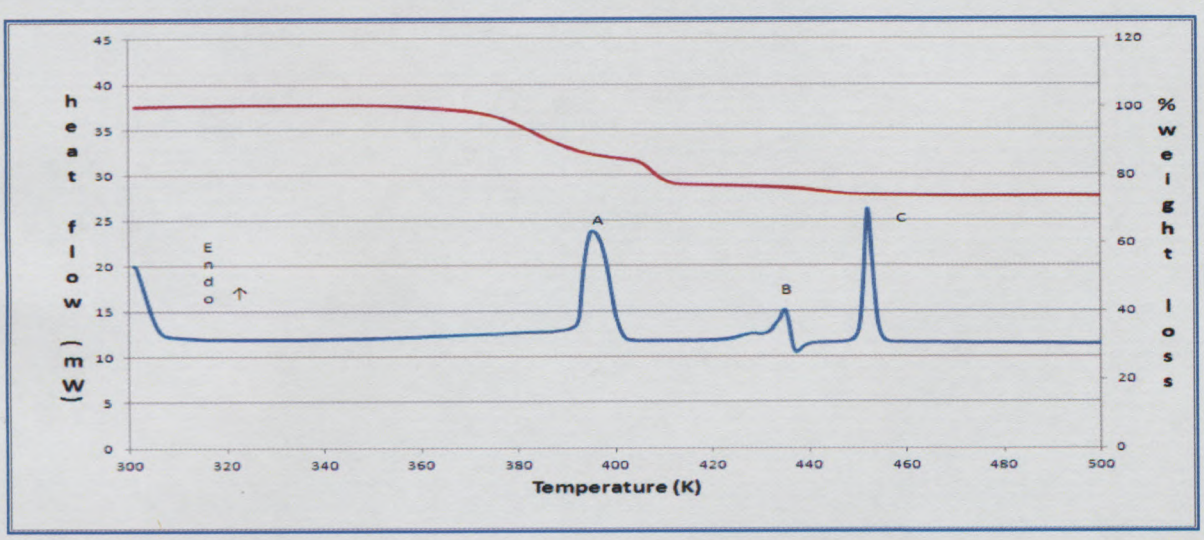

Figure 3.9 DSC and TG traces of **H·2PYR.**

3.1.10 Thermal analysis of H·2MORPH

The DSC and TG traces of **H·2MORPH** are shown in Figure. 3.10. The TG trace shows a three step mass loss. In the first step the mass loss is 22.6 % followed by mass losses of 2.2 % and 3.5 % respectively. The total mass loss (28.3 %) can be attributed to the loss of two guest molecules. The DSC shows four endotherms. Endotherm A is due to the loss of guest whereas endotherms B, C host phase change and D can be attributed to the host melt. The onset temperatures and percentage mass losses are given in Table 3.10.

Table 3.10 Thermal analysis results of **H·2MORPH**

	Endotherm	T_{onset} (K)	Normal bp of MORP (K)
DSC	A	387.8	
	B	436.4	402
	C	443.3	
	D (melt)	449.7	
	Exp. % weight loss	Calc. % weight loss	H:G ratio
TG	28.3	28.3	1:2

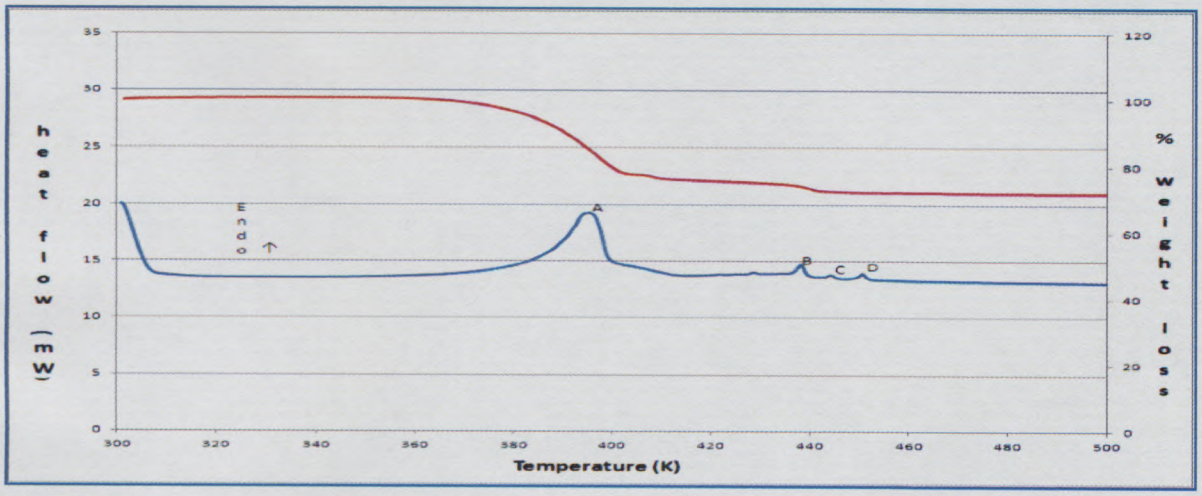

Figure 3.10 DSC and TG traces of **H·2MORPH**.

3.1.11 Summary of thermal analysis results

The thermal analysis results are summarised in Table 3.11. The TG results show that seven of the nine compounds gave H:G ratios of 1:2, **H·NMF** and **H·2PIC** gave H:G ratios of 1:1. The experimental % weight loss values for all the compounds closely correspond to that of the calculated % weight loss therefore there is good agreement in the results. The DSC results show that endotherms occur at temperatures below that of the normal boiling point (bp) of the guest solvent. The T_{on}/T_b values for **H·2DMA**, **H·2DMF**, **H·2NMA** and **H·NMF** were calculated and found to be 0.85, 0.94, 0.84, and 0.84 respectively. The T_{on}/T_b values for **H·2PIC**, **H·2(3PIC)**, **H·2(4PIC)**, **H·2MORP**, **H·2PYR** were calculated and found to be 0.94, 0.87, 0.93, 0.95 and 0.93 respectively.

Table 3.11 Summary of thermal analysis results.

	Host-H	H·2DMA	H·2DMF	H·2NMA	H·NMF	H·2PIC	H·2(3PIC)	H·2(4PIC)	H·2PYR	H·2MORP
DSC										
A	433.2	371.3	401.1	401.6	397.8	364.0	363.6	387.4	292.2	387.8
B	443.2	422.2	426.0	420.0	411	442.5	433	430.4	431.8	436.4
C	450.6	-	449.7	-	-	-	449	450.2	450.6	443.3
D melt	-								-	449.7
bp		**438-439**	**426**	**479-481**	**471-472**	**388**	**417**	**418**	**388**	**402**
TG										
H:G		1:2	1:2	1:2	1:1	1:1	1:2	1:2	1:2	1:2
%exp		27.7	24.7	24.6	11.9	17.9	29.2	28.6	26.1	28.3
% cal		**28.3**	**24.8**	**24.8**	**11.8**	**17.4**	**29.6**	**29.6**	**26.3**	**28.3**
T_{on}/T_b		0.85	0.94	0.84	0.84	0.94	0.87	0.93	0.93	0.95

3.2 Hot-stage Microscopy (HSM)

Crystals were dried using filter paper then analyzed under HSM, all the structures were analyzed with the exception of **H·2PIC** and **H·2(3PIC)** as the crystals for these could not be regrown, a sticky oily residue would form. The series of photographs showing the thermal events are given in figures listed below.

3.2.1 Hot-stage analysis of H·2DMA

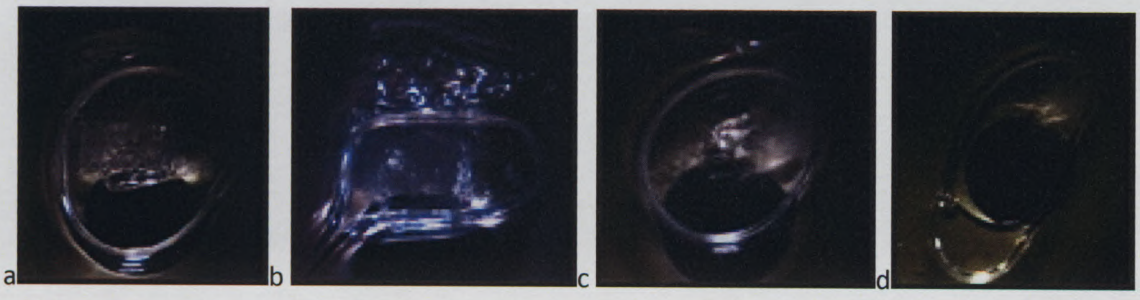

Figure 3.11 Crystals of **H·2DMA** during thermal decomposition a-initial stage the crystal at 303K b-bubbles formed and crystal becomes transparent indicating the guest release at 375.5K c- crystal clears and d- at 424K the host melts.

3.2.2 Hot-stage analysis of H·2DMF

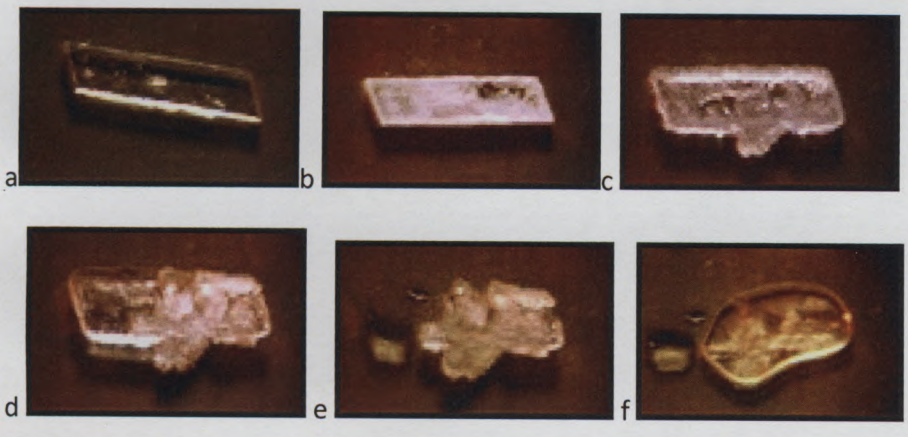

Figure 3.12 Crystals of **H·2DMF** during thermal decomposition a- initial stage the crystal at 303K b-the crystal changes to an opaque colour showing a change in morphology at 386K c and d- bubbles formed indicating the release of guest at 401K and 449.4K. e and f show the host in its amorphous form and melting of the host at 452K and 456.3K respectively.

3.2.3 Hot-stage analysis of H·2NMA

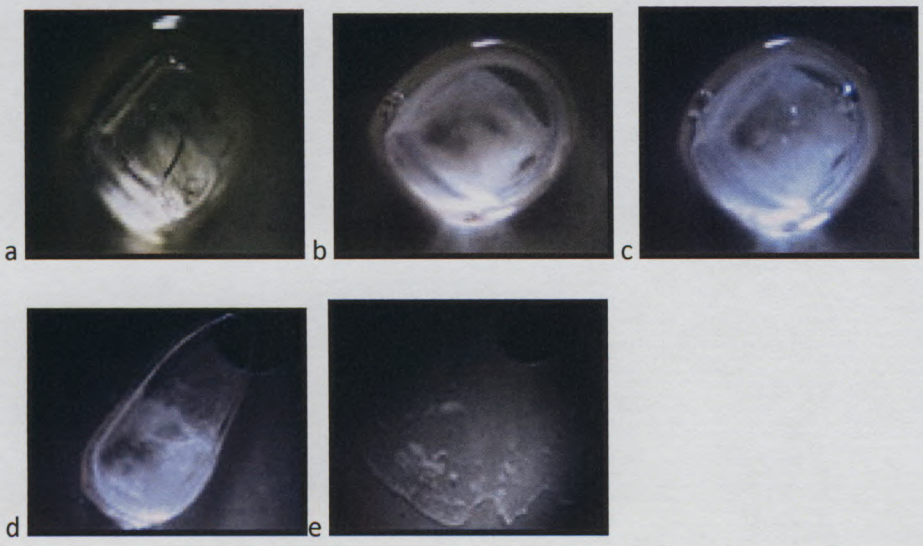

Figure 3.13 Crystals of **H·2NMA** during thermal decomposition a-crystal immersed in silicone oil at room temperature b- the crystal starts to change to an opaque colour and bubbles start to form c- further bubbling as guest is released at 401.9K d- host starts its melting process at 412K and e-host melts at 413K.

3.2.4 Hot-stage analysis of H·NMF

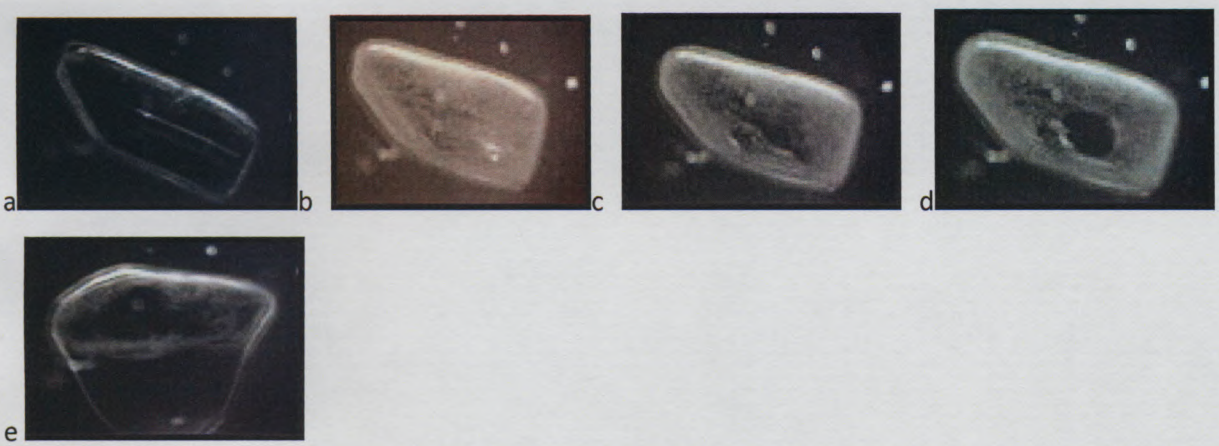

Figure 3.14 Crystals of **H·NMF** during thermal decomposition a- crystal at room temperature b- colour of crystal has fully changed to opaque this change can be attributed to the guest being released at 392.2K c- remaining guest is concurrently released d- host starts to melt at 412.5K e - host melt at 419K.

3.2.5 Hot-stage analysis of H·2(4PIC)

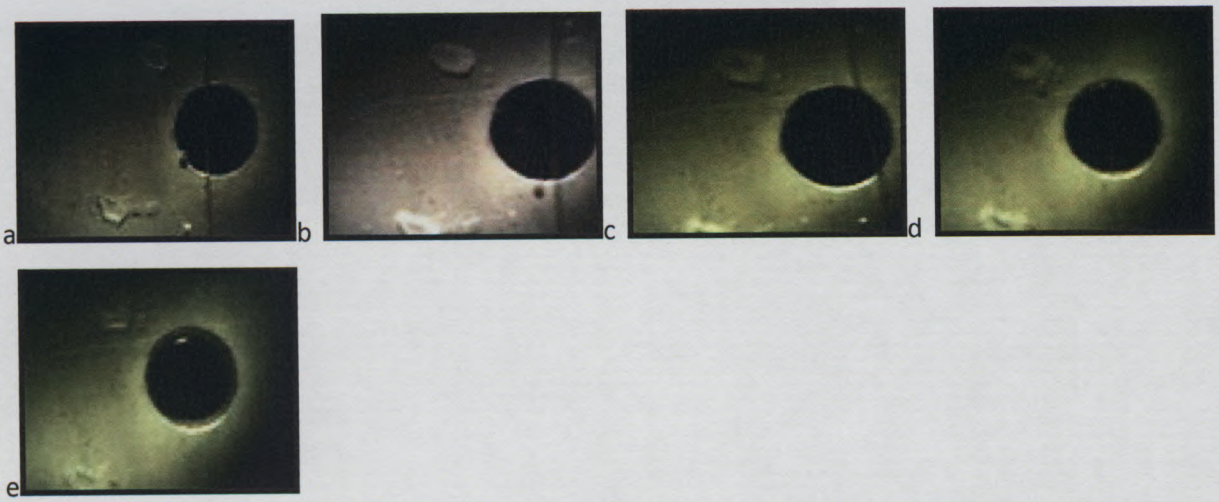

Figure 3.15 Crystals of **H·2(4PIC)** during thermal decomposition a-the crystals at room temperature b- the crystals change colour to opaque at 392K c- the guest is released at 416K d- the host starts to melt e-host melt at 450K.

3.2.6 Hot-stage analysis of H·2PYR

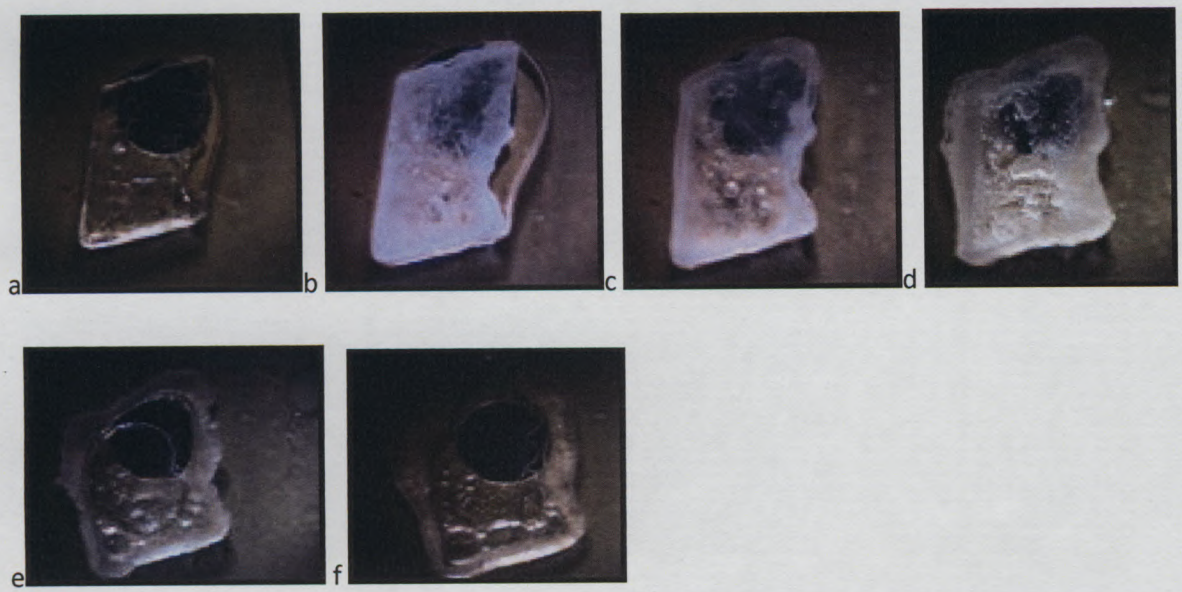

Figure 3.16 Crystals of **H·2PYR** during thermal decomposition a- at room temperature b- at 383.2K the host changes colour due to the initial stage of guest release c-bubbles form depicting guest release at 393 K d- continuation of guest release e- the host begins to disintegrate during the first stage of host melting at 450K f- the host melts at 455K.

3.2.7 Hot-stage analysis of H·2MORPH

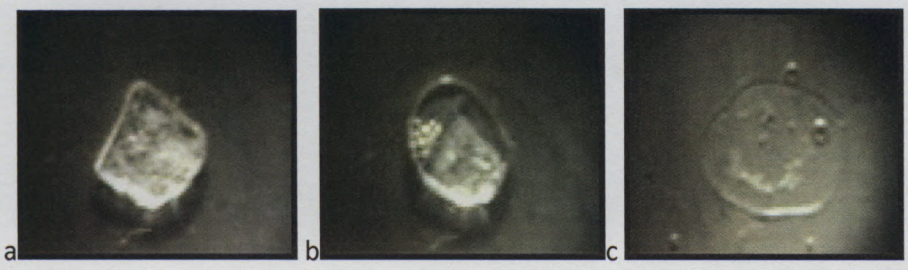

Figure 3.17 Crystals of **H·2MORPH** during thermal decomposition a- crystal at room temperature b- bubbles formed as guest is released at 387.5K c-host melts at 403.9K.

3.3 Structural Analysis

Table 3.12 Crystal Data Parameters

Compound	H·2DMA(a)	H·2DMA(b)	H·2DMF	H·2NMA	H·NMF	H·2H$_2$O
Structural Formula	H^a·2C$_4$H$_9$NO	H^a·2C$_4$H$_9$NO	H^a·2C$_3$H$_7$NO	H^a·2C$_3$H$_7$NO	H^a·C$_2$H$_5$NO	H^a·2H$_2$O
Molecular Mass(gmol^{-1})	616.77	616.77	588.72	588.72	501.60	478.56
Data collection temp. (K)	173(2)	173(2)	173(2)	173(2)	173(2)	173(2)
Crystal system	Orthorhombic	Monoclinic	Triclinic	Monoclinic	Triclinic	Triclinic
Space group	Pbca	P2$_1$/c	P$\bar{1}$	P2$_1$/c	P$\bar{1}$	P$\bar{1}$
a (Å)	11.2630(6)	12.263(3)	7.6923(11)	7.5460(12)	8.2760(17)	10.3078(6)
b (Å)	16.4363(8)	13.918(3)	9.1752(13)	26.221(4)	8.9920(18)	10.82(6)
c (Å)	17.4733(9)	11.155(2)	12.7495(18)	9.1335(13)	18.972(4)	11.6724(6)
α (°)	90.00	90.00	77.960(3)	90.00	84.68(3)	77.[illegible]01(2)
β (°)	90.00	115.55(3)	76.026(3)	113.272(2)	89.23(3)	77.6420(1)
γ (°)	90.00	90.00	66.760(2)	90.00	67.92(3)	88.4400(1)
Volume (Å^3)	3234.7(3)	1717.8(6)	795.9(2)	1660.2(4)	1302.4(5)	1241.56(1)
Z	4	2	1	2	2	2
D$_c$, Calc density (g cm^{-3})	1.266	1.192	1.2[illegible]8	1.178	1.279	1.280
Absorption coefficient (mm^{-1})	0.081	0.076	0.079	0.076	0.081	0.083
F(000)	1320	660	314	628	532	508
Reflections collected/ unique	12767/4901	28533/3290	8988/3939	6476/3372	51799/6440	9799/5087
Goodness-of-fit on F^2	1.025	1.088	1.036	1.022	1.042	1.027
Final R indices [I>2sigma(I)]	R$_1$ = 0.0457; wR$_2$ = 0.1173	R$_1$ = 0.0595; wR$_2$= 0.1638	R$_1$ = 0.0411; wR$_2$ = 0.1068	R$_1$ = 0.0538; wR$_2$ = 0.1303	R$_1$ = 0.0462; wR$_2$ = 0.1059	R$_1$ = 0.0376; wR$_2$ = 0.0945
R indices (all data)	R$_1$ = 0.0630; wR$_2$ = 0.1281	R$_1$ = 0.0685; wR$_2$= 0.1739	R$_1$ = 0.0499; wR$_2$ = 0.1127	R$_1$= 0.0785 wR$_2$= 0.1445	R$_1$ = 0.0694; wR$_2$ = 0.1213	R$_1$ = 0.0432; wR$_2$ = 0.0990
Largest diff. peak and hole (eÅ^{-3})	0.340; -0.221	0.432; -0.598	0.306, -0.206	0.343, -0.414	0.256, -0.260	0.292, -0.188

[a] = $C_{32}H_{26}O_2$

3.3.1 Crystal structure of H·2DMA(a)

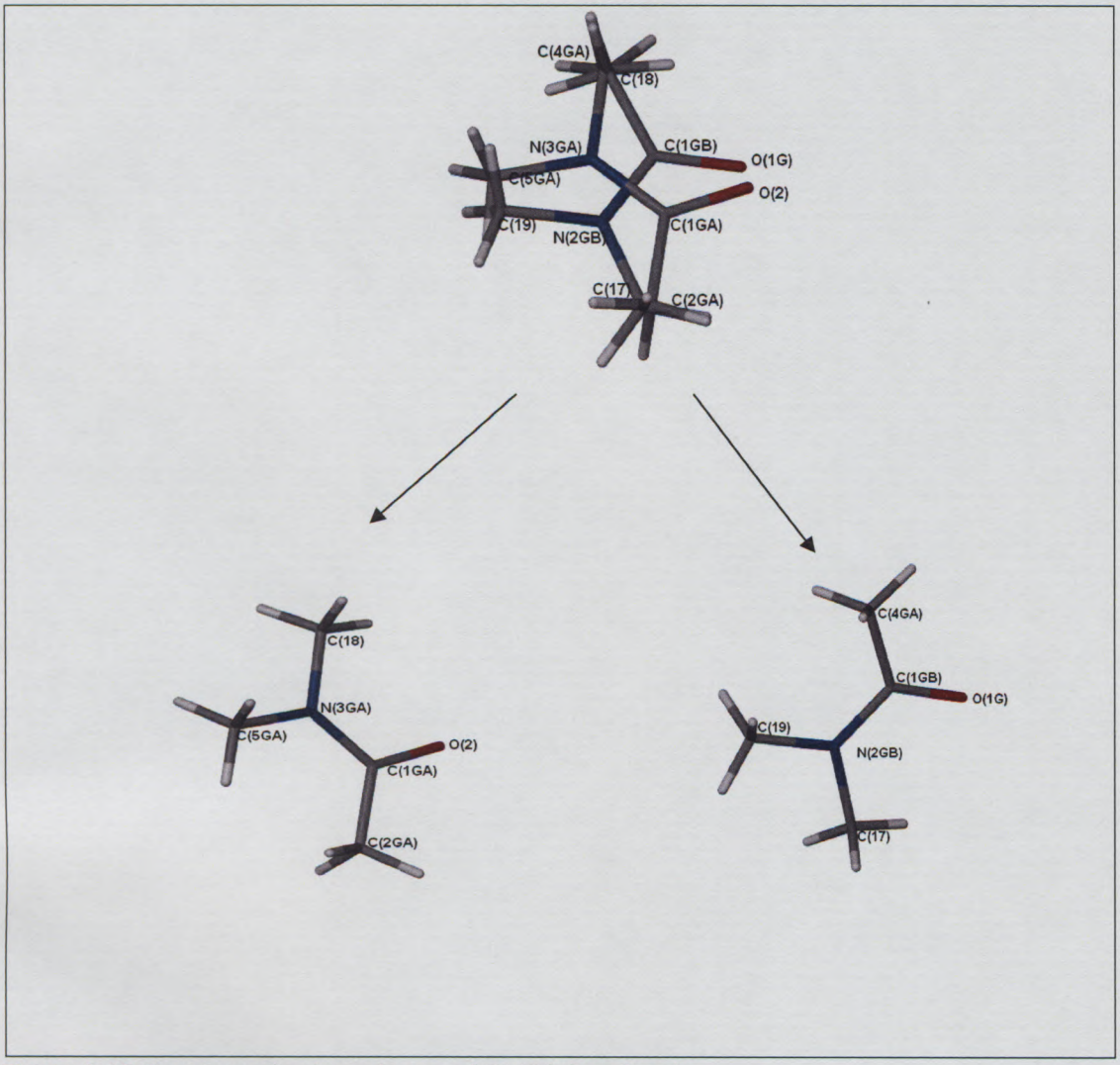

Figure 3.18 Guest numbering scheme of **DMA(a)** molecule.

H·2DMA(a) crystallizes in an orthorhombic crystal system (space group Pbca) consisting of one half of a host molecule and one guest molecule in the asymmetric unit. The host molecule is located on a centre of inversion at Wyckoff position *a*. The guest molecule is disordered as shown in Figure 3.18, with site occupancies of 50/50%. All the non-hydrogen host and guest atoms in the asymmetric unit were refined anisotropically. The host hydroxyl hydrogen was located in the difference electron density map and allowed to refine with a simple bond length constraint dependent on the O•••O distance.[1] The structure refined successfully to $R_1 = 0.0457$ with $wR_2 = 0.1173$.

There are four host molecules and eight guest molecules in each unit cell giving a H:G of 1:2 with Z = 4. This is illustrated in the packing diagram in Figure 3.19. These molecules pack to form channels in the [100] direction shown in Figure 3.20 where the host is shown with its van der Waals radii. The guest molecules are omitted.

Sections[2] through the unit cell were viewed with the guest molecules omitted (Figure 3.21). The section plot confirms the presence of channels in which the guests are packed.

The structure is stabilized by (host)**O-H···O**(guest) hydrogen bonds. The host-guest hydrogen bonding is illustrated in Figure 3.22. Hydrogen bonding details are listed in Table 3.13. The hydrogen bond lengths indicate relatively weak hydrogen bonding.[3]

Further considerations of the intermolecular interactions show **C–H···π** contacts that further stabilize the structure. The closest **C–H···π** contact between the guest and the host occurs between **C17GA–H17A···Cg1** [ring C2, C3, C4, C5, C6 to C7] with an intermolecular distance of 2.790 Å between **H17A···Cg1** and 3.5798 Å between **C17GA···Cg1** bonding at **⟨ (C17GA–H17A···Cg1)** = 138°. The **C–H···π** distances are in the expected average ranges for organic inclusion compounds as mentioned by Braga et al.[4]

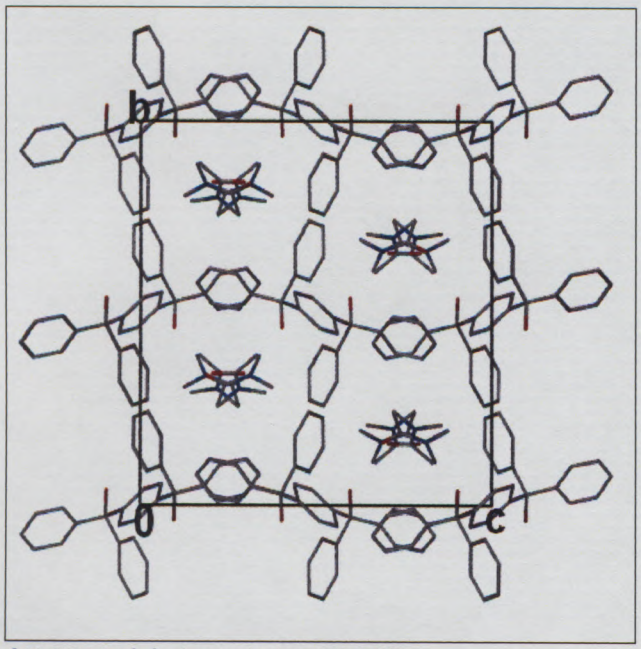

Figure 3.19 Packing diagram of **H·2DMA(a)** viewed along [100].

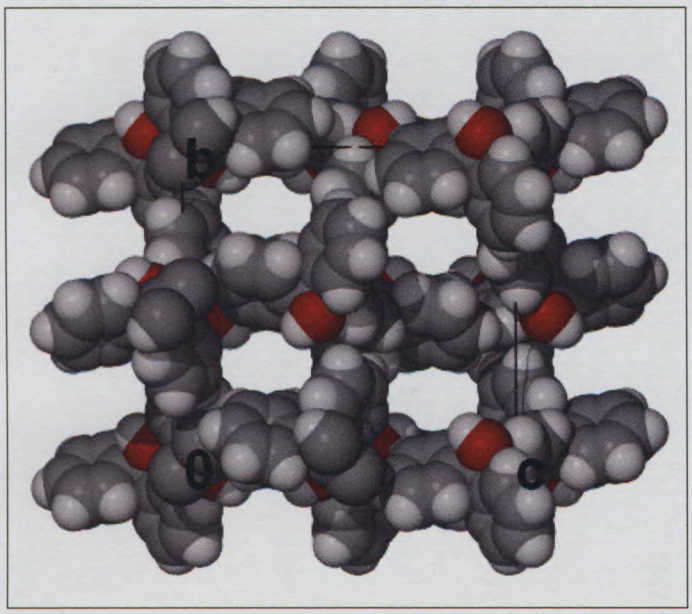

Figure 3.20 Space filled diagram viewed along [100] for **H·2DMA(a).** The guest molecules reside in channels (the guests are omitted).

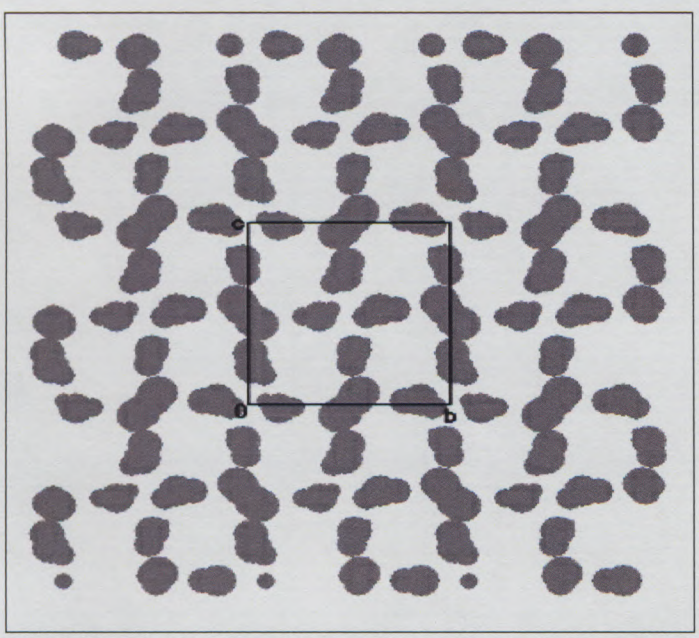

Figure 3.21 Sections shown through a unit cell with guest molecules omitted located along [100] at a section height of 5.76 Å.

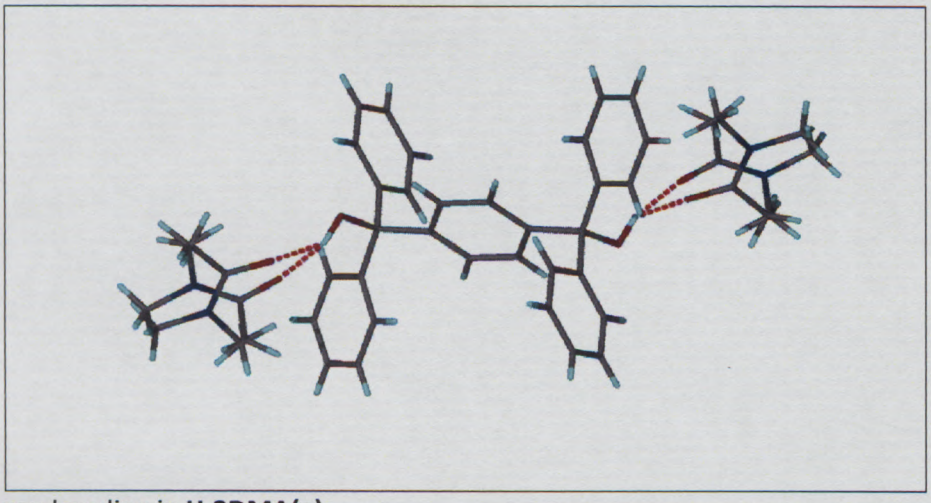

Figure 3.22 Hydrogen bonding in **H·2DMA(a).**

Table 3.13 Hydrogen bonding details of **H·2DMA(a)**

Donor D	**Acceptor A**	**D···A/Å**	**D-H/ Å**	**H···A/ Å**	**D-H···A/ Å**
O1	O(1G)	2.661(4)	0.982(1)	1.800(1)	144(1)
O1	O2	2.751(1)	0.982(1)	1.802(1)	161(1)

3.3.2 Crystal structure of H·2DMA(b)

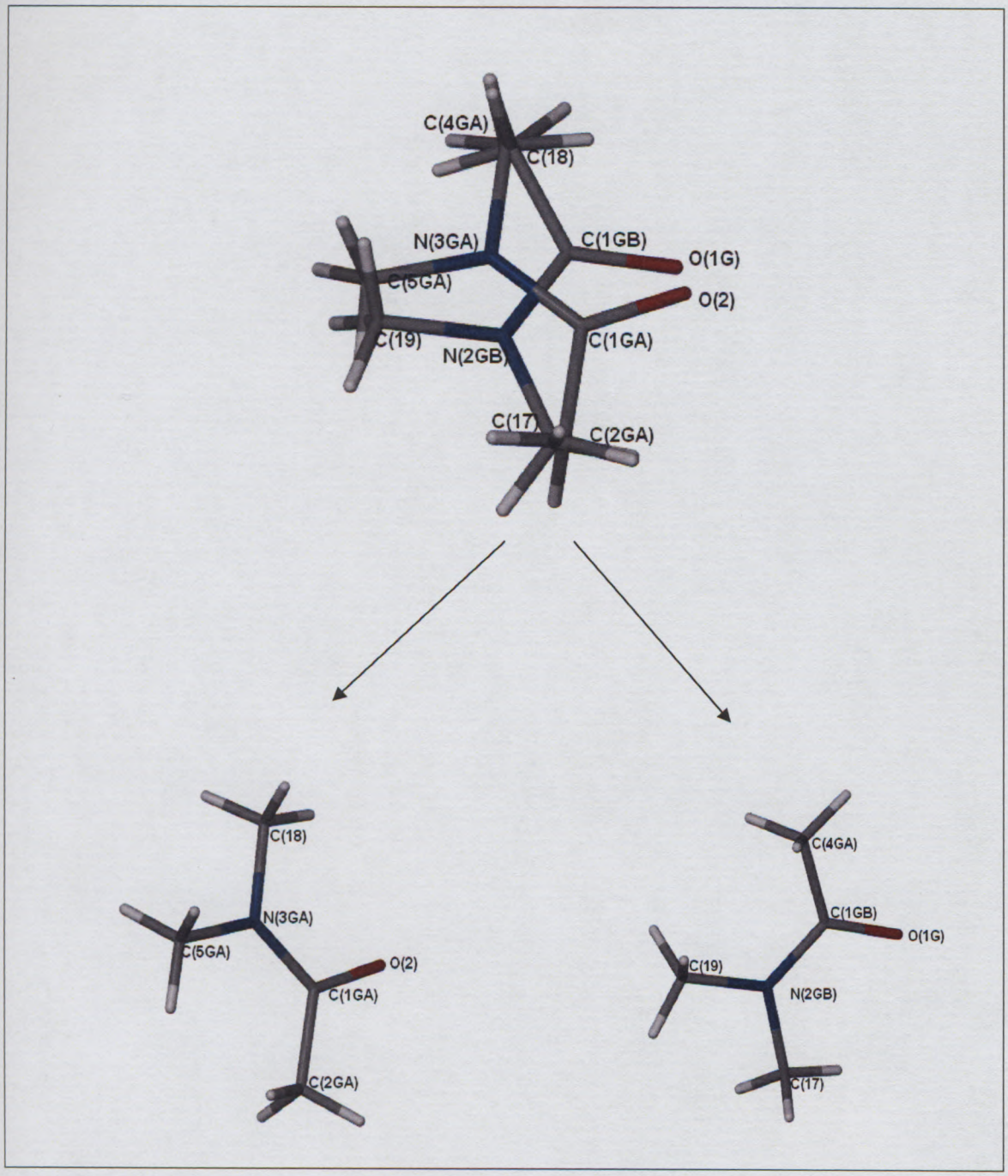

Figure 3.23 Guest numbering scheme of the **DMA(b)** molecule.

The host was dissolved in an equimolar mixture of DMA and NMF. A **polymorph** of the DMA inclusion compound was formed by slow evaporation of this solution. The crystal structure of **H·2DMA(b)** is arranged similarly to that of **H·2DMA(a)** in that both have the same host-guest molecular arrangement and in both cases the guest is disordered (Figure 3.23). The **H·2DMA (b)**

molecule is disordered with site occupancies of 55/45%. **H·2DMA(b)** crystallizes in a monoclinic system in the $P2_1/c$ space group. The host molecule is located on a centre of inversion at Wyckoff position *b*. All the non-hydrogen host and guest atoms in the asymmetric unit were refined anisotropically. The host hydroxyl hydrogen was located in the difference electron density map and subsequently refined with a simple bond length constraint dependent on the O•••O distance. The structure refined successfully to $R_1 = 0.0595$ with $wR_2 = 0.1638$.

There are two host molecules and four guest molecules in each unit cell giving a H:G of 1:2 with Z = 2. The packing diagram in Figure 3.24 shows the channels formed down [001]. The host molecules pack to form an open structure in which the guests are located in intersecting channels down [010] and [001].

The structure is stabilized by a (host)**O-H···O**(guest) hydrogen bond. The host-guest hydrogen bonding is shown in Figure 3.25, where the host is hydrogen bonded to two guest molecules. The hydrogen bonding details are given in Table 3.14.

The structure is further stabilized by **C–H···π** contacts. The closest **C–H···π** contact between the guest and the host occurs between **C18–H18B···Cg1** [ring C2, C3, C4, C5, C6 to C7] with the intermolecular distance of 2.600 Å between **H18B···Cg1** and 3.6459 Å between **C18 ···Cg1** with **⟨ (C18–H18B···Cg1) =** 174°.

These two polymorphs **H·2DMA(a)** and **H·2DMA(b)** can be characterized by their different packings, with polymorph (a) displaying channels running along [100] in which the guests are accommodated (Figure3.26) and polymorph (b) has a more open structure in which the guest are found in intersecting channels down [010] and [001], Figure 3.27 and 3.28.

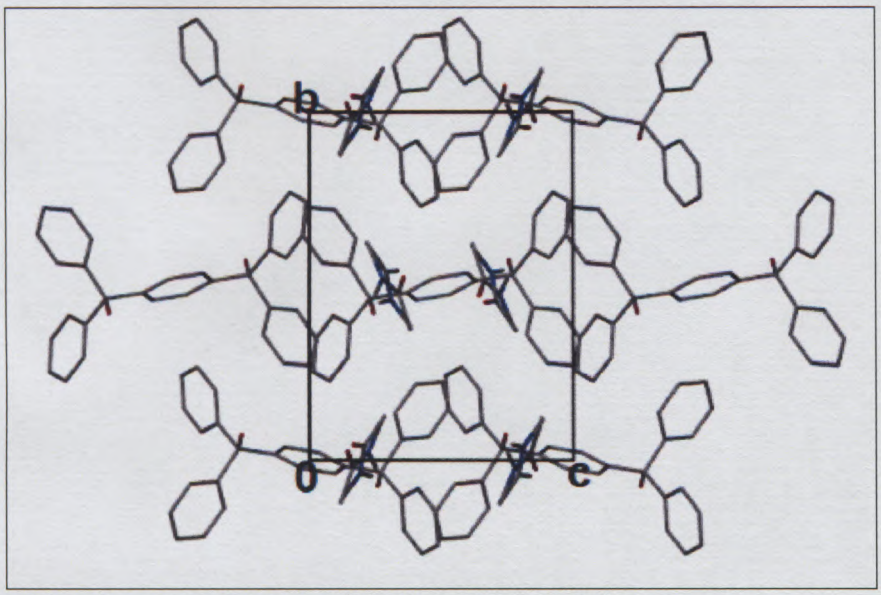

Figure 3.24 Packing diagrams of **H·2DMA(b)** viewed along [001].

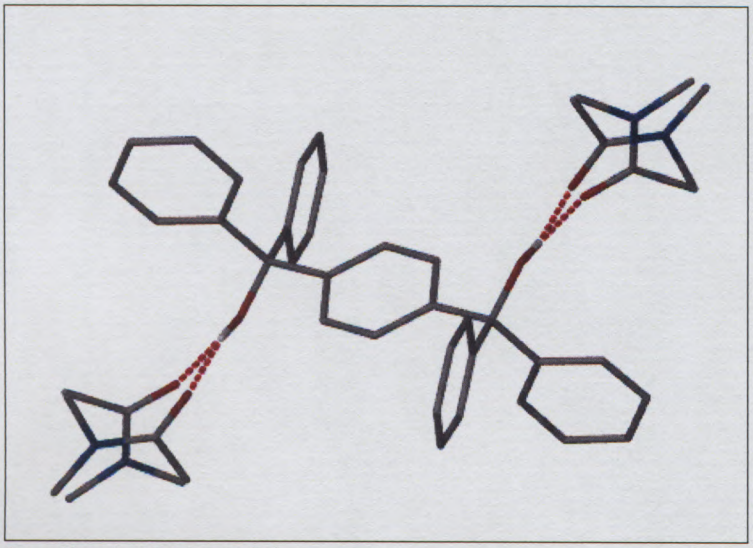

Figure 3.25 Hydrogen bonding in **H·2DMA(b)**.

Table 3.14 Hydrogen bonding details of **H·2DMA(b)**.

Donor D	**Acceptor A**	**D···A/Å**	**D-H/ Å**	**H···A/ Å**	**D-H···A/ Å**
O1	0(1G)	2.6997(1)	0.955(1)	1.772(1)	163(2)
O1	O2	2.785(1)	0.955(1)	1.853(1)	169(1)

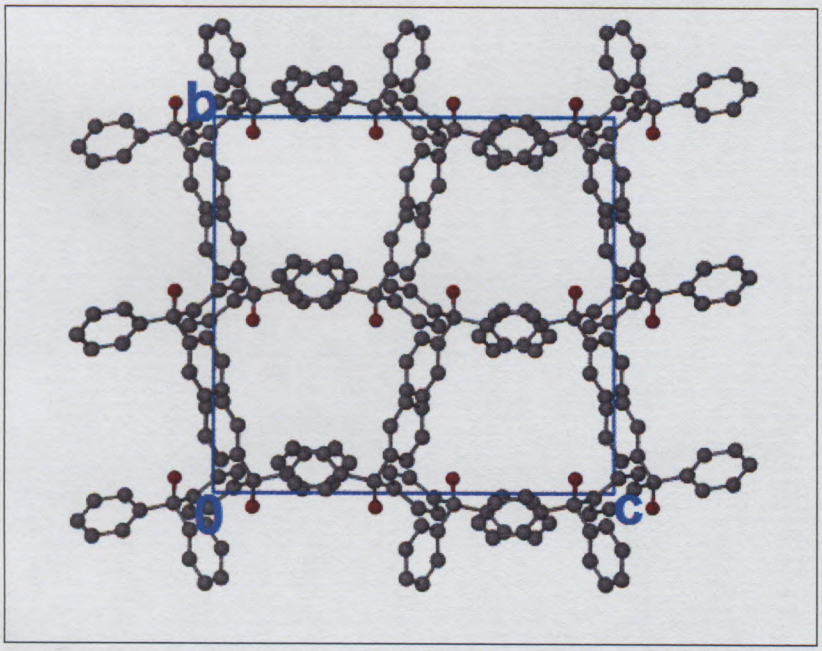

Figure 3.26 Packing diagrams of **H·2DMA(a)** viewed down [100] (the guests are omitted).

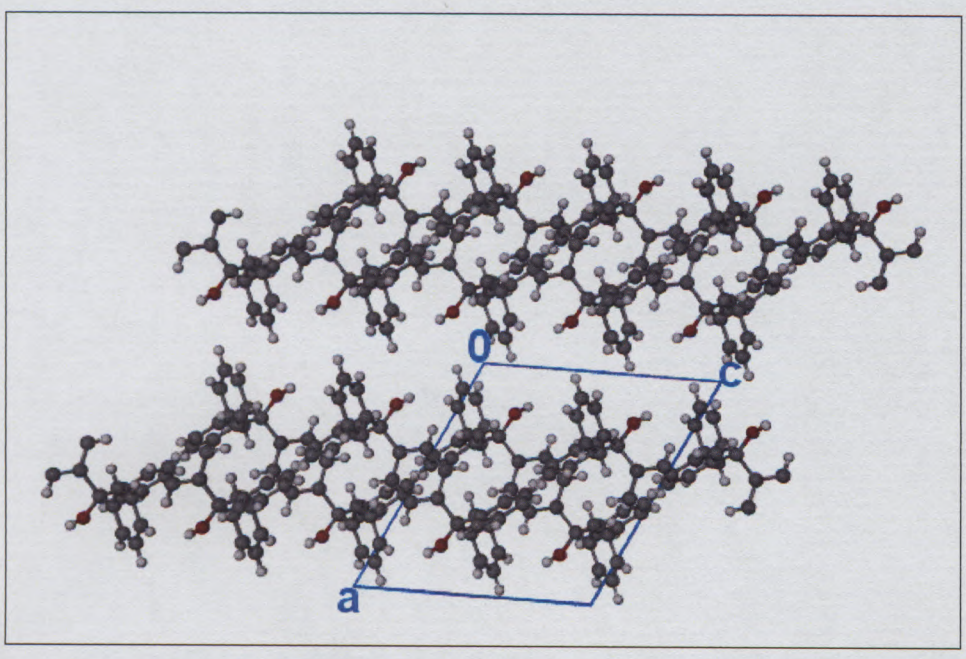

Figure 3.27 Packing diagrams of **H·2DMA(b)** viewed down [010] (the guests are omitted).

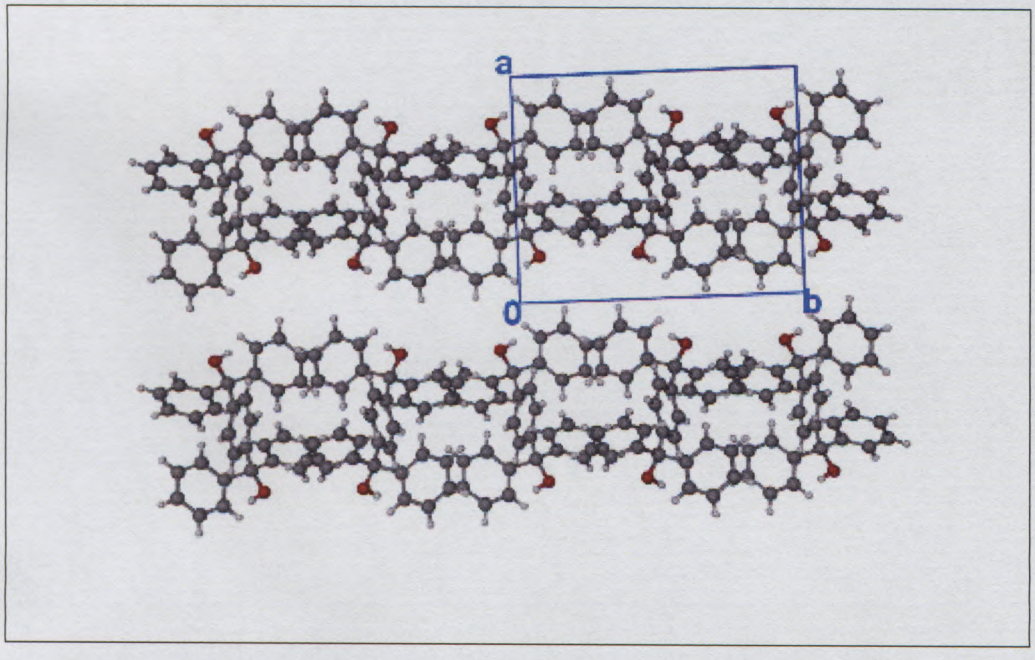

Figure 3.28 Packing diagrams of **H·2DMA(b)** viewed down [001] (the guests are omitted).

3.3.3 Crystal structure of H·2DMF

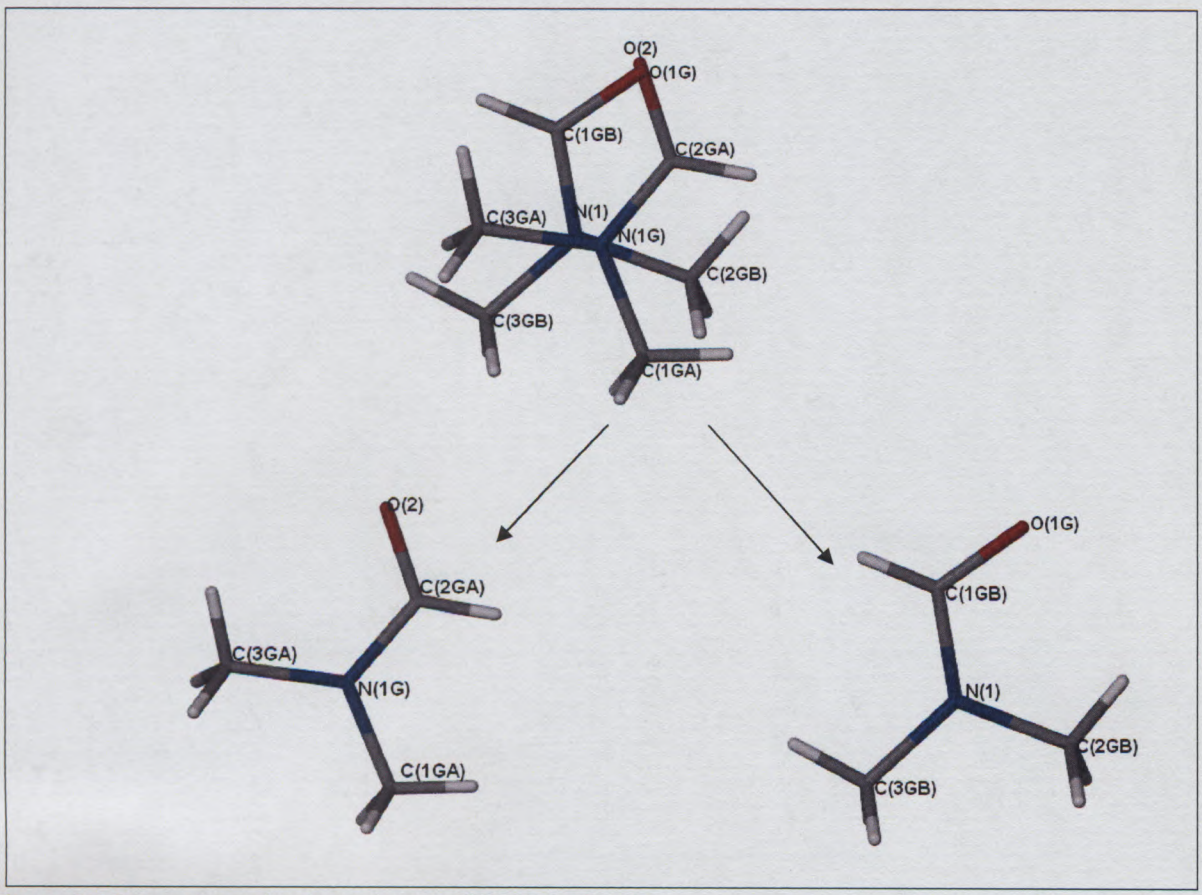

Figure 3.29 Guest numbering scheme of **DMF** molecule.

H·2DMF crystallizes in the triclinic system, space group $P\bar{1}$. The host molecule is located at the centre of inversion at Wyckoff position *d*. The DMF molecule is disordered and refined to site occupancies of 85/15%. All the non-hydrogen host and guest atoms in the asymmetric unit were refined anisotropically. The host hydroxyl hydrogen was located in the difference electron density map. The structure refined successfully to $R_1 = 0.0411$ with $wR_2 = 0.1068$.

There is one host molecule and two guest molecules in each unit cell giving a H:G of 1:2 with Z = 1. This is illustrated in the packing diagram in Figure 3.30. The host molecules pack to form channels down [100] shown in Figure 3.31 where the host is shown with its van der Waals radii, with the guest molecules omitted. Sections through the unit cell were viewed with the guest molecules omitted (Figure 3.32). The section plot confirms the presence of channels in which the guests are packed located along [100].

The structure is stabilized by (host)**O-H···O**(guest) hydrogen bonds. The host-guest hydrogen bonding is illustrated in Figure 3.33. The closest **C–H···π** contact between the guest and the host occurs between **C2GA–H2GA···Cg1** [ring C2, C3, C4, C5, C6 to C7] with the bonding distance of 2.56 Å between **H2GA···Cg1** and

3.4198 Å between **C2GA···Cg1** with ⟨ **(C2GA–H2GA···Cg1)** = 150°. The hydrogen bonding details are given in Table 3.15.

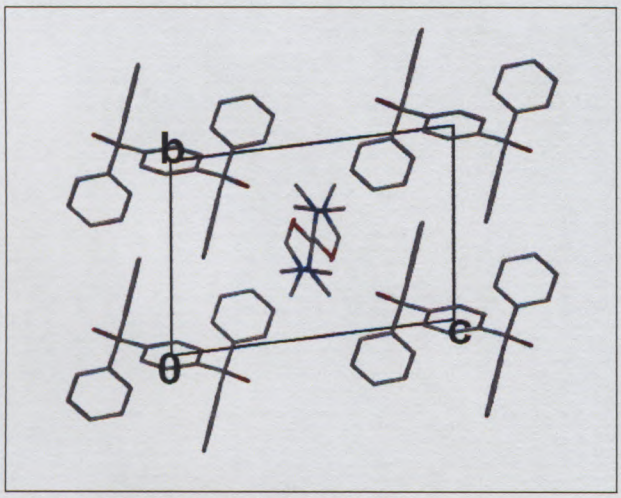

Figure 3.30 Packing diagram of **H·2DMF** viewed along [100].

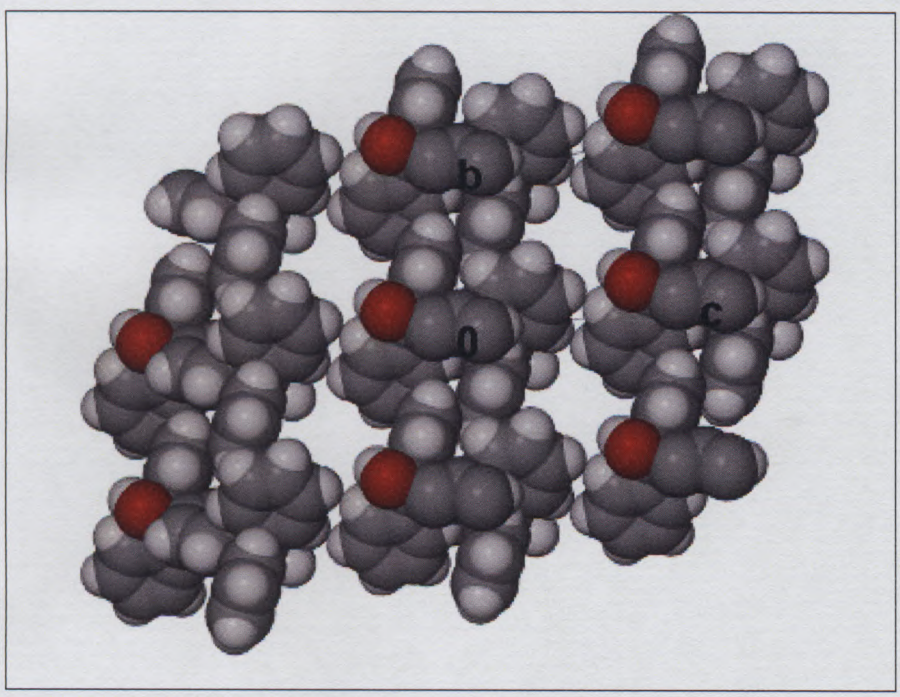

Figure 3.31 Space filled diagram for **H·2DMF** viewed along [100]. The guest molecules reside in the open channels (the guests are omitted).

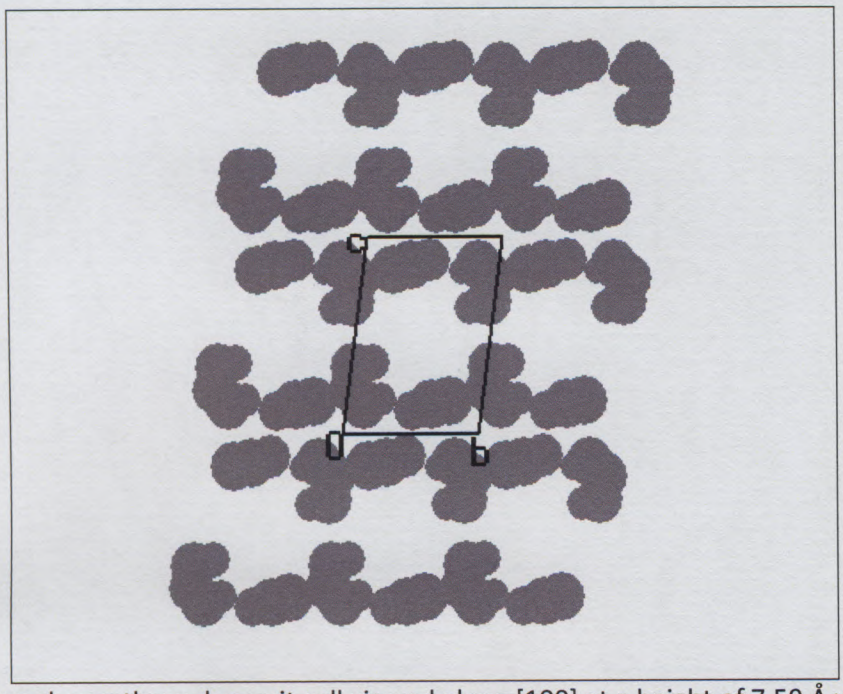

Figure 3.32 Section shown through a unit cell viewed along [100] at a height of 7.59 Å with guest molecules omitted.

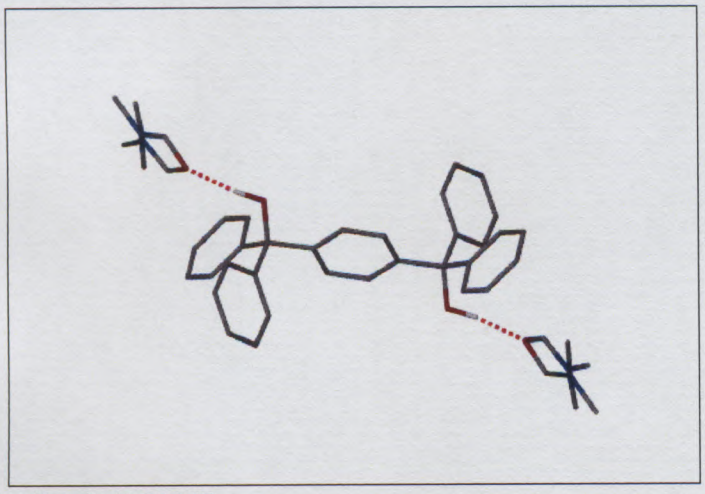

Figure 3.33 Hydrogen bonding in **H·2DMF**.

Table 3.15 Hydrogen bonding details of **H·2DMF.**

Donor D	Acceptor A	D···A/Å	D-H/ Å	H···A/ Å	D-H···A/Å
O1	O(1G)	2.760(1)	0.980(1)	1.786(1)	172(1)
01	O2	2.749(1)	0.980(1)	1.776(1)	171(1)

3.3.4 Crystal structure of H·2NMA

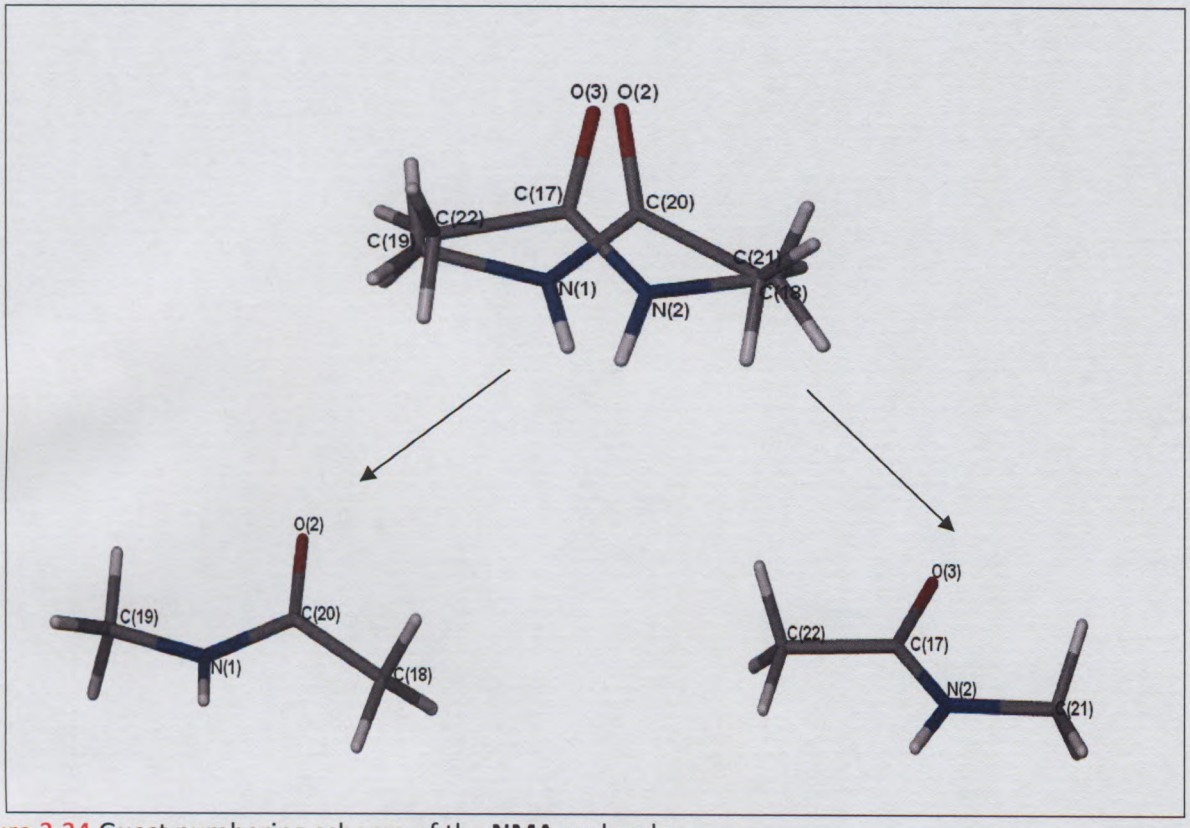

Figure 3.34 Guest numbering scheme of the **NMA** molecule

H·2NMA crystallizes in a monoclinic system in the $P2_1/c$ space group. The host molecule is located on the centre of inversion at Wyckoff position *b*. The asymmetric unit contains one half of a host molecule and one guest molecule. The NMA molecule is disordered with site occupancies of 80/20%. All the non-hydrogen host and guest atoms in the asymmetric unit were refined anisotropically. The host hydroxyl hydrogens were located in the difference electron density map and allowed to refine. The structure refined successfully to $R_1 = 0.0538$ with $wR_2 = 0.1303$.

There are two host molecules and four guest molecules in each unit cell giving a H:G of 1:2 with Z = 2. This is illustrated in the packing diagram in Figure 3.35. The host molecules pack to form layers parallel to [101], Figure 3.36. The guests occupy the voids between the layers of host molecules.

The structure is stabilized by (host)**O-H···O**(guest) hydrogen bonds(Figure 3.37) and (guest)**N-H···O**(guest). The hydrogen bond motif forms a quadrilateral with the Etter[5] notation of $R_6^6(38)$. Hydrogen bonding details are listed in Table 3.16. The hydrogen bonding pattern is arranged in cyclic patterns, in such a manner that the chains of hydrogen bonded guest molecules bond with each other, also hydrogen bonded to the host molecule via the carbonyl group forming an accepting bifurcated hydrogen bond.

The structure is also stabilized by **C–H···π** contacts. The closest **C–H···π** contact between the guest and the host occurs between **C22–H22A···Cg2** [ring C8, C9, C10, C11, C12 to C13] with the intermolecular distance of 2.790 Å between **H22A···Cg2** and 3.5798 Å between **C22 ···Cg2** with ⟨ **(C22–H22A···Cg2)** = 132°.

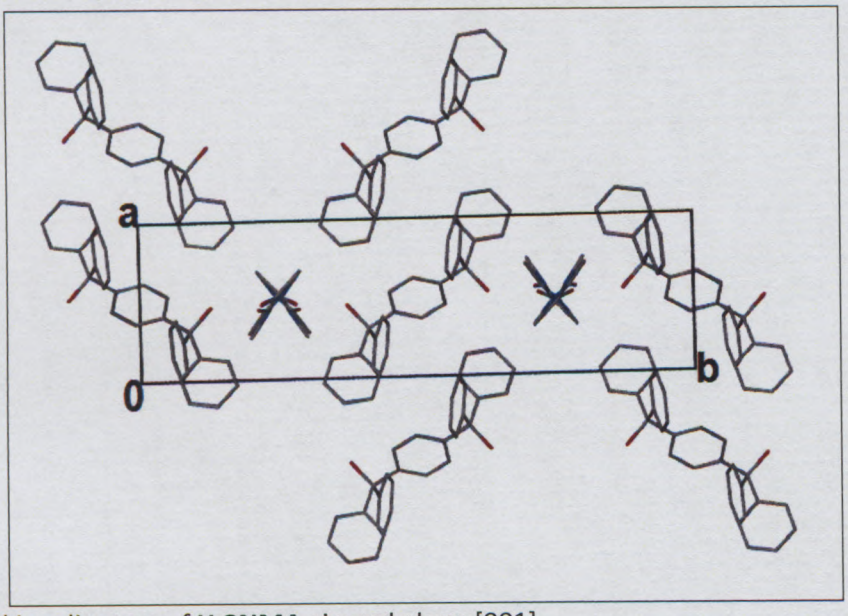

Figure 3.35 Packing diagram of **H·2NMA** viewed along [001].

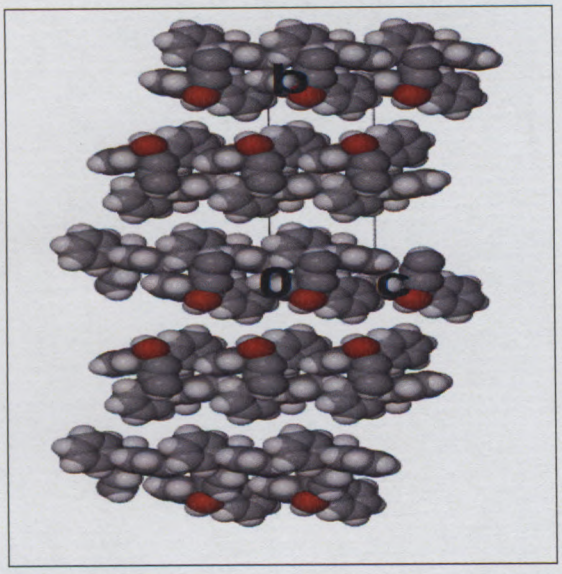

Figure 3.36 Space filled diagram viewed along [100] for **H·2NMA** the guest molecules reside in the layers between the molecules (the guests are omitted).

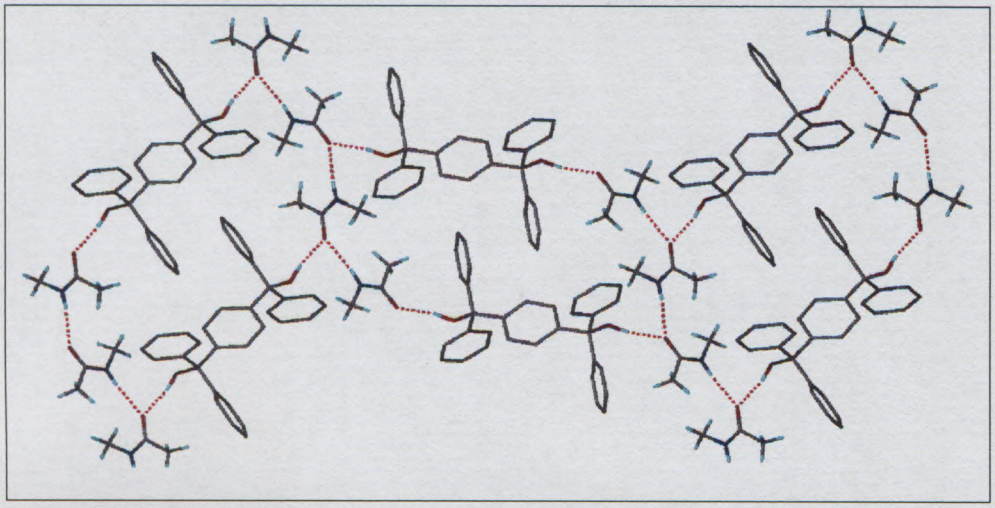

Figure 3.37 Hydrogen bonding in **H·2NMA,** only one of the disordered guests is represented for clarity.

Table 3.16 Hydrogen bonding details of **H·2NMA**

Donor D	**Acceptor A**	**D···A/Å**	**D-H/ Å**	**H···A/ Å**	**D-H···A/ Å**
O1	O(2)	2.757(1)	0.976(1)	1.893(1)	146(1)
O1	O(3)	2.754(1)	0.976(1)	1.832(1)	156(3)
N1(x,1/2-y,z-1/2)	O(2)	2.289(1)	0.880(1)	1.900(1)	153(1)
N1(x,1/2-y,z-1/2)	O(3)	2.163(1)	0.880(1)	2.067(1)	145(1)
N2(x,1/2-y,z-1/2)	O(2)	2.228(1)	0.880(1)	1.910(1)	174(1)
N2(x,1/2-y,z-1/2)	O(3)	2.233(1)	0.880(1)	2.109(1)	168(1)

3.3.5 Crystal structure of H·NMF

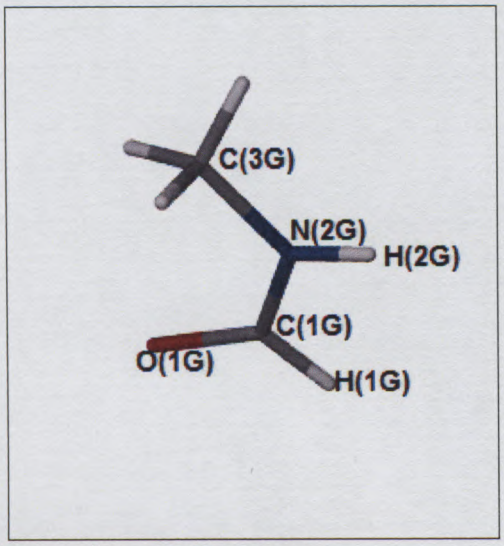

Figure 3.38 Guest numbering scheme of the **NMF** molecule

H·NMF crystallizes in a triclinic system in the $P\bar{1}$ space group. The asymmetric unit consists of two half host molecules and one guest molecule. Each of the two half host molecules lie on a centre of symmetry at Wyckoff positions *b* and *e*. The guest molecules are found in general positions. All the non-hydrogen host and guest atoms in the asymmetric unit were refined anisotropically. The host hydroxyl hydrogens were located in the difference electron density map and allowed to refine. The structure refined successfully to $R_1 = 0.0462$ with $wR_2 = 0.1059$.

There are two host molecules and two guest molecules in each unit cell giving a H:G of 1:1 with Z = 2. This is illustrated in the packing diagram in Figure 3.39. The host molecules pack to form cavities down [010].

The structure is characterized by a ribbon of (host)-O-H•••O(host) hydrogen bonds (Figure 3.40) and in accordance with the Etter graphical notation this ladder motif is characterized as $R_6^6(30)$ with hydrogen bonds running along [011]. The hydrogen bonding details are given in Table 3.17. The structure is further stabilized by **C–H···π** contacts. The closest **C–H···π** contact between the guest and the host occurs between **C11–H11···Cg1** [ring C2, C3, C4, C5, C6 and C7] with a bonding distance of 2.840 Å between **H11···Cg1** and 3.6369 Å between **C11···Cg1** with ⟨ **(C11–H11···Cg1)** = 142°.

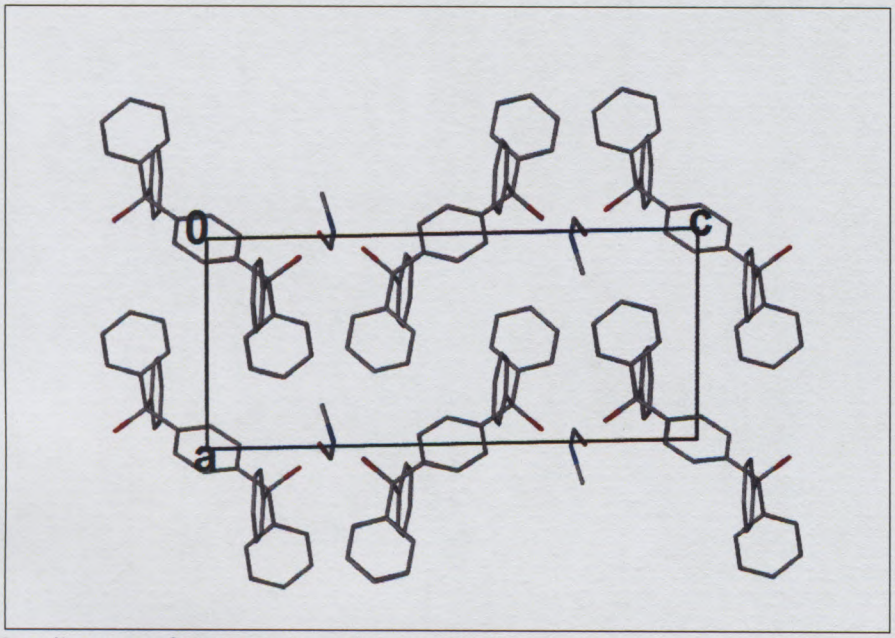

Figure 3.39 Packing diagram of **H·NMF** viewed down [010].

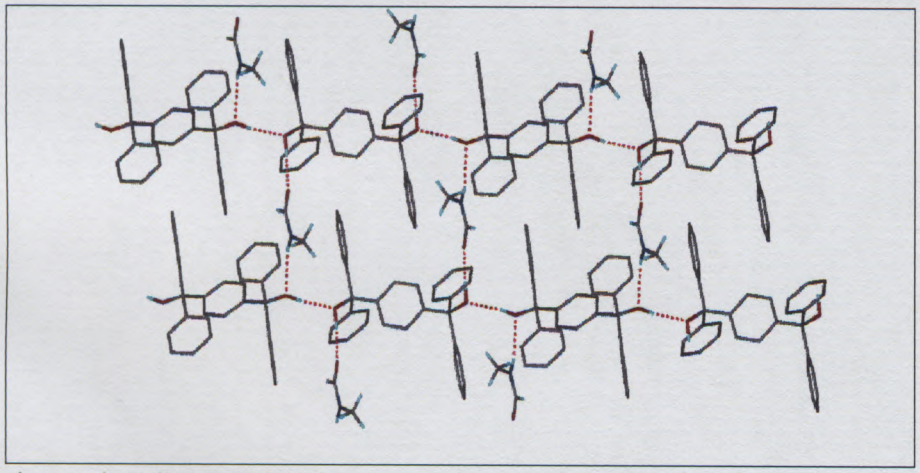

Figure 3.40 Hydrogen bonding in **H·NMF**

Table 3.17 Hydrogen bonding details of **H·NMF**

Donor D	Acceptor A	D···A/Å	D-H/ Å	H···A/ Å	D-H···A/ Å
O1	O(1G)	2.755(2)	0.975(1)	1.839(1)	155(1)
O1A	O1	2.946(1)	0.960(1)	2.017(1)	162(1)
N(G2)	O1A	3.049(1)	0.880(1)	2.242(1)	152(1)

3.3.6 Crystal structure of $H{\cdot}2H_2O$

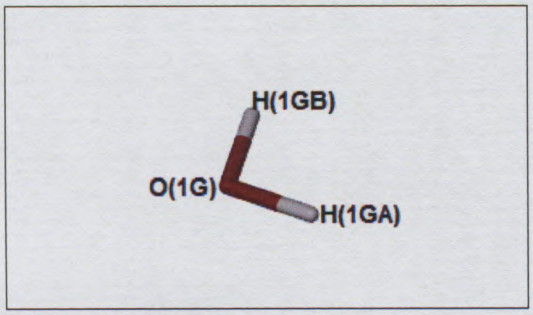

Figure 3.41 Guest numbering scheme of the **H_2O** molecule

$H{\cdot}2H_2O$ crystallizes in a triclinic system, space group $P\bar{1}$. The asymmetric unit contains two half host molecules, each lie on a centre of symmetry at Wyckoff positions *b* and *g*, as well as two water molecules in general positions. All the non-hydrogen host and guest atoms in the asymmetric unit were refined anisotropically. The host hydroxyl hydrogens were located in the difference electron density map and allowed to refine. The structure refined successfully to $R_1 = 0.0376$ with $wR_2 = 0.0945$.

There are two host molecules and four guest molecules in each unit cell giving a H:G of 1:2 with Z = 2, this is illustrated in the packing diagram in Figure 3.42. Two host molecules on opposite ends lie across each other by the centre phenyl rings in such a way that the water molecules occupy cavities.

The structure is stabilized by (host)**O-H···O**(guest) hydrogen bonds. The H-bond pattern is characterized by repeating rings of host hydroxyls and water molecules which may be described as $R_4^4(8)$ and $R_6^5(26)$, a cyclic pattern built by hydrogen bonded hosts with water molecules as shown in Figure 3.43. The hydrogen bonding details are given in Table 3.18.

The closest **O–H···π** contact between the guest and the host occurs between **O1G–H1GB···Cg1** [ring C2, C3, C4, C5, C6 and C7] with a bonding distance of 2.580 Å between **H1GB···Cg1** and 3.3927 Å between **O1G···Cg1** with ⟨ **(O1G–H1GB···Cg1)** = 158°.

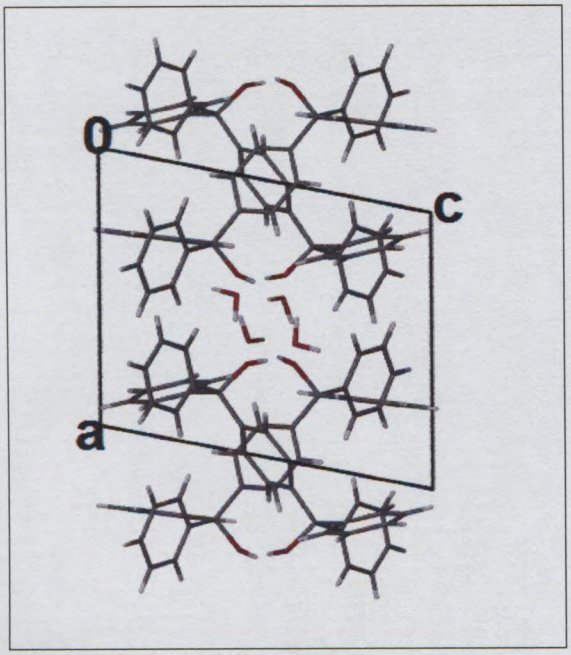

Figure 3.42 Packing diagram of **H·2H$_2$O** viewed along [010].

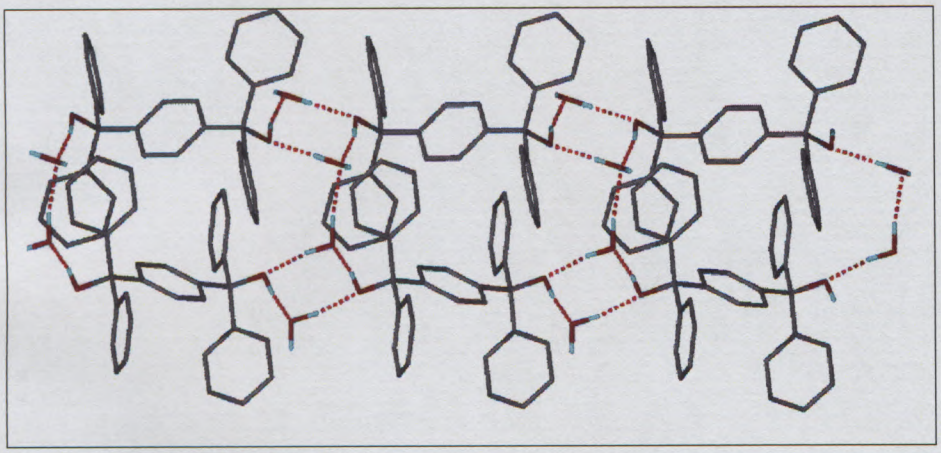

Figure 3.43 Hydrogen bonding in **H·2H$_2$O.**

Table 3.18 Hydrogen bonding details of **H·2H$_2$O.**

Donor D	**D···A/Å**	**D-H/ Å**	**H···A/ Å**	**D-H···A/ Å**
O1–H1···O(2G) [-x+1, -y, -z+1]	2.695(2)	0.980(1)	1.721(1)	172(1)
O1A–H1A···O(1G) [-x-1, -y+1, -z+1]	2.757(2)	0.975(1)	1.799(1)	167(1)
O(1G)-H(1GA)···O1A	2.716(2)	0.975(1)	1.768(1)	163(1)
O(2G)-H(2GA)···O1	2.713(2)	0□980(1)	1.766(1)	161(1)
O(2G)-H(2GB)···O(1G) [1-x, 1-y, 1-z]	2.855(1)	0.962(1)	1.907(1)	168(1)

Table3.19 Crystal data parameters.

	H·2PIC	H·2(3PIC)	H·2(4PIC)	H·2PYR	H·2MOR□H
Compound	$H^a \cdot C_6H_7N$	$H^a \cdot 2C_6H_7N$	$H^a \cdot 2C_6H_7N$	$H^a \cdot 2C_5H_5N$	$H^a \cdot 2C_4H_9NO$
M/g mol^{-1}	535.65	628.78	628.78	600.73	616.80
T/K	173	173	173	173	173
Crystal System	Monoclinic	Triclinic	Triclinic	Triclinic	Monoclinic
Space group	$P2_1/c$	$P\bar{1}$	$P\bar{1}$	$P\bar{1}$	$P2_1/c$
a/Å	10.416(□)	8.7348(17)	9.0717(9)	8.2910(8)	9.1043(18)
b/Å	9.5708(19)	10.187(2)	10.2536(10)	8.8810(8)	16.124(3)
c/Å	28.897(6)	11.376(2)	11.3009(12)	11.9486(11)	11.377(2)
α/º	90.00	97.64(3)	64.027(2)	82.901(3)	90.00
β/º	93.26(3)	111.56(3)	89.021(2)	82.865□2)	102.51(3)
γ/º	90.00	112.02(3)	66.086(2)	68.559(2)	90.00
V/Å^3	2876.0(10)	828.6(3)	847.27(15)	809.66(13)	1630.4(6)
Z	4	1	1	1	2
μ/mm^{-1}	0.075	0.077	0.075	0.075	0.081
F(000)	1136	334	334	318	660
Reflections collected/unique	32464/ 5461	19356/3138	8586□4235	11186 / 5803	7064 / 3606
ρ_{calc}/g cm^{-3}	1.237	1.260	1.232	1.232	1.256
Final R indices [I > 2σ(I)]	R_1 = 0.0598, wR_2 = 0.1048	R_1 = 0.0403, wR_2 = 0.0997	R_1 = 0.0492, wR_2 = 0.1216	R_1 = 0.0547, wR_2 = 0.1396	R_1 = 0.0960, wR_2 = 0.1822
R indices (all d□ta)	R_1 = 0.0407, wR_2 = 0.0943	R_1 = 0.0356, wR_2 = 0.0940	R_1 = 0.0418, wR_2 = 0.114	R_1 = 0.0463, wR_2 = 0.1307	R_1 = 0.0630, wR_2 = 0.1670
Largest difference peak and hole /e Å^{-3}	0.208 ; -0.198	0.222 ;-0.289	0.480 ; -0.232	0.436 ; -0.266	0.727 ; -0.391

[a] $C_{32}H_{26}O_2$

3.3.7 Crystal structure of H·2PIC

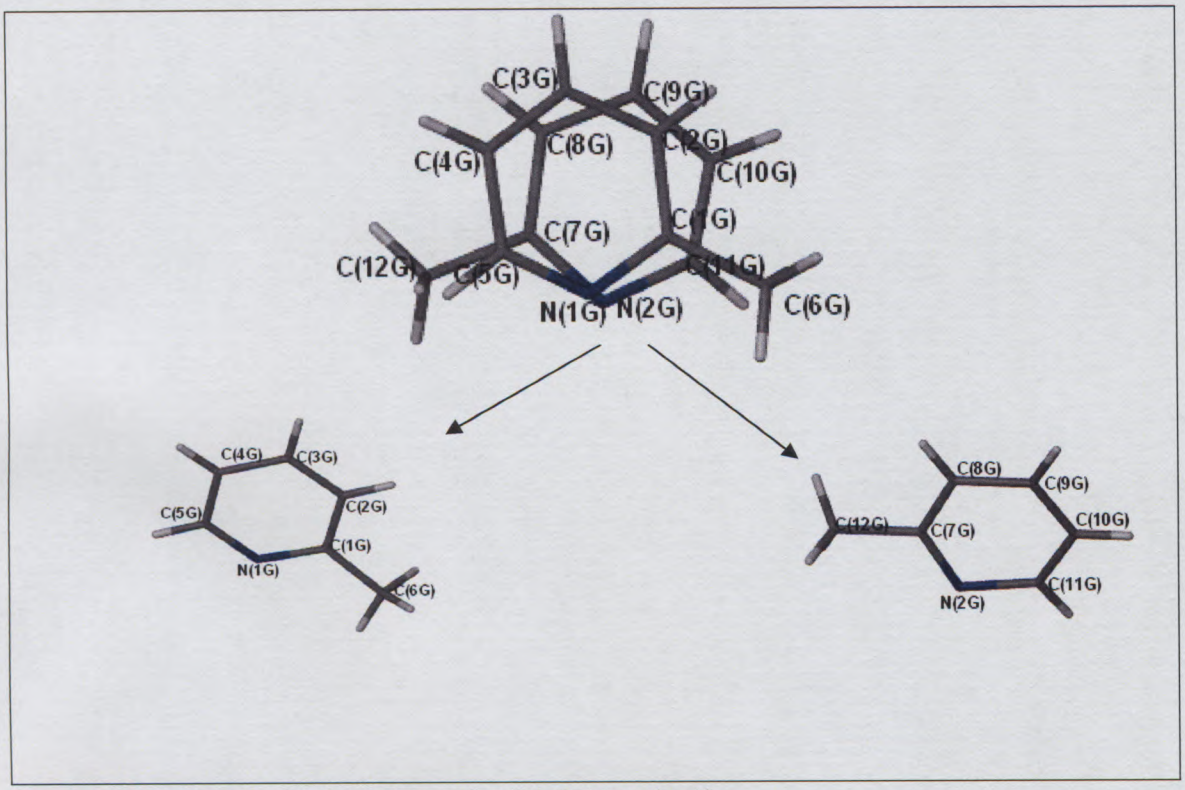

Figure 3.44 Guest numbering scheme for the **2PIC** molecule.

H·2PIC crystallizes in a monoclinic crystal system (space group $P2_1/c$) containing one host molecule and one guest molecule in the asymmetric unit. All the non-hydrogen host and guest atoms in the asymmetric unit were refined anisotropically. The host hydroxyl hydrogens were located in the difference electron density map and allowed to refine. The atoms N1G and N2G displayed the highest peak magnitude within the guest pyridine ring and could therefore be confidently assigned. The structure refined successfully to $R_1 = 0.0598$ with $wR_2 = 0.1048$.

There are four host molecules and four guest molecules in each unit cell giving a H:G of 1:1, this is illustrated in the packing diagram in Figure 3.45 with Z = 4. The host molecules pack to form channels in the [010] direction shown in Figure 3.46 where the host is shown with its van der Waals radii and the guest molecules are omitted for clarity.

Sections through the unit cell were viewed with the guest molecules omitted (Figure 3.47) The section plot confirms the presence of channels in which the guests are packed.

The structure is stabilized by (host)**O-H···N**(guest) hydrogen bonds. The host-guest interactions are illustrated in Figure 3.48. The hydroxyl groups of the host were found to be trans with a torsion angle of 161.1°. The host is hydrogen bonded to one guest molecule, leaving a vacant bonding site on the second hydroxyl group. The nearest adjacent molecule is a host compound with a bonding distance of 3.587 Å between the host heteroatom **O1A** and the neighbouring host centroid (**Cg3**). The hydrogen bonding details are given in Table 3.20.

The closest **C–H···π** contact between the guest and the host occurs between **C7G–H7CG···Cg6** [ring C8, C9, C10, C11, C12 and C13] with a bonding distance of 2.80 Å between **H7CG···Cg6** and 3.5314 Å between **C7G···Cg6** with ⟨ **(C7G–H7CG···Cg6)** = 132°.

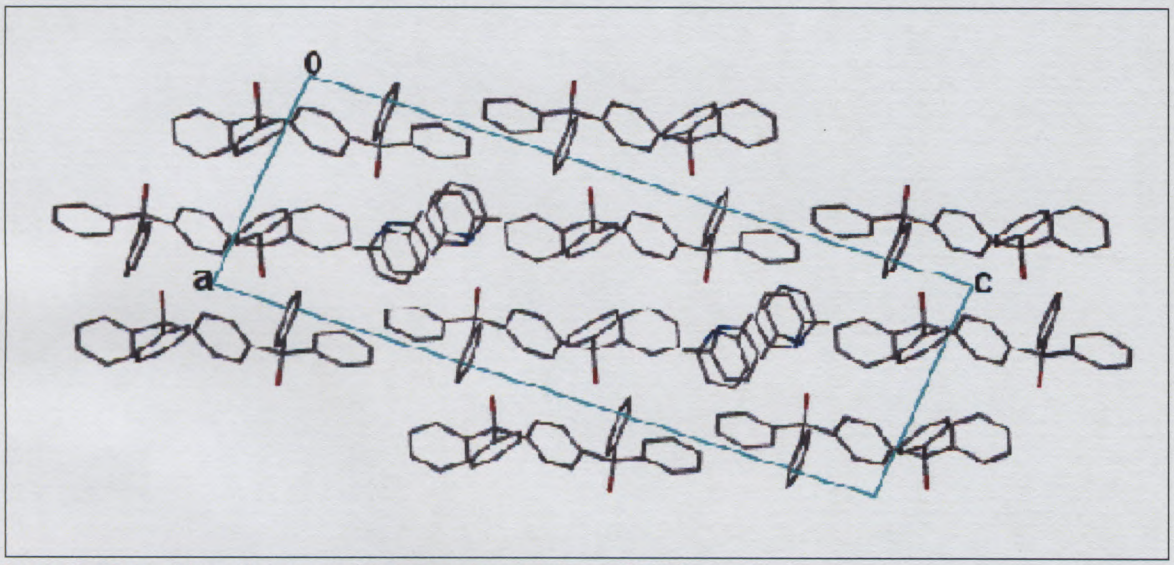

Figure 3.45 Packing diagram of **H·2PIC** viewed down [010].

Figure 3.46 Space filled diagram viewed down [010] for **H·2PIC.** The guest molecules reside in the channels (the guest are omitted).

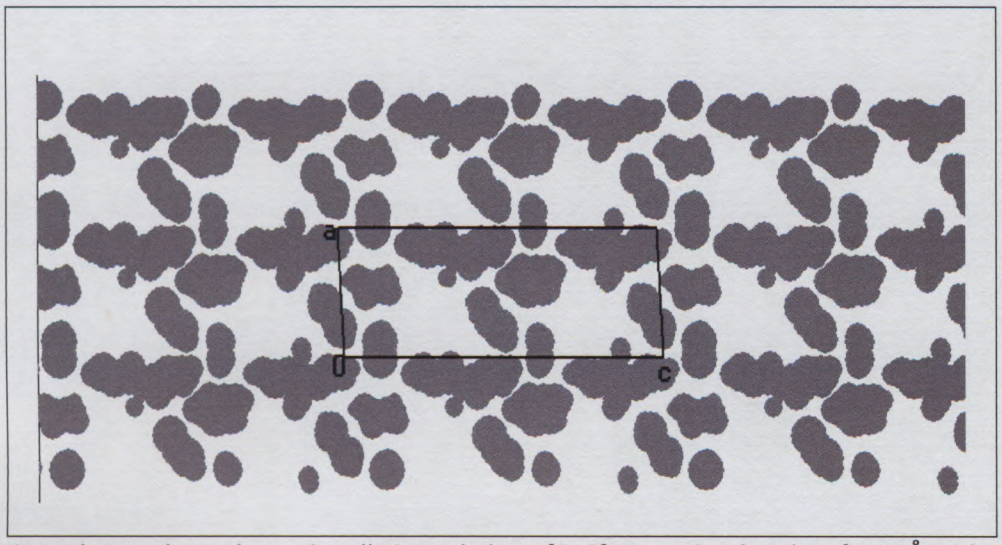

Figure 3.47 Sections shown through a unit cell viewed along [010] at section height of 7.57Å with guest molecules omitted.

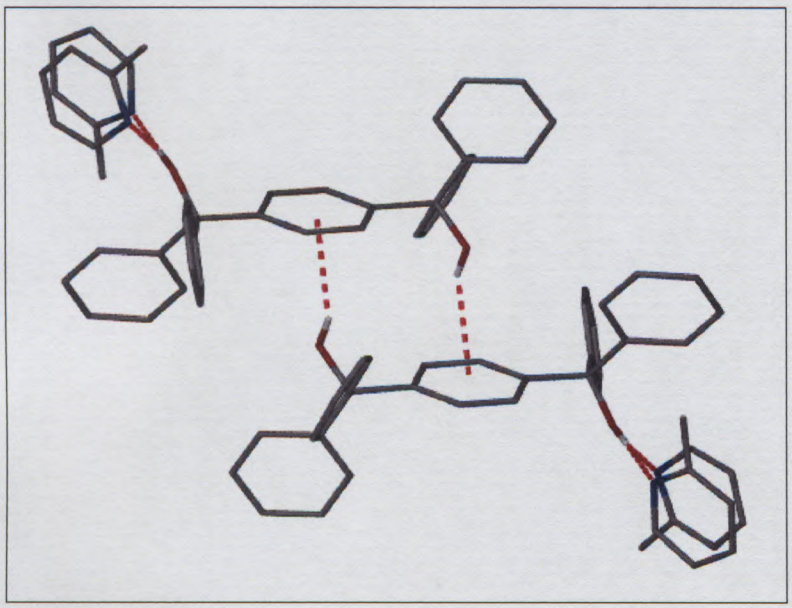

Figure 3.48 Hydrogen bonding in **H·2PIC.**

Table 3.20 Hydrogen bonding details of **H·2PIC.**

Donor D	**Acceptor A**	**D···A/ Å**	**D-H/ Å**	**H···A/ Å**	**D-H···A/ Å**
O1	N(1G)	2.825(1)	0.977(1)	1.862(1)	172(1)
O1	N(2G)	2.711(1)	0.977(1)	1.738(1)	173(1)

3.3.8 Crystal structure of H·2(3PIC)

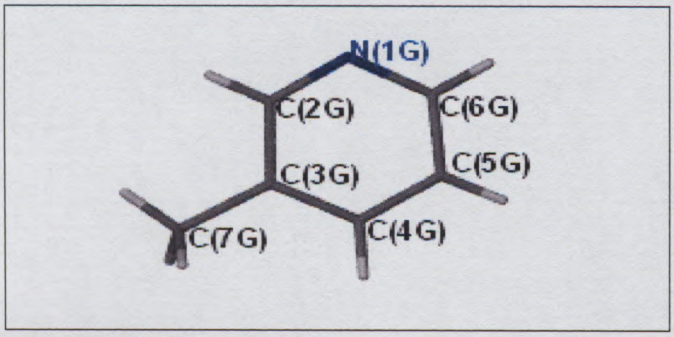

Figure 3.49 Guest numbering scheme of **3PIC** molecule

H·2(3PIC) crystallizes in a triclinic crystal system (space group $P\bar{1}$) consisting of one half of a host molecule and one guest molecule in the asymmetric unit. The host was located at Wyckoff position *c*. Atom N1G of the guest was confidently placed as it had the highest peak intensity in the pyridine guest ring, within the hydrogen bonding distance of the hydroxyl oxygen of the host. All the non-hydrogen host and guest atoms were refined anisotropically. The host hydroxyl hydrogen atom was located in the difference electron density map. The rest of the host and guest hydrogen atoms were placed in geometrically constrained positions and refined with common isotropic atomic displacement parameters for the atoms of the same type. The structure refined successfully to $R_1 = 0.0403$ with $wR_2 = 0.0997$.

The packing diagram is shown in Figure 3.50. There is one host molecule and two guest molecules in each unit cell which confirms a H:G ratio of 1:2 and Z=1. The guest molecules are packed down channels formed by the host compound (Figure 3.51).

The structure is stabilized by (host)**O-H···N**(guest) hydrogen bonding illustrated in Figure 3.52. The hydrogen bonding details are given in Table 3.21.

The closest **C–H···π** contact between the guest and the host occurs between **C6–H6···Cg2** [ring C8, C9, C10, C11, C12 and C13] with a bonding distance of 2.76 Å between **H6···Cg2** and 3.641 Å between **C6···Cg2** with ⟨ **(C6–H6···Cg2)** = 154°.

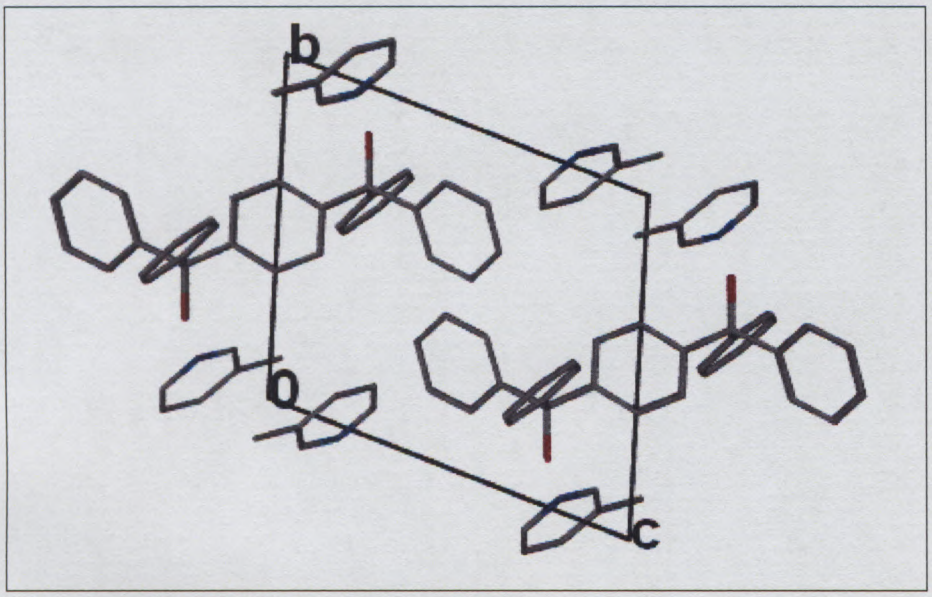

Figure 3.50 Packing diagram of **H·2(3PIC)** viewed down [100].

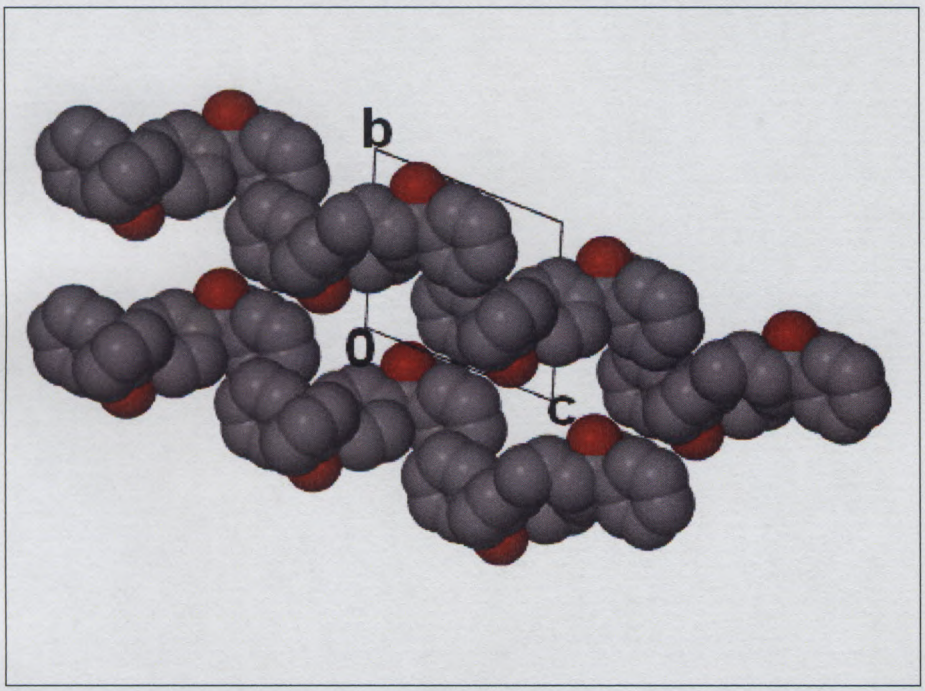

Figure 3.51 Space filled diagram of **H·2(3PIC)** viewed down[100] showing the the packing of the host, the vacant spaces are channels where the guests fit.

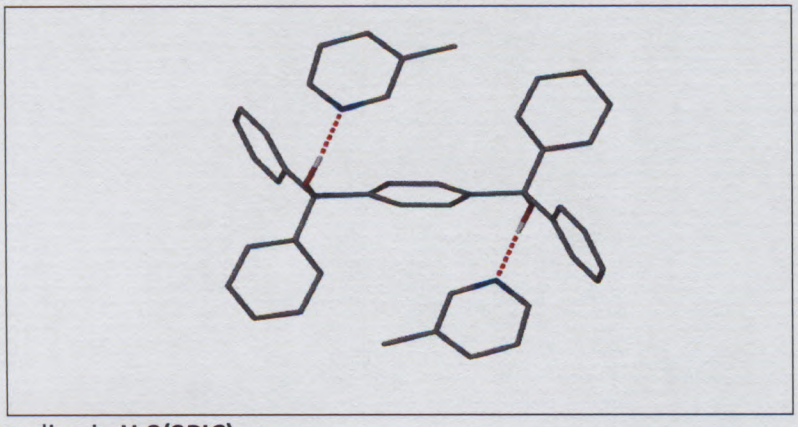

Figure 3.52 Hydrogen bonding in **H·2(3PIC).**

Table 3.21 Hydrogen bonding details **H·2(3PIC).**

Donor D	Acceptor A	D···A/ Å	D-H/ Å	H···A/ Å	D-H···A/ Å
O1	N(1G)	2.814(1)	0.970(□)	1.853(1)	169(1)

3.3.9 Crystal structure of H·2(4PIC)

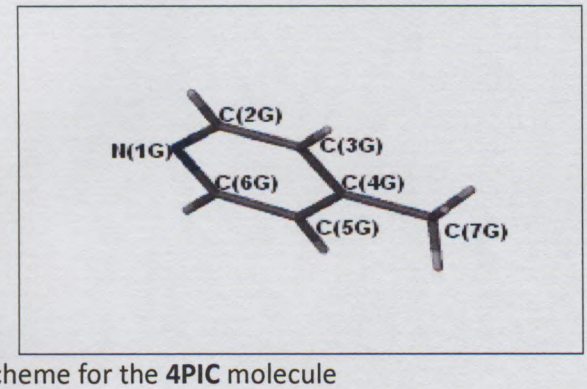

Figure 3.53 Guest numbering scheme for the **4PIC** molecule

Similarly to **H·2(3PIC), H·2(4PIC)** crystallizes in a triclinic crystal system ($P\bar{1}$) consisting of one half of a host molecule and one guest molecule in the asymmetric unit. The host was located on the centre of inversion at Wyckoff position *g*, and the guests found in general positions. All the non-hydrogen host and guest atoms were refined anisotropically. The host hydroxyl hydrogen was located in the difference electron density map and allowed to refine freely. The structure refined successfully to $R_1 = 0.0492$ with $wR_2 = 0.1216$.

The packing diagram is shown in Figure 3.54. There is one host molecule and two guest molecules in each unit cell which confirms a H:G ratio of 1:2 and Z=1. The guest molecules are packed in channels formed by the host

compound in the [100] direction. Figure 3.55 shows the host framework with its van der Waals radii forming channels which the guest inhabits.

The structure is stabilized by (host)**O-H···N**(guest) bonding illustrated in Figure 3.56. The hydrogen bonding details are given in Table 3.22.

The closest **C–H···π** contact between the guest and the host occurs between **C6–H6G···Cg1** [ring C2, C3, C4, C5, C6 and C7] with a bonding distance of 2.73 Å between **H6G ···Cg1** and 3.6287 A° **C6···Cg1** with ⟨ **(C6–H6G···Cg1)** = 163°.

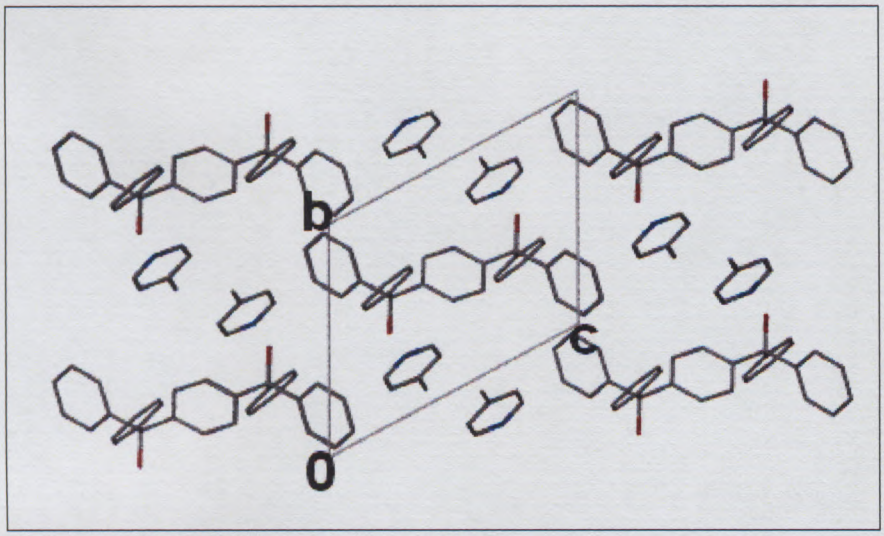

Figure 3.54 Packing diagrams of **H·2(4PIC)** viewed down [100].

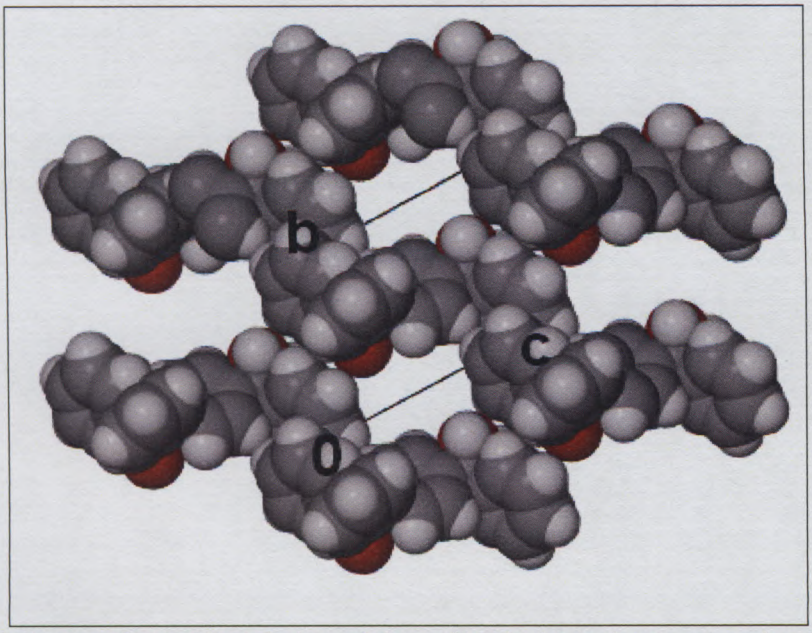

Figure 3.55 Space filled diagram for **H·2(4PIC)** viewed down [100] where the guest molecules reside in channels (guests are omitted).

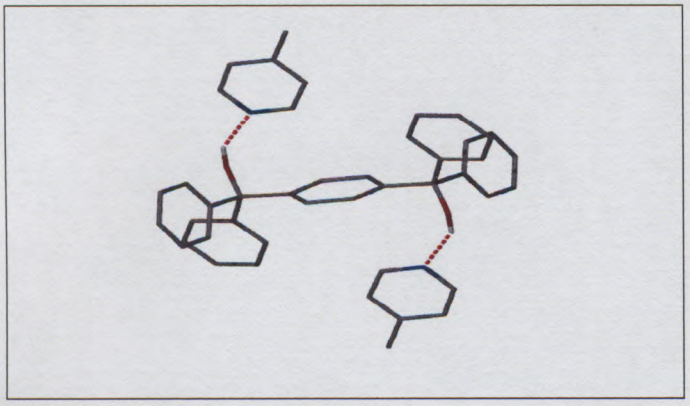

Figure 3.56 Hydrogen bonding in **H·2(4PIC).**

Table 3.22 Hydrogen bonding details.

Donor D	Acceptor A	D···A/Å	D-H/ Å	H···A/ Å	D-H···A/ Å
O1	N(1G)	2.810(2)	1.00(2)	1.818(2)	149(14)

3.3.10 Crystal structure of H·2PYR

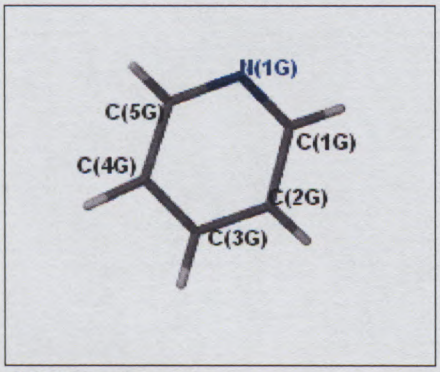

Figure 3.57 Guest numbering scheme of **PYR** molecule.

H·2PYR crystallizes in a triclinic crystal system (space group $P\bar{1}$) consisting of one half of a host molecule and one guest molecule in the asymmetric unit. All the non-hydrogen host and guest atoms were refined anisotropically. The host was located at Wyckoff position *e*. The host hydroxyl hydrogen was located in the difference electron density map and allowed to refine. The rest of the host and guest hydrogen atoms were placed in geometrically constrained positions and refined with common isotropic atomic displacement parameters for the atoms of the same type. The structure refined successfully to $R_1 = 0.0547$ with $wR_2 = 0.1369$.

The packing diagram in Figure 3.58 illustrates one host molecule and two guest molecules in each unit cell giving a H:G of 1:2 with Z = 1. The host molecules pack to form channels in the [100] direction shown in Figure 3.59 where the host is shown with its van der Waals radii and the guests are omitted.

Sections through the unit cell were viewed with the guest molecules omitted, shown in Figure 3.60. The section confirms the presence of channels in which the guests are able to pack located along [010] at a section height of 6.39 Å.

The structure is stabilized by (host)**O-H···N**(guest) hydrogen bonding illustrated in Figure 3.61. The hydrogen bonding details are given in Table 3.23.

The closest **C–H···π** contact between the guest and the host occurs between **C5–H5 ···Cg2** [ring C8, C9, C10, C11, C12 and C13] with a bonding distance of 2.70 Å between **H5 ···Cg2** and 3.934 Å between **C5 ···Cg2** with ⟨ **(C5–H5 ···Cg2)** = 143°.

The structure is further stabilized by face- to- face **π ···π** stacking between aromatic rings of adjacent host

molecules. The shortest distance between two centroids of the aromatic rings of neighbouring host molecules is approximately 5.79 Å. (Figure 3.62)

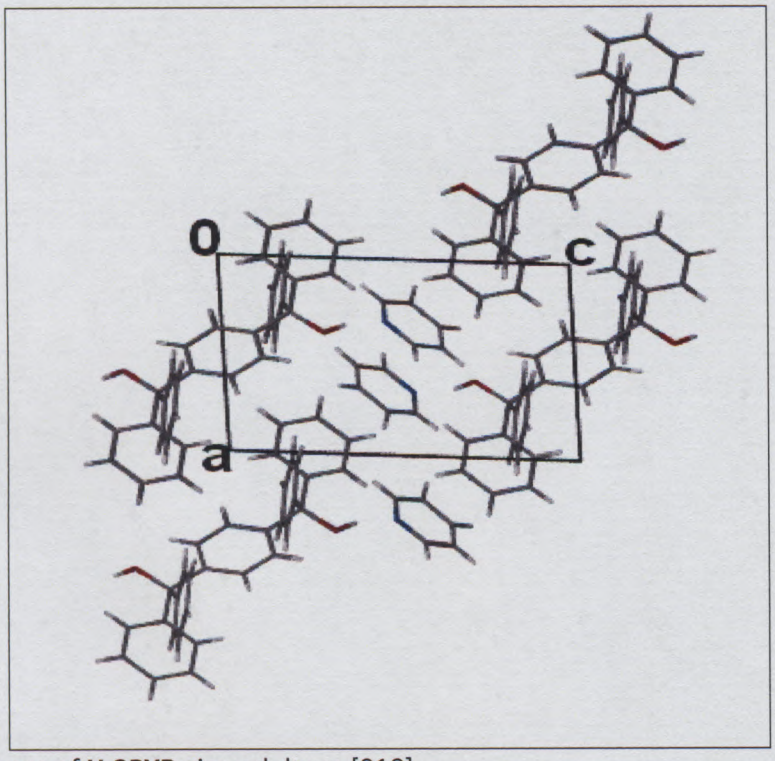

Figure 3.58 Packing diagram of **H·2PYR** viewed down [010].

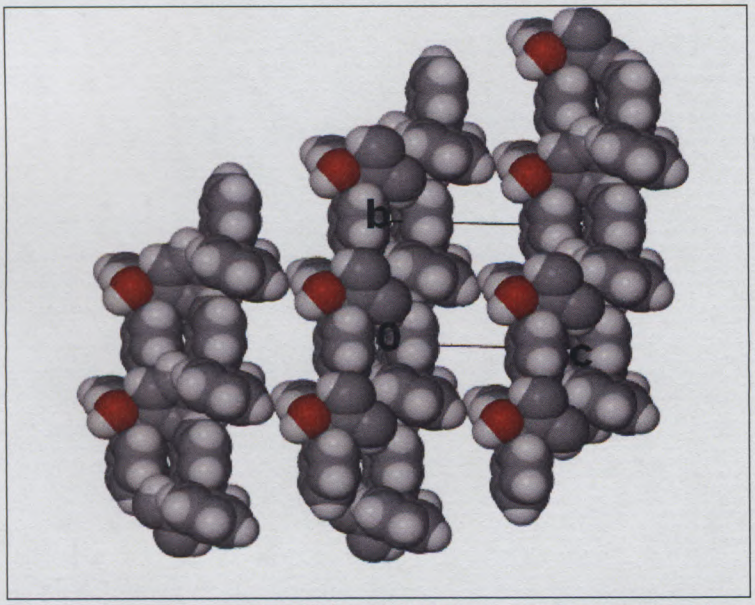

Figure 3.59 Space filled diagram viewed down [100] for **H·2PYR** where the guest molecules reside in channels (the guest are omitted).

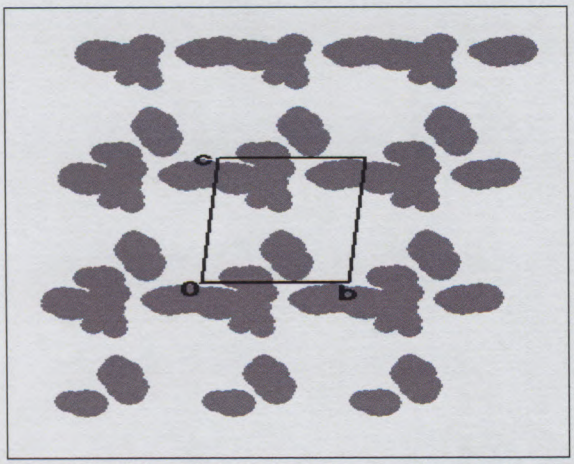

Figure 3.60 Section shown through a unit cell with guest molecules omitted, viewed down [100] at a section height of 6.19 Å.

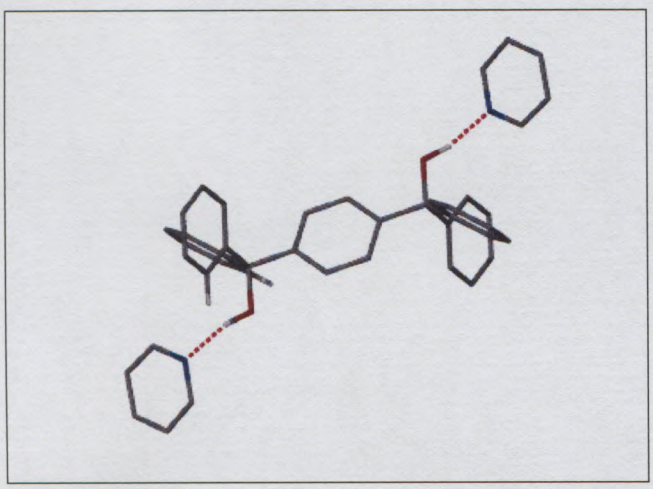

Figure 3.61 Hydrogen bonding in **H·2PYR.**

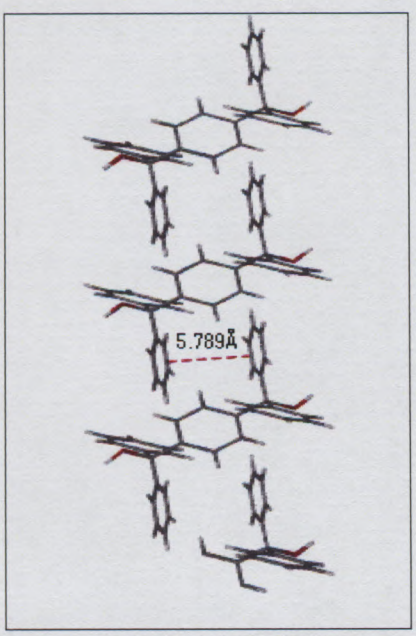

Figure 3.62 Illustration faces- to- face π ···π stacking in **H·2PYR**.

Table 3.23 Hydrogen bonding details

Donor D	Acceptor A	D···A/A°	D-H/ A°	H···A/ A°	D-H···A/ A°
O1	N(1G)	2.806(1)	0.970(1)	1.854(1)	167(1)

3.3.11 Crystal structure of H·2MORPH

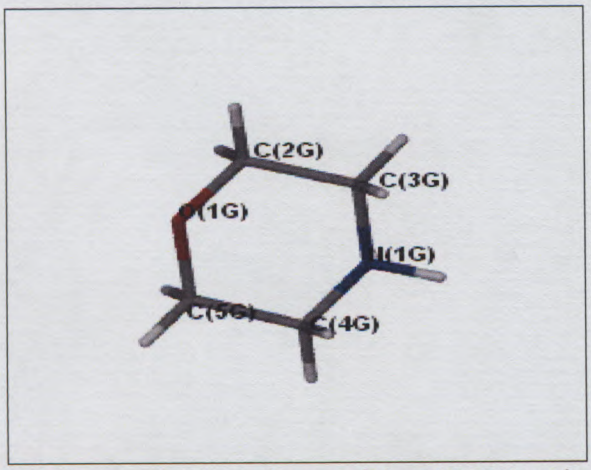

Figure 3.63 The numbering scheme of the **MORPH** molecule.

H·2MORPH crystallizes in a monoclinic crystal system (space group $P2_1/c$) consisting of one half of a host molecule and a guest molecule in the asymmetric unit. The host was located on a centre of inversion at Wyckoff position *b* and the guests found in general positions. The structure refined successfully to $R_1 = 0.0960$ with $wR_2 = 0.1822$.

The packing diagram in Figure 3.64 shows two host molecules and four guest molecules in each unit cell giving a H:G of 1:2 with Z = 2. The host molecules pack to form channels along the [001] direction shown in Figure 3.65 and 3.66.

Sections through the unit cell were viewed with the guest molecules omitted, these are shown in Figure 3.67. The section confirms the presence of channels in which the guests are able to pack located along [001] at a section height of 6.08 Å.

The hydrogen of the secondary amine was located in the difference electron density map. The expected trigonal bipyramidal arrangement was maintained around the nitrogen of the morpholine. The morpholine is in the expected chair conformation and structure is stabilized by (host)**O-H···N**(guest) and (guest)**N-H···O**(guest) hydrogen bonding (Figure 3.68). The host form layers in such a way that the guests are packed inside the channels formed, and are hydrogen bonded to the guest. The guests further chain linkages within the channels

via amine and carboxyl group. The hydrogen bonding details are given in Table 3.24.

The closest **C–H···π** contact between the guest and the host occurs between **C3G–H3BG ···Cg2** [ring C8, C9, C10, C11, C12 and C13] with a bonding distance of 2.61 Å between **H3BG ···Cg2** and 3.5518 Å between **C3G ···Cg2** with an angle of ⟨ **(C3G–H3BG ···Cg2)** = 146°.

The structure is further stabilized by face- to- face **π ···π** stacking between aromatic rings of adjacent host molecules. The shortest distance between two centroids of the aromatic rings of neighbouring host molecules is approximately 4.80 Å.

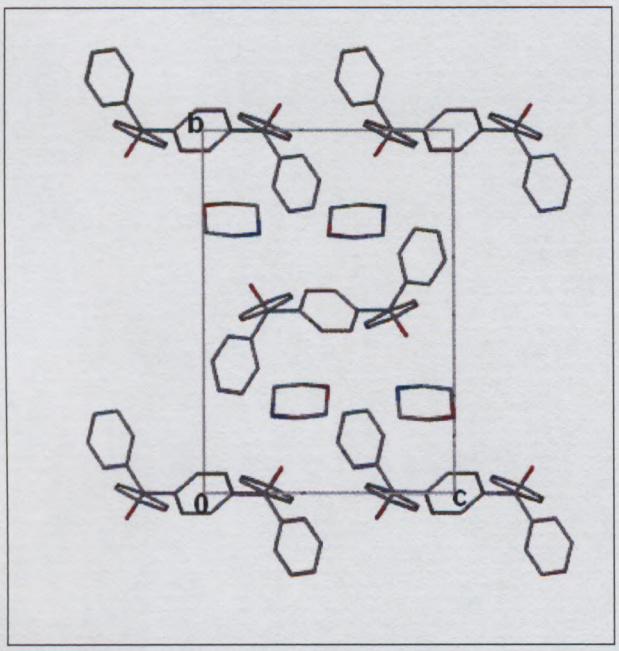

Figure 3.64 Packing diagram of **H·2MORPH** viewed down [100].

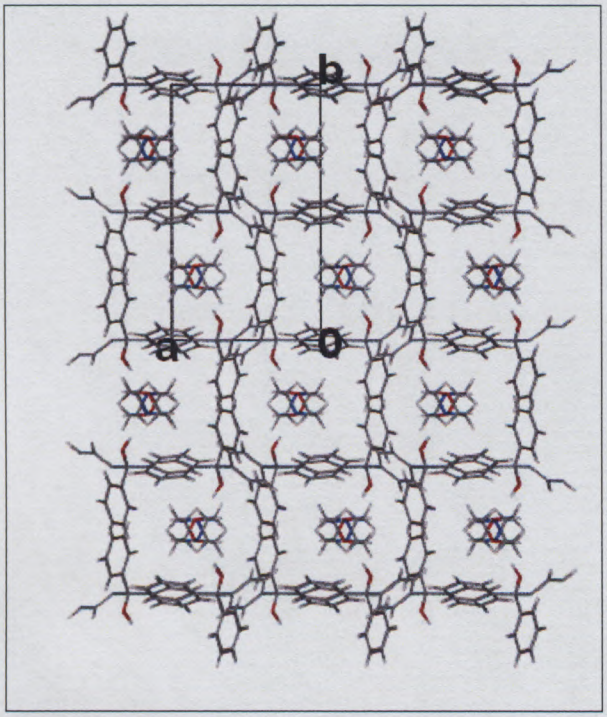

Figure 3.65 Packing of **H·2MORPH** viewed down [001].

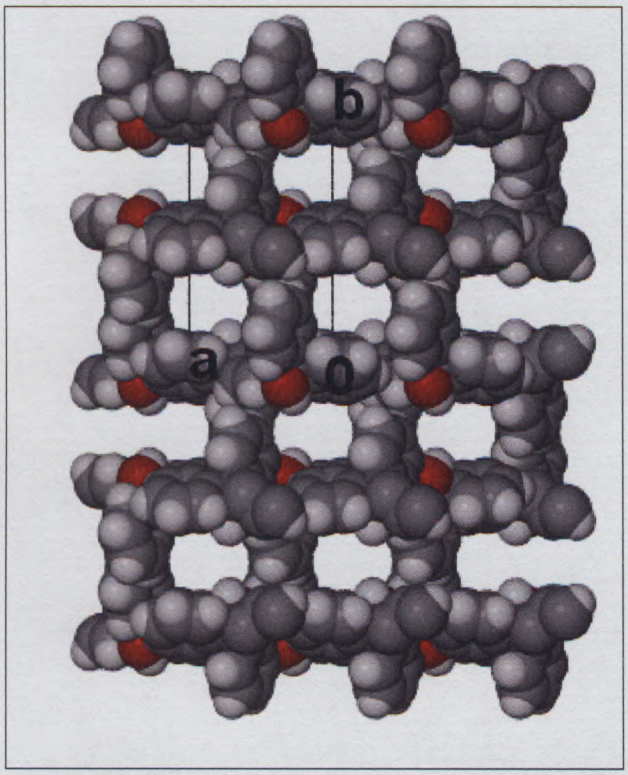

Figure 3.66 Space-filling projection down [001] showing channels of **H·2MORPH** (guest molecules are omitted).

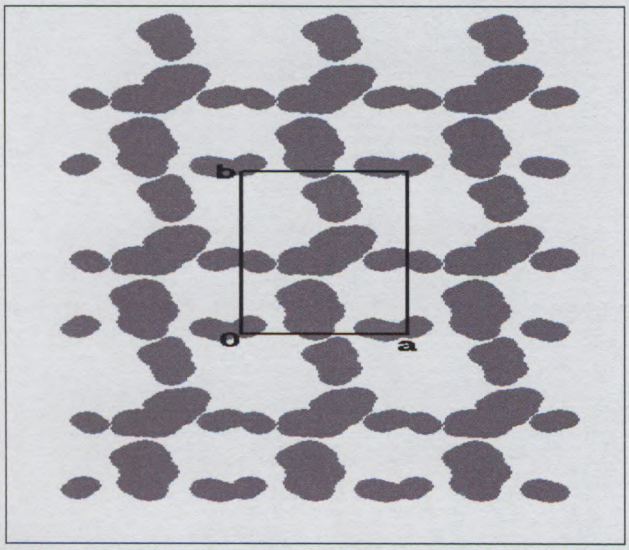

Figure 3.67 Section shown through a unit cell with guest molecules omitted viewed along [001] at a section height of 6.08 Å.

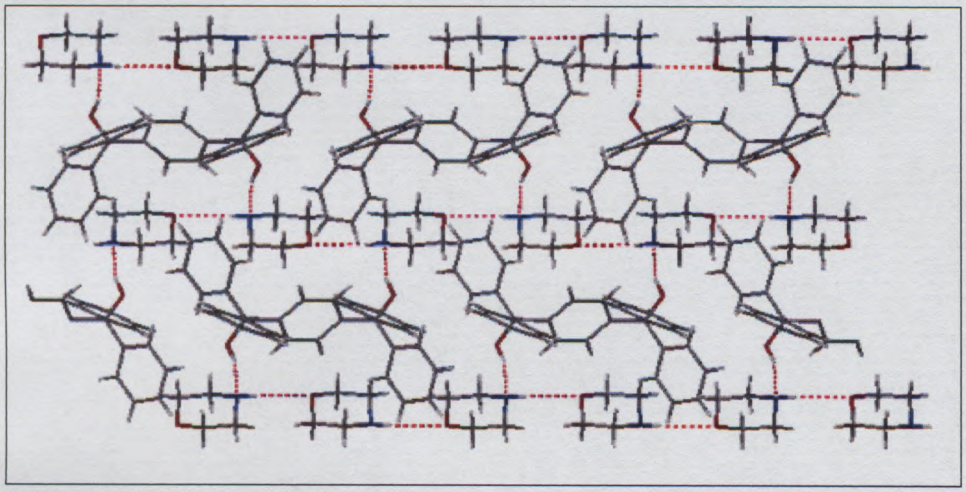

Figure 3.68 The hydrogen bonding in **H·2MORPH.**

Table 3.24 Hydrogen bonding details

Donor D	**Acceptor A**	**D···A/ Å**	**D-H/ Å**	**H···A/ Å°**	**D-H···A/ Å**
O1	N(1G)	2.813(1)	0.970(1)	1.874(1)	162(1)
N(1G)	O(1G)	2.801(1)	0.938(1)	2.347(1)	151(1)

3.4 Kinetics of Desolvation

Kinetic studies have become a crucial point in thermal analysis,[6] in which the main purpose is to determine the mechanism of reactions and to calculate the parameters of the Arrhenius equation. In this section, the decomposition behaviour of **H·2DMF** was studied by thermogravimetery (TG). Non-isothermal methods were used to determine the kinetics of desolvation. **H·2DMF** was selected for kinetic analysis as it is the only compound which displayed a TG decomposition curve with a single mass loss step. Crystals were crushed prior to analysis and the weight loss as a function of temperature change at different scan rates was measured. A series of TG runs over a temperature range of 30 to 200 °C were performed at heating scan rates of 2, 4, 8, and 16 °C min^{-1} (Figure 3.69). Notably there is an increase in the onset temperature of the decomposition as the heating rate is increased. The weight loss is then converted to a normalized form called the conversion fraction (α), the measure of reaction progress as a function of temperature (Figure. 3.70). The value ranges from 0 to 1.

The results of the non-isothermal method[7] gave a series of log β vs. 1/T where β = scan rate and T = absolute temperature. The plots for the 2.5, 5.0, 7.5 and 12.5% decompositions are shown in Figure 3.71. The α range 0.1-0.5 was studied because for α > 0.5 the TGA mass loss no longer follows a single step. The parallel lines indicate a constant mechanism of desorption in the chosen range and the activation energy was determined to be 65.1-83.9 kJ mol^{-1}, which is comparable with inclusion compounds of this type.[8]

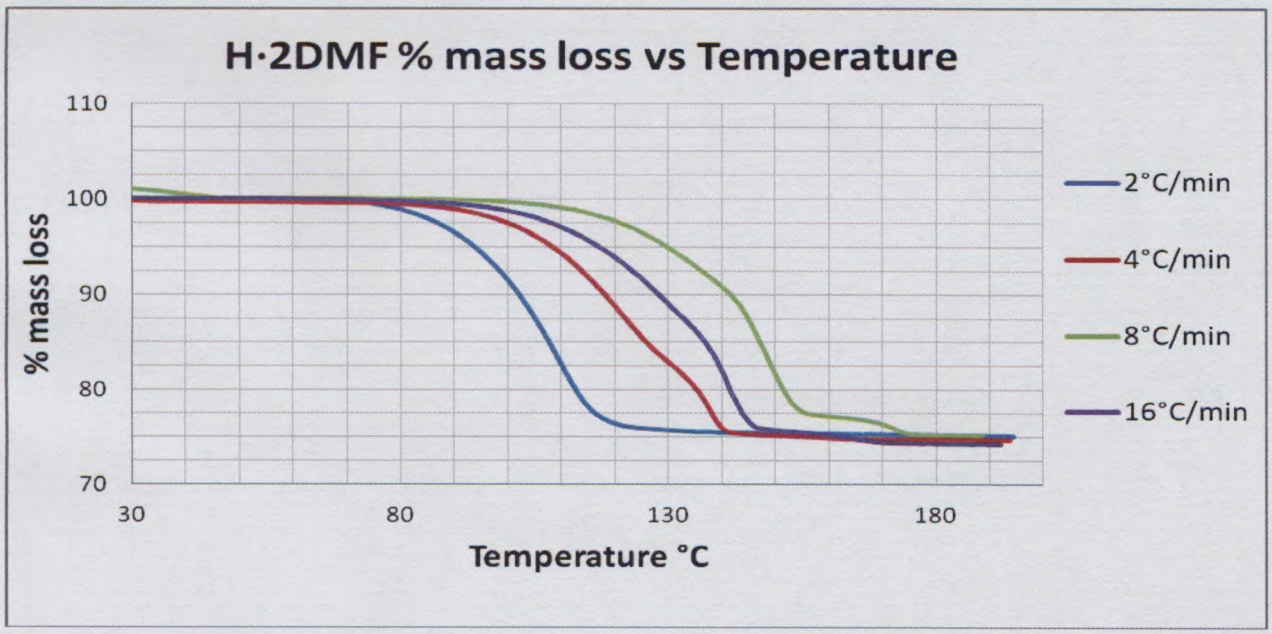

Figure 3.69 TG traces of **H·2DMF** at different scan rates.

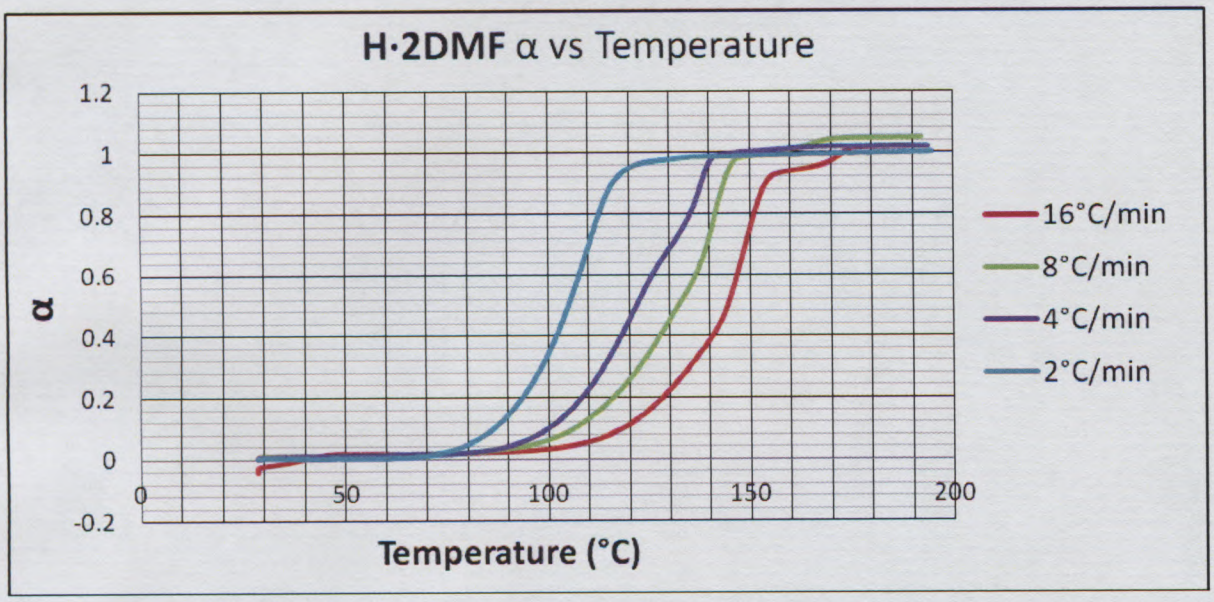

Figure 3.70 Conversion of TG curve to **α** vs. **Temp** curve.

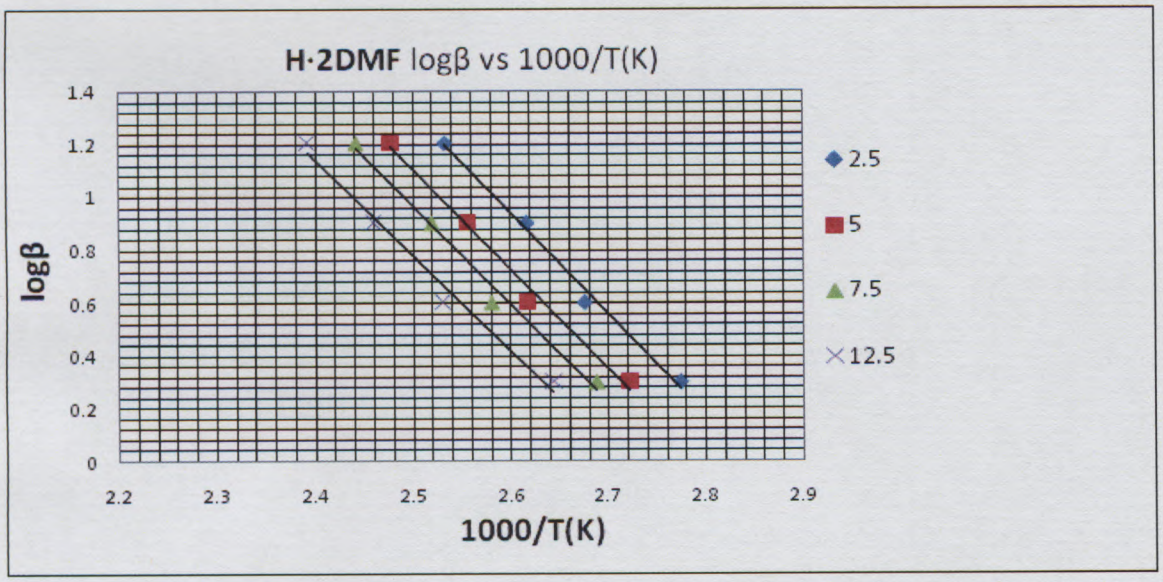

Figure 3.71 Logarithmic plots of logβ vs 1000/T(K) for **H·2DMF.**

3.5 Competition experiments

3.5.1 X-ray Powder Diffraction (PXRD)

Experiments were performed by dissolving approximately 30 mg of **H** (host) in 50:50 guest pair mixtures. The crystals were harvested and analyzed using PXRD. NMR experiments were also explored but could not be pursued due to overlapping of guest peaks. Investigations were carried out using PXRD, where a selection of crystals prepared from equimolar guest pairs were crushed and placed on a Mylar film. PXRD plots were generated and the results depicted in a diffractogram in which the diffracted intensity I is shown as a function of the scattering angle 2θ. These were then overlaid and compared with the PXRD plots of the individual clathrates. The results are tabulated in Table 3.24.

The PXRD plots of **H** with **DMF:NMF, DMF:NMA** and **DMF:DMA** guest pairs were compared with their corresponding individual clathrate plots as shown in Figures 3.72, 3.73 and 3.74, respectively. The results show that the host displays a strong preference for the **DMF** guest in all three instances. The plots for **H** with **DMA:NMF** and **NMA:DMA** guest pairs (Figures 3.75 and 3.76) were compared in a similar manner. The **NMA:DMA** experiment showed that the host preferred **NMA** as a guest. The **H** with **DMA:NMF** PXRD plot matched the **H·NMF** PXRD pattern. The **NMA:NMF** experiment gave a PXRD plot (Figure 3.77) which matched that of **H·2NMA.** To ascertain the overall preference of **DMF** an equimolar four component mixture of the amides and **H** was prepared, **DMF:DMA:NMA:NMF** and the PXRD plot obtained (Figure 3.78) matched the PXRD plot obtained for the **H·2DMF** compound. Thus the guest stability trend is DMF > NMA > NMF > DMA.

Table 3.24 Results of competition experiments.

Starting Mixture	Major Component
DMF/NMF	DMF
DMF/NMA	DMF
DMF/DMA	DMF
NMA/NMF	NMA
DMA/NMF	NMF
DMA/NMA	NMA
DMF/DMA/NMF/NMA	DMF

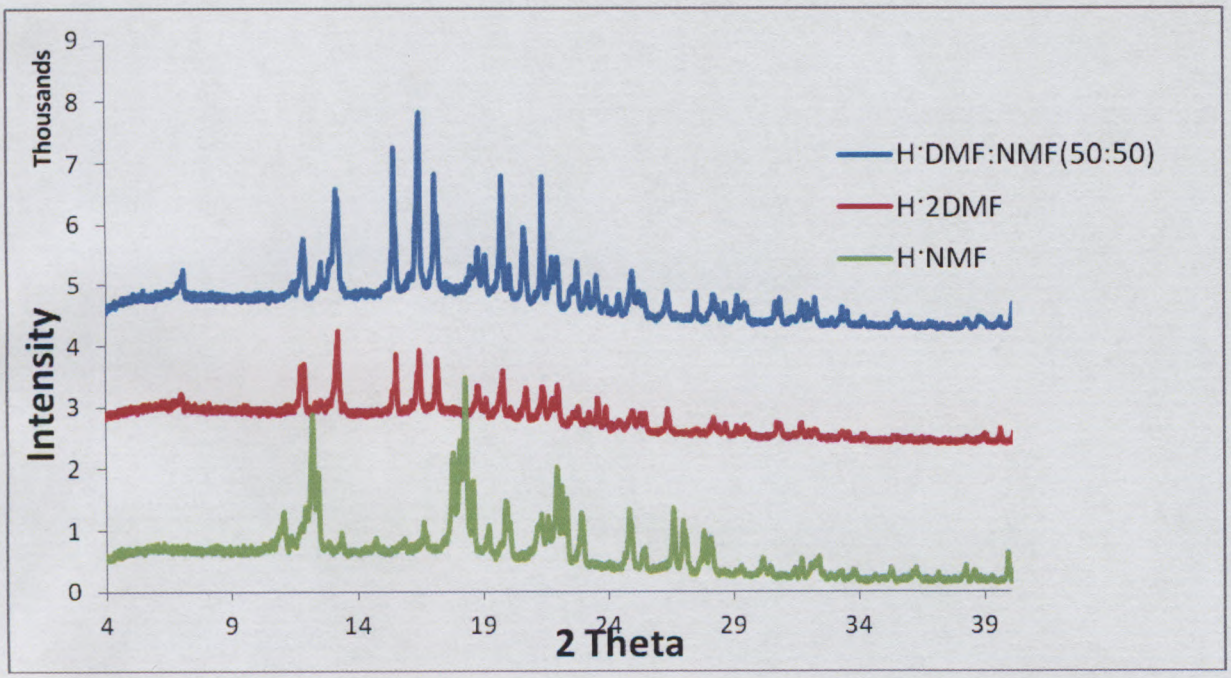

Figure 3.72 PXRD trace of competing guest pairs.

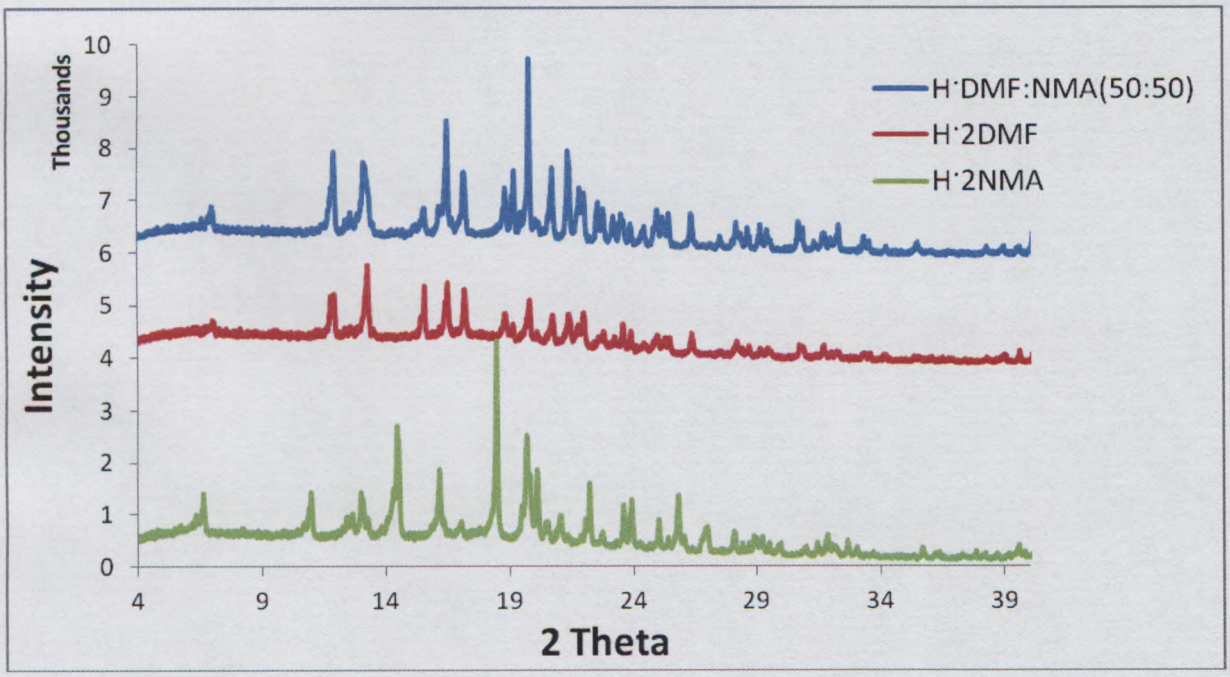

Figure 3.73 PXRD trace of competing guest pairs.

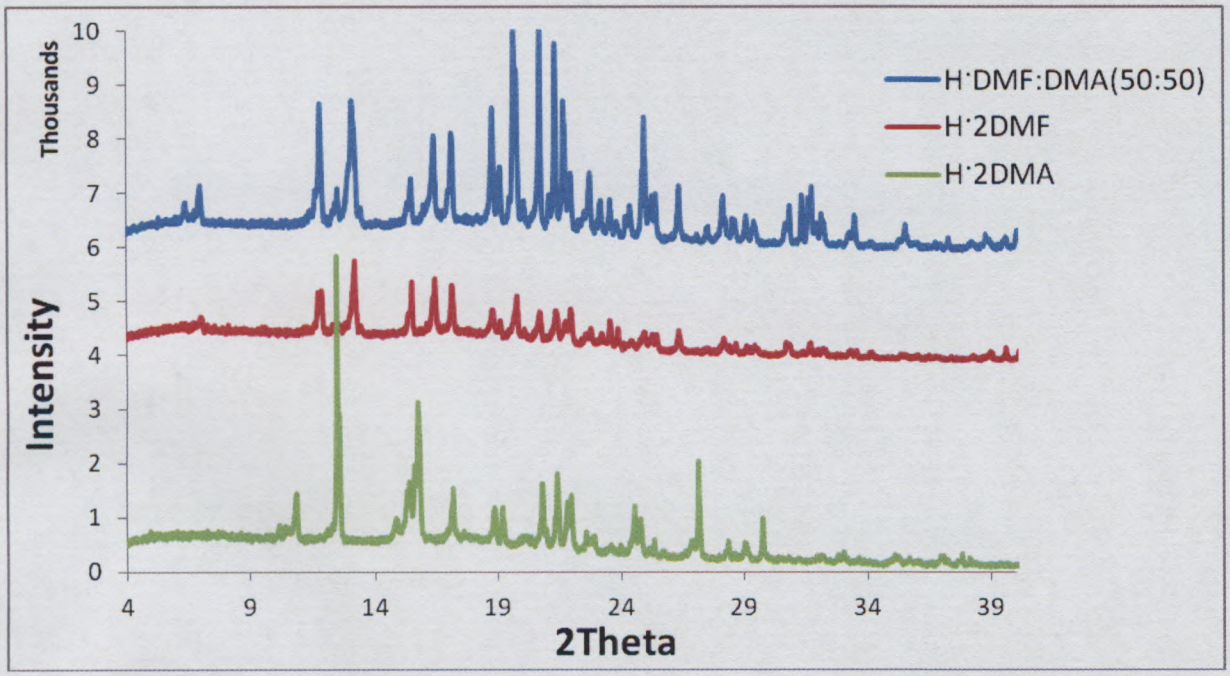

Figure 3.74 PXRD trace of competing guest pairs.

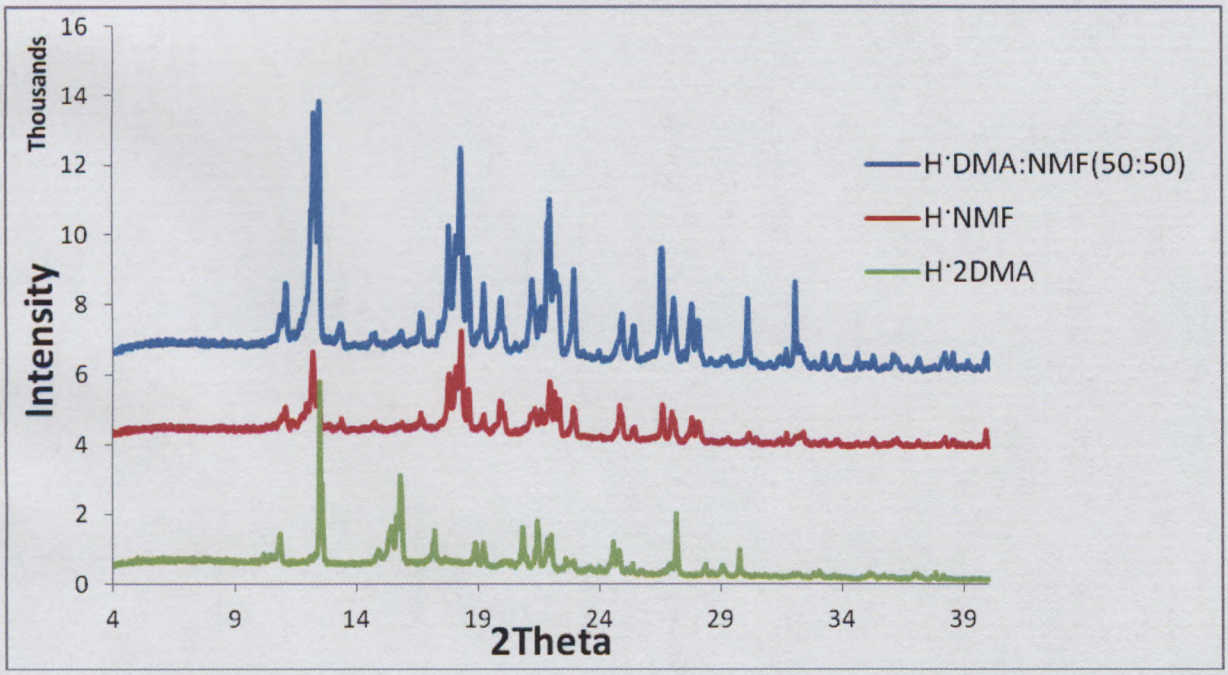

Figure 3.75 PXRD trace of competing guest pairs.

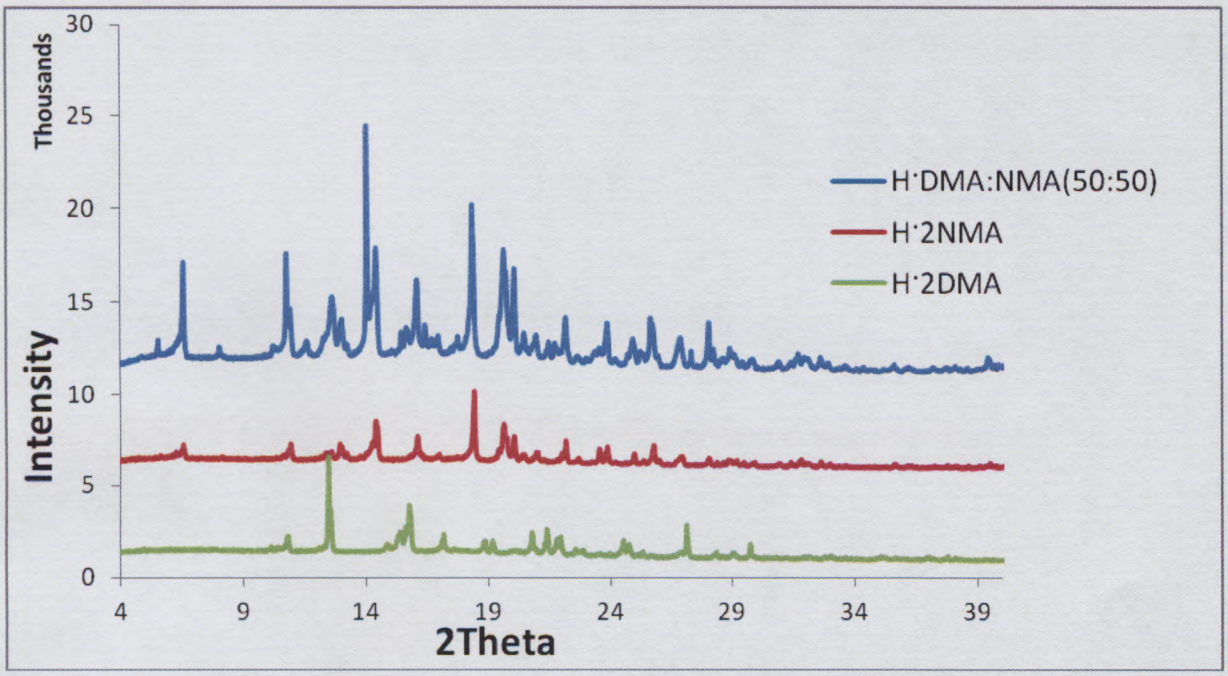

Figure 3.76 PXRD trace of competing guest pairs.

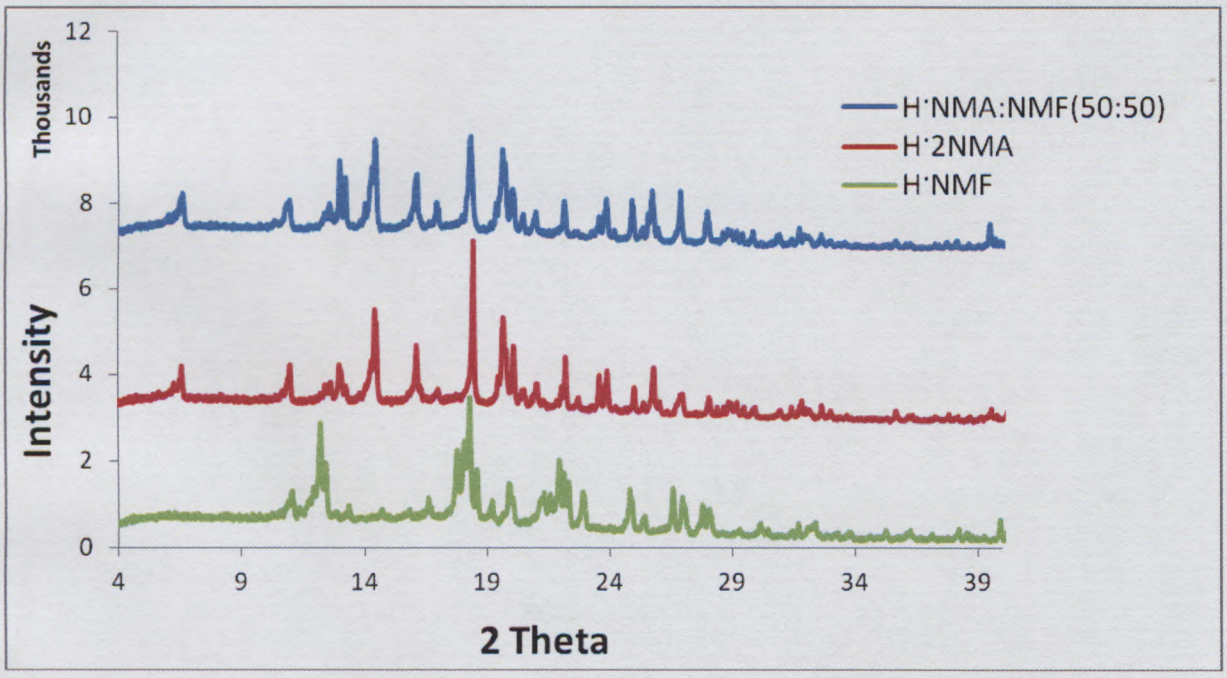

Figure 3.77 PXRD trace of competing guest pairs.

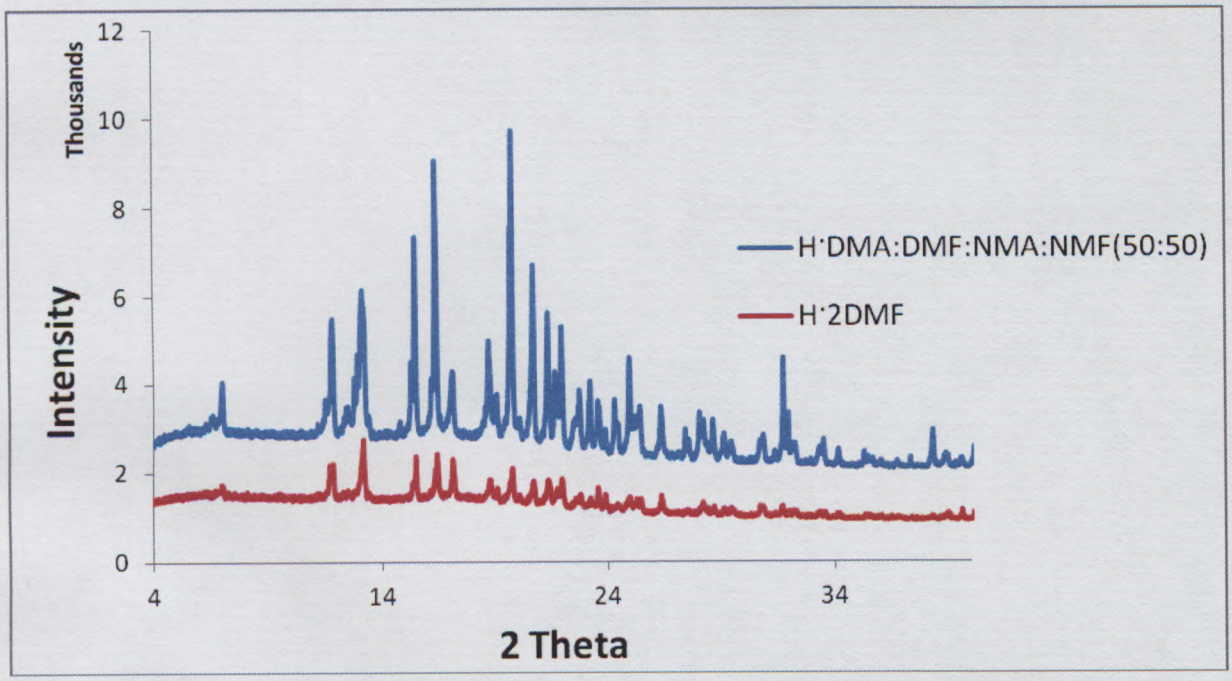

Figure 3.78 PXRD trace of four competing amide guests.

3.5.2 Solubility studies

The solubility of the host was measured, to study the force of interaction of the the various amide guests with our host and was correllated with results obtained from PXRD experiments. This was achieved by adding the liquid guest dropwise to a fixed mass of host until dissolution was possible. The procedure was carried out at 25 °C with gentle stirring. The results obtained (milligram of host per gram of guest) were DMF 2.8, NMA 4.6, NMF 49.7 and DMA 149.8. The host is therefore least soluble in DMF. The solubility trend is therefore DMF<NMA<NMF<DMA. These results could be linked with the results obtained from the competition experiments in that the preferred guest is the one in which the host compound is the least soluble.

3.5.3 Gas Chromatography (GC)

Experiments were set-up by dissolving 30 mg of host in 50:50 guest mixtures of 2PIC:3PIC, 2PIC:4PIC, 2PIC:PYR, 2PIC:MORPH; 3PIC:4PIC, 3PIC:PYR, 3PIC:MORPH; 4PIC:PYR, 4PIC:MORPH; PYR:MORPH. The crystallization process proved to be difficult as for most of the samples an oily residue formed at the base of the vial. Crystals were grown from 50:50 2PIC:PYR and 4PIC:PYR mixtures.

The experiments were performed using GC. The components were extracted by diluting samples with chloroform. The results of crystal grown from 50:50 2PIC:PYR showed that 2PIC was preferred over pyridine, upon analysis of results from crystal grown from 50:50 4PIC:PYR the host favoured 4PIC. These experiments could not be completely analysed due to paucity of the host material and the lack of resultant precipitates from competition experiments.

3.6 REFERENCES

1. I. Olovsson and P. Jönsson in The Hydrogen Bond – Structure and Spectroscopy, eds. P. Schuster, G. Zundel and C. Sardify, North Holland Publishing Company., Amsterdam, 1975
2. L. J Barbour, SECTION, A computer program for the graphic display of cross sections through a unit cell, *J. Appl. Cryst.*, 1999, **32**, 353
3. J.W. Steed, J.L. Atwood, Supramolecular Chemistry, John Wiley & Sons., Chichester, 2000
4. D. Braga, F. Grepioni, E. Tedesco, *Organometallics.*, 1998, **17**, 2669
5. M. C. Etter, J. C. MacDonald, J. Bernstein, *Acta Crystallogr.*, 1990, **B46**, 256
6. M. R. Caira, A. Jacobs, L.R. Nassimbeni and F. Toda, *CrystEngComm.*, 2003, **5(28)**, 150.
7. J. H. Flynn, L. A Wall , *J. Res. Nat Bur. Stand.*, 1966, **70A**, 487
8. A. Jacobs, L. R. Nassimbeni, K. L. Nohako, G. Ramon and B. K. Sebogisi, *J. Chem. Cryst.*, 2011, **41(5)**, 610

4. CHAPTER 4- Host Conformation

4.1 Host conformation

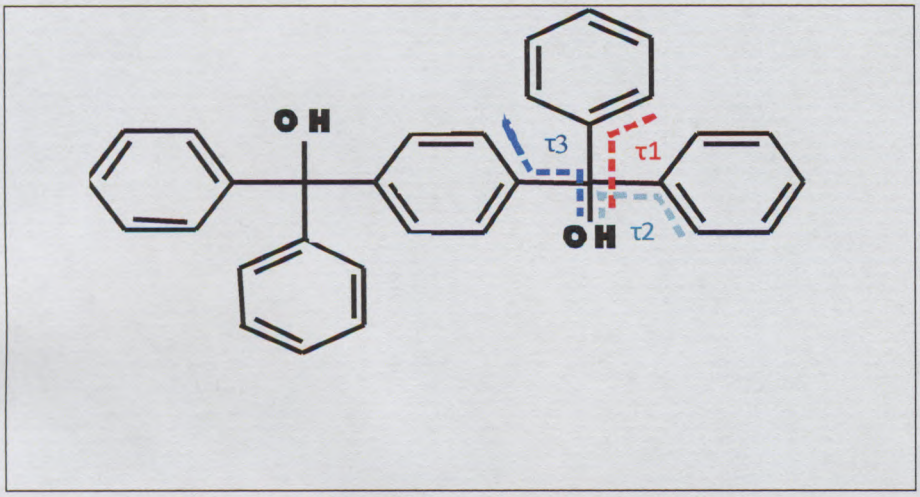

Figure 4.1 Illustration of torsion angles for H.

Table 4.1 Torsion angles for inclusion compounds.

Torsion angles	*H·2DMA (a)	*H·2DMA (b)	*H·2DMF	*H·2NMA	**H·NMF	**H·NMF	**H·2H_2O	**H·2H_2O
τ 1/°	+85.5	+35.3	+54.2	+18.9	+12.7	+16.3	+47.3	+30.2
τ 2/°	+10.1	+19.1	+25.4	+55.4	+56.6	+59.3	+36.9	+31.6
τ 3/°	+27.3	+44.1	+36.6	+39.9	+40.6	+28.3	+47.9	+68.6

* These structures have half a host molecule in their asymmetric unit.

** These structures have one complete host in their asymmetric unit

The conformation of the host is governed by three torsion angles (Figure 4.1).The torsion angles where **τ 1** is measured involved atoms O1-C1-C2-C3 or O1-C1-C2-C7, **τ 2** O1-C1-C8-C9 or O1-C1-C8-C13 and **τ 3** O1-C1-C14-C15 or O1-C1-C14-C16. From these two points of measurements the lowest angle value was recorded. The crystal structures of the amide inclusion compounds display considerable variability in the torsion angles. τ1 varies from a minimum of 12.7° to a

maximum of 85.5°, with a change of 72.8° (Table 4.1). Similarly the changes in τ2 and τ3 are 69.4° and 41.3°. There are also considerable changes within the same structure of **H·NMF** and **H·2H$_2$O**.

Table 4.2 Torsion angles for inclusion compounds.

Torsion angles	**H·2PIC	**H·2PIC	*H·2(3PIC)	*H·2(4PIC)	*H·2PYR	*H·2MORPH
τ 1/°	+18.0	+61.6	+16.6	+48.8	+61.3	+11.7
τ 2/°	+42.9	+37.9	+51.4	+22.6	+8.2	+77.1
τ 3/°	+56.2	+39.9	+35.6	+47.8	+29.6	+10.6

*These structures have a half host molecule in the asymmetric unit.

**This structure has one host molecule in the asymmetric unit.

Table 4.2 shows the torsion angle list for the crystal structures of **H·2PIC, H·2(3PIC), H·2(4PIC), H·2PYR** and **H·2MORPH** which again shows variability e.g. τ1 varies from a minimum of 18.0° to a maximum of 61.6°. These torsion angles confirm the flexibility of the host molecule, which adapts and allows the conformation of the phenyl moieties to accommodate the various guests in the packing of the structures. This pliability of the phenyl rings can be regarded as one of the reasons for the success of this host in enclathrating a large range of guest molecules.

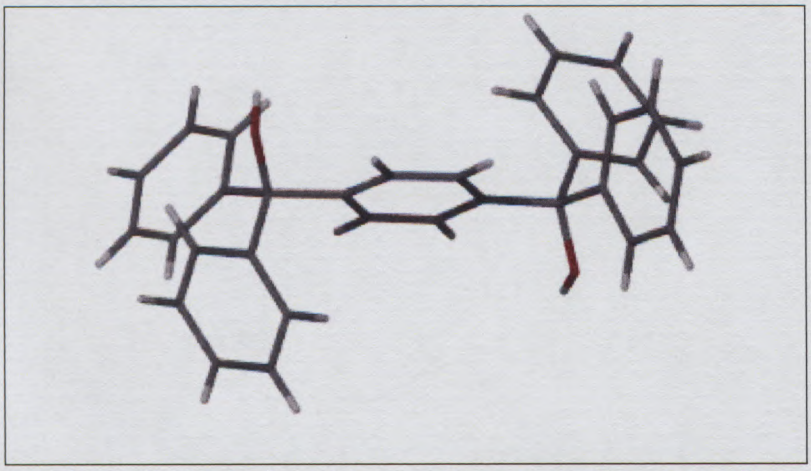

Figure 4.2 Conformation of **H** with the hydroxyl groups in trans conformation (from **H·2PIC**).

The host hydroxyl groups are in the *trans* conformation in all the structures. The torsion angles between the hydroxyl moieties (O1-C1-C20-O1A) are 180°, by crystallographic

symmetry, for all the structures where one half of the host molecule was present in the asymmetric unit. The only exception was **H·2PIC** where a complete host molecule was found in the asymmetric unit and O1- C1-C20-O1A was measured as 161.1°.

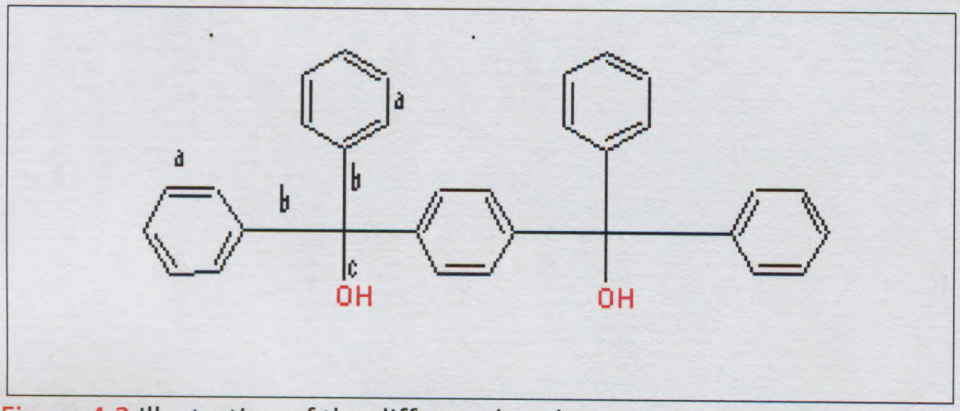

Figure 4.3 Illustration of the different bond types.

Three different types of bonds are present in the **host** (Figure 4.3). These were measured and listed in Table 4.3; and were found to be comparable with standard values[1].

Table 4.3 The different bonds present in **H**.

Structure	a- C_{ar}-C_{ar}	b-C_{ar}-C_{sp3}	c-C_{sp3}-O
H·2DMAa	1.382(1) - 1.399(1)	1.542(3)	1.432(2)
H·2DMAb	1.377(1) - 1.393(2)	1.541(3)	1.428(2)
H·2DMF	1.376(2) - 1.395(2)	1.537(3)	1.432(2)
H·2NMA	1.371(6) - 1.397(2)	1.536(3)	1.436(2)
H·NMF	1.383(2) - 1.396(5)	1.534(3)	1.442(2)
H·NMF	1.379(5) - 1.398(4)	1.538(3)	1.442(2)
H·2H_2O	1.378(2) - 1.393(4)	1.537(3)	1.438(2)
H·2H_2O	1.376(6) - 1.396(1)	1.537(3)	1.438(2)
H·2PIC	1.352(2) - 1.401(5)	1.546(3)	1.431(2)
H·2(3PIC)	1.379(11) - 1. 398(14)	1.545(3)	1.428(2)
H·2(4PIC)	1.378(5) - 1.398(6)	1.539(3)	1.427(2) - 1.539(4)
H·2PYR	1.382(10)- 1.398(3)	1.563(3)	1.428(2)
H·2MORPH	1.379(1) - 1.399(2)	1.542(3)	1.433(2) - 1.542(4)

4.2 REFERENCES

1. F. H Allen, O. Kennard and D. G Watson, *J. Chem. Soc. Perkin Trans II*, 1987.

5. CHAPTER 5 - Conclusions

5.1 Concluding Remarks

According to the analysis of experiments performed in this project, the main conclusions are:

1,4-bis(diphenylhydroxymethyl)benzene **(H)** has proven to be a good host compound. The host formed eleven clathrates, four of which were obtained with amides **H·2DMA, H·2DMF, H·2NMA** and **H·NMF** and three with picolines **H·2PIC, H·3PIC AND H·4PIC.** Furthermore inclusion compounds of pyridine **H·2PYR** and morpholine **H·2MORPH** and two serendipitous compounds with the inclusion of water molecules **H·2H_2O** and the secondary **H·2DMA** (polymorph) were also formed. This proved that our host possesses good inclusion ability.

The question of thermal stability then arises. It is a known fact that it is difficult to correlate the features recorded with the thermal events taking place.[1] The TG and DSC results showed good correlation which was confirmed by photographic images using HSM. Although temperature shifts are noticed when comparing DSC and HSM, consideration was taken into account that the DSC analysis was conducted under carefully defined enclosed sample conditions, slow heating, cooling rates so that equilibrium would be approached.

The T_{on}/T_b values calculated for the amides gave a good indication of the stability profile of our compounds. T_{on}/T_b of **H·2DMF** was calculated to be 0.94 which was considerably high when compared to that of **H·2DMA**, **H·2NMA** and **H·NMF** 0.85, 0.84 and 0.84. Upon comparison for pyridine, substituted pyridines and morpholine compounds, **H·2MORPH** has a high T_{on}/T_b 0.95 compared **to H·2PIC, H·2(3PIC), H·2(4PIC)** and **H·2PYR**.

The structural analysis showed credible quality as the final R indices [$I>2\sigma(I)$] results were less than 10% for all the structures. The H:G obtained for the single crystal analysis were in agreement with those found in TG analysis for all the structures obtained. H:G=1:2 for all structures except **H·2PIC** and **H·NMF**. The amide structures were strongly stabilized by (host)**O-H···O**(guest) hydrogen bonds while the pyridine, substituted pyridines and

morpholine structures were governed by (host)**O-H···N**(guest) hydrogen bonds, with **H·2NMA and H·2MORPH** further stabilized by (guest)**N-H···O**(guest) hydrogen bonds.

The kinetics of desolvation could only be conducted for **H·2DMF** since it was the only compound that displayed a one step dissolution process. The activation energy was determined to be 65.1 - 83.9 $kJmol^{-1}$.

The competition experiment results obtained from crystals grown from the host dissolved in equimolar guest mixtures of amide guests showed that DMF was favoured in all the guest pair set ups. These results showed that the enclathration takes place in the preferential order **DMF>NMA>NMF>DMA.** These results could then be linked with the solubility results which proved DMF to be the least soluble guest. The picolines\pyridine\morpholine competition results were inconclusive due to inability to form precipitates.

NMR methods could not be employed in the competition experiments due to overlaps between signals of host, G_A and G_B.

The host is discriminatory and is highly selective towards the DMF guest molecule. It can therefore be deemed as being a compound that shows good molecular recognition ability. Enhanced inclusion ability is obtained owing to the large voids created by the bulky terminal groups.

5.2 References

1. Brown M, E. 'Introduction to thermal analysis' Chapman and Hall, London 1988